Università degli Studi di Padova

DIPARTIMENTO DI TECNICA E GESTIONE DEI SISTEMI INDUSTRIALI
Corso di Laurea Magistrale in Ingegneria dell'Innovazione del Prodotto

Low-GWP Refrigerants: The Importance of the Thermophysical Properties for HVAC Design

Laureando:
Ivan Greselin
Matricola 1236527

Relatore:
Prof. Claudio Zilio

Correlatore:
Ing. Sergio Bobbo

Anno Accademico 2021-2022

Sommario

La presente tesi verte sulla nuova generazione di refrigeranti conformi ai trattati internazionali sulle sostanze climalteranti, e ritenuti come l'alternativa promettente ai fluidi operativi tradizionali per il settore della refrigerazione e del condizionamento dell'aria. In particolare, questo lavoro si focalizza sulle proprietà termodinamiche e di trasporto dei refrigeranti, attraverso una disamina della loro rilevanza ingegneristica per il dimensionamento e le prestazioni dei moderni impianti HVAC basati su cicli a compressione di vapore. Per una selezione di refrigeranti si conduce un confronto critico tra le misure sperimentali di alcune proprietà fondamentali, tratte da pubblicazioni scientifiche ricercate attraverso un'indagine della letteratura, e quelle ad esse relative estrapolate attraverso REFPROP 10.0, la versione attuale del database di fluidi che ai fini ingegneristici rappresenta lo standard di riferimento. L'obiettivo ultimo è valutare l'affidabilità delle correlazioni matematiche integrate nel software, attraverso un'analisi delle deviazioni dei dati sperimentali da quelli calcolati per ciascuna proprietà e per ogni refrigerante considerati. Una significativa discrepanza tra i valori misurati e quelli calcolati è stata riscontrata per le proprietà termodinamiche di alcuni fluidi, in particolari condizioni a basse temperature e pressioni, nonché in prossimità del punto critico e delle curve di saturazione. Per le proprietà di trasporto, la differenza si è rivelata in generale maggiormente accentuata. Dai risultati dello studio emerge che, per i refrigeranti esaminati, vi è l'esigenza di aumentare l'attendibilità del software, attraverso lo sviluppo di nuove correlazioni basate su una maggiore disponibilità di dati sperimentali precisi ed accurati, per meglio agevolare la progettazione di sistemi HVAC innovativi ed efficienti.

Abstract

This thesis addresses the novel generation of refrigerants which comply with the international regulations on climate-forcing pollutants and that, in the mid-long term, are considered as promising alternatives to the traditional working fluids for the refrigeration and air-conditioning industry. Particularly, this work focuses on refrigerant thermodynamic and transport properties, and provides an insight on their technical relevance for the design and performance of modern HVAC equipment based on the refrigeration vapor-compression cycles. For a selection of refrigerants, a comparison is critically performed between the experimental measurements of some fundamental properties, retrieved from scientific publications by means of a literature review, and their relative values computed with REFPROP 10.0, the current version of the engineering reference-standard fluid database. The purpose is to assess the effectiveness of the mathematical correlations included in the software, by analysing the deviations for the experimental data from the calculated values, for each considered property and refrigerant. A significant disagreement between the available experimental measurements and the calculated values for the thermodynamic properties of some fluids was observed, under particular conditions at low temperatures and pressures, as well as near the critical point and the saturation curves. For the transport properties, the difference further increased in general. The results of the study reveal that, for the investigated refrigerants, it is necessary to improve the software reliability, through the development of new correlations fitted on a higher amount of precise, accurate experimental data, to better promote the design of efficient, innovative HVAC systems.

Ringraziamenti

Difficile condensare questa doverosa parte in poche parole, e nonostante non farò il nome di tutti, gli stessi credo si riconosceranno per certo in queste righe.

Un "grazie" speciale va al prof. Claudio Zilio e all'ing. Sergio Bobbo per la disponibilità nei miei confronti, e per avermi consentito di conciliare l'attività di tesi con il lavoro. In particolare, ringrazio l'ing. Sergio per avermi guidato nella stesura dell'elaborato. Rivolgo il mio ringraziamento anche a Laura Fedele, Giulia Lombardo e Mauro Scattolini, che ho avuto la fortuna di incontrare quest'anno. La simpatia di ciascuno mi ha accompagnato in questa caldissima estate trascorsa a Padova, rendendo il periodo ancora più intenso e piacevole.

Ringrazio i miei compagni di corso e amici, e soprattutto i "biondi" della triade poco seriosa vorrei quasi dire. . . la rifacciamo? Ai miei genitori, alla mia famiglia, desidero esprimere la mia gratitudine per avermi sostenuto in questo percorso, e per avermi dato l'opportunità di cogliere tutto ciò che di questa esperienza è possibile apprezzare. Grazie, infine, a tutte le persone che mi offrono la loro preziosa amicizia.

Contents

Introduction

Refrigeration and air-conditioning are regarded among the twenty most important engineering achievements during the last century, along with electrification, internet, and cars. The long-term ability to preserve food and drugs as well as to control and adapt the environmental comfort resulted the foundation to the technological, economical, and social development of modern society. The disruptive change was only made possible thanks to the industrialization of appliances that have used refrigerants as the core elements of their functioning. As the climate impact of these working fluids was discovered and progressively better understood, research efforts made available more sustainable, alternative molecules. This thesis addresses the fourth generation of refrigerants, which is characterized by a low greenhouse effect as well as a negligible ozone-depleting potential. A sound knowledge of refrigerant properties is essential to accurately describe their behavior in the HVAC systems: it highly influences the requirements in terms of sizing and performance, and depends on the ability of simulation software to represent it by means of mathematical properties correlations.

This thesis is structured in five chapters. Chapter 1 introduces to refrigerants and depicts their background. Chapter 2 delves into the most relevant refrigerant properties for the design of HVAC systems and their components. Chapter 3 illustrates the evolution of properties prediction correlations focusing in particular on the state-of-the-art, and describes the relation between these tools and the effects on some key parameters related to the equipment performance. Chapter 4 outlines the most established methods for measuring the useful refrigerant properties from which the mathematical correlations are derived. Chapter 5 presents the analysis performed in this thesis on the recommended refrigerant models for promising molecules in the HVAC sector. In light of a substantial lack of available studies reporting key properties for a selected set of new refrigerants, the scope was to explore the reliability of latest NIST reference database REFPROP to compute fluid properties. The analysis, which was carried out in coordination with the Refrigerants and Nanofluids Research Group from the Construction Technologies Institute of the National Research Council (ITC-CNR), identified some issues of technical concern that might suggest future software improvements.

Chapter 1

Climate change and its drivers: an overview

1.1 Latest key findings

Droughts, floods, heatwaves and heavy rainfalls are just some of the most common extreme natural events that human kind have been experiencing recurrently in the last decades. They are happening more frequently than ever, and the symptoms of a faulty environmental equilibrium can now be found anywhere, worldwide.

Since the beginning of the 19th century, several campaigns of studies have been carried out to relate *anthropic* (i.e. human-induced) activities to global warming. The evidence of severe, time-extended effects has widely been confirmed by the scientific community and periodic reports draw widespread attention to climate change, recognizing that it is likely the toughest challenge for the present and immediate future, but as the time span to act effectively is narrowing, decisive, ground-breaking solutions and strategies are to be adopted by governments in the near term. With this purpose, the International Panel on Climate Change (IPCC) — established in 1988 by the World Meteorological Organisation (WMO) and the United Nations Environment Programme (UNEP) — has been working to investigate and predict the magnitude of the environmental crisis, providing guidelines for policymakers to coordinate the pledges in tackling climate changes. The organization is built on the contribution of currently 195 members from all over the world, that pertains to the assessment of full scientific, technical and socio-economical well-established knowledge on climate change, including also evolving and multiple perspectives in the literature.

One of the latest releases by the IPCC is an high-level summary of the current state of the climate, provided with the Sixth Assessment Report (AR6) by the Working Group I (WGI). To underline the awareness of climate change, the

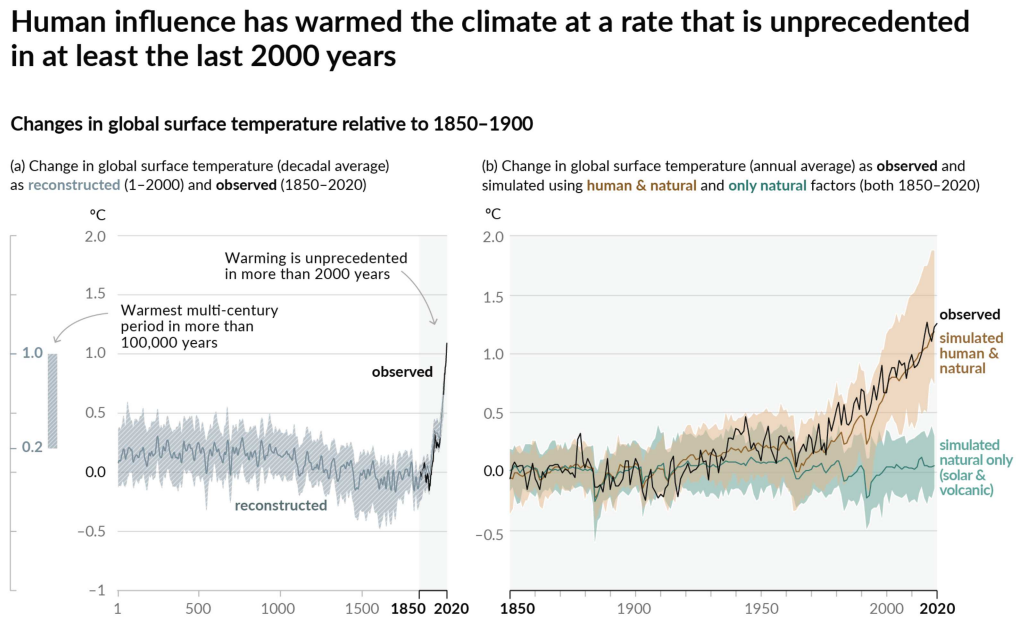

Figure 1.1: Global historical temperature change (a) and close-up view of recent temperature trends (b) [1].

proceeding begins with the key finding: "It is unequivocal that human influence has warmed the atmosphere, ocean and land. Widespread and rapid changes in the atmosphere, ocean, cryosphere and biosphere have occurred [1]." The whole ecosystem, in fact, has been affected by an abrupt mutation, which is in general described in terms of temperature rise. Fig. 1.1 illustrates the recorded global surface temperature change: the "observed" curve in panel (b) shows that, apart from slight annual deviations, between 1850 and 1900 the temperature remained approximately steady.

From the first decades of the 20th century, western countries underwent a decisive population growth and industrialization, which rapidly took to an increased demand of energy, and that paved the way to mass productions of goods. Primary energy sources, however, were fossil fuels — and they still are nowadays (see Fig. 1.2) — whose consumption was responsible not only for air pollution and its severe consequences on health, but also for an increased atmospheric concentration of gases responsible for the *greenhouse effect*, therefore called "greenhouse gases" (GHGs). More lately, in the last forty years, the climate has been significantly warmer than ever reported (see Fig. 1.1): in 2019, the best estimation of the effective human-induced global temperature rise is of 1.07 °C [1, 3], and it is likely to reach 1.5 °C between 2030 and 2052 if it continues to increase with the same rate [4]. Significantly, signs of warming have been related to an increase of "well-mixed

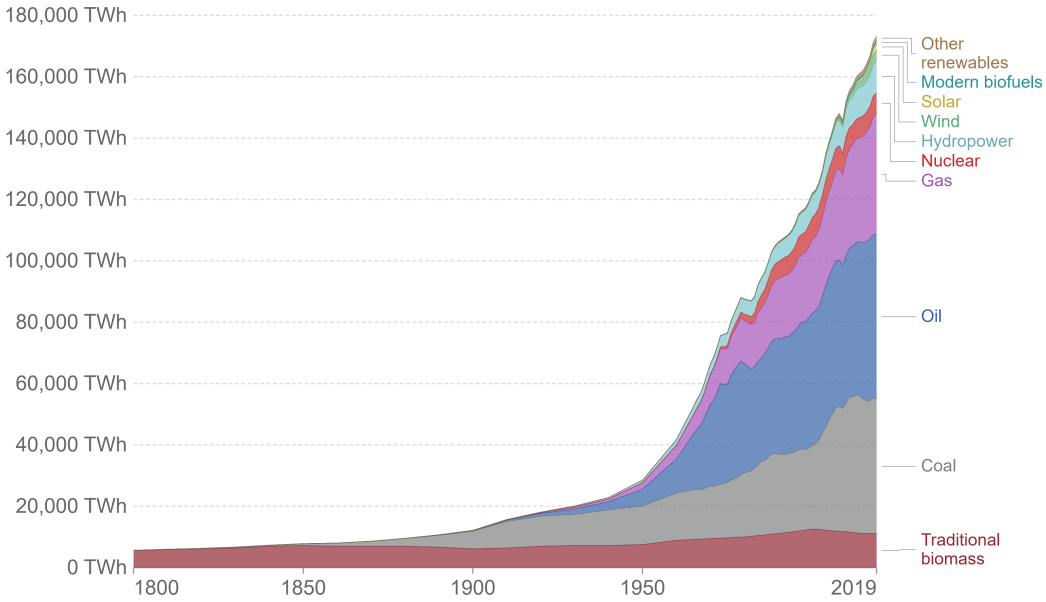

Figure 1.2: Global primary energy consumption (also accounting inefficiencies in fossil fuel production). Source: Vaclav Smil (2017) & BP Statistical Review of World Energy [2].

GHGs", i.e., those GHGs that remain in the atmosphere long enough to have the same concentration all over the world.

1.2 The greenhouse effect

1.2.1 Agents of global warming

There is proof the impact on global warming depends heavily on its drivers, that are both natural and human caused. Some GHGs are released by natural sources: for instance, by oceans and through respiration and decomposition of plants, or they are emitted from forest fires, wetlands and volcanoes [5]. Some of these also occur naturally in the atmosphere, such as carbon dioxide, methane, water vapor and nitrous oxide. Nevertheless, as depicted in Fig. 1.3 by panel (b), the contribution from environmental phenomena like solar and volcanic activities is negligible if compared to human-induced emissions, although the amount of anthropogenic and natural GHGs are of the same order of magnitude [5]. Overall, each contribute adds up to the GHGs in the atmosphere, that mainly includes:

- carbon dioxide (CO_2), with the highest share of around 89% of total emission from fossil-fuel combustion,
- methane (CH_4), caused mainly by fossil-fuel production and ruminant

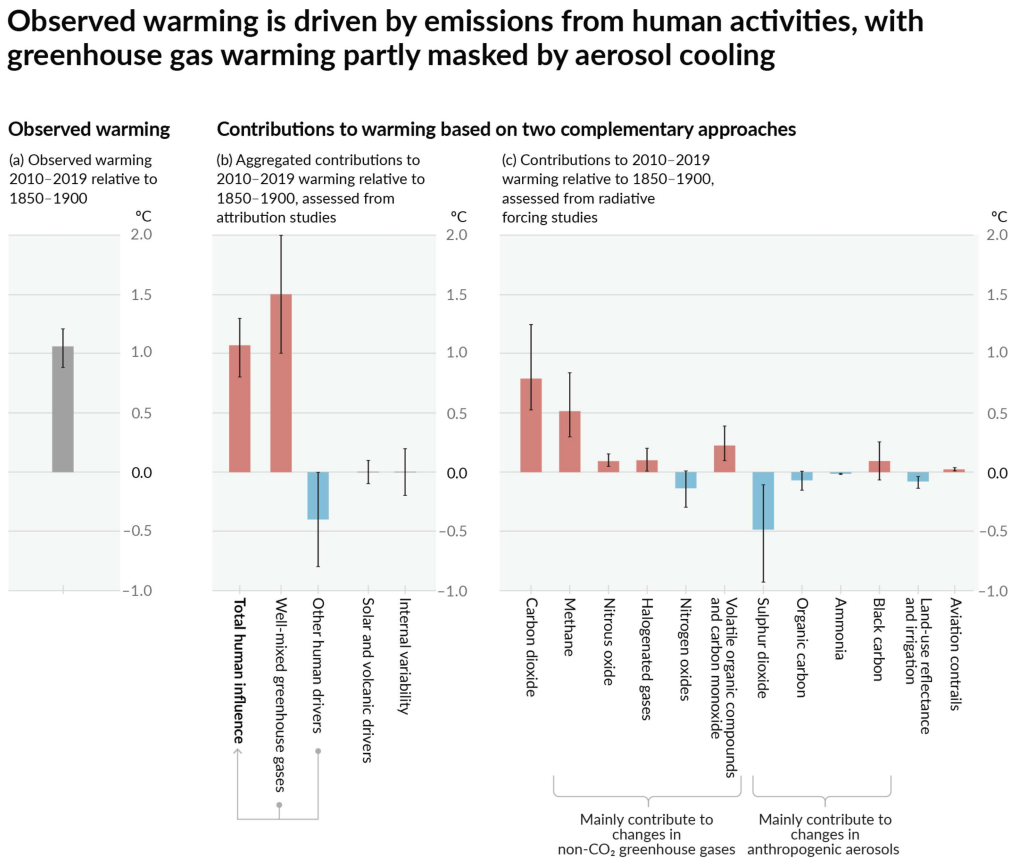

Figure 1.3: Assessed contributions to observed warming in 2010–2019 relative to 1850–1900 [1].

livestock,

- nitrous oxide (N_2O), originated predominantly (about two-thirds) by agricultural activities.

In numbers, in 2019 they were the 73%, 19% and 5% respectively of global total GHG emissions [6]. These values, however, do not consider water vapor, which is actually the most abundant gas in the atmosphere. In fact, scientists believe that its anthropic production does not have a noticeable effect on global warming if compared to the amount that is naturally present (i.e. in clouds), but it is rather an important feedback to the climate: its quantity increases indirectly as a result of global warming, and therefore it is a "mechanism" to evaluate the greenhouse effect. Ozone (O_3) is technically also a GHG, but its impact mainly depends on where it is in the atmosphere: a natural presence at high elevations in the stratosphere is fundamental to block ultraviolet (UV) light, that is harmful for plant and animal

life, from reaching the Earth's surface, and this benefit prevails over its warming effect.

Unlike the previous, halogenated gases are synthetic, human made. They consist of hydrocarbon compounds where at least one atom of hydrogen is replaced by halogens (bromine, chlorine, fluorine and iodine), hence they are also called "halogenated hydrocarbons" or "halocarbons". Essentially, halogenated gases are produced to satisfy a set of properties, (that will be discussed in Chapter 2) and they can be found in a variety of applications, serving as aerosol propellants, foams and insulation blowing agents, and refrigerants. These chemicals contribute with a low share of the total GHG emissions [6], however, as described in Panel (c) of Fig. 1.3, their impact on the climate is not negligible as it reflects effectively on global warming.

In fact, over the last 170 years, human activities have massively increased the amount of both natural and synthetic gases in the atmosphere, causing global warming [1], but the greenhouse effect itself is a natural phenomenon that makes the Earth a livable place: without it, the global surface temperature would be around $-15\,^{\circ}\mathrm{C}$ instead of the current mean, which is around $16\,^{\circ}\mathrm{C}$. Nonetheless, the global scale and the magnitude of phenomena caused by climate change suggest that to measure, compare and control the impact of these drivers is of a major importance. Following Sections 1.2.2 and 1.2.3 will describe two of the most common tools for the purpose: the *radiative forcing* and *global warming potential*.

1.2.2 Radiative forcing

As mentioned previously, the increase in global surface temperature is due to the presence of GHGs in the atmosphere; although having a low share on the total amount if compared to that of oxygen and nitrogen naturally occurring, they absorb an amount of the infrared (IR) thermal radiation emitted by the Earth. The atmosphere itself emits radiation, part of which is directed downward to the Earth and adds to the energy income by the sunlight, yielding to an additional warming [7]. The absorbed radiation causes a net change in the energy balance of the Earth in terms of *radiative forcing* (RF), measured in watts per square metre ($\mathrm{W\,m^{-2}}$), and estimated from the change between 1750 (RF set to zero) and today, i.e., the "Industrial Era". Technically, it is the difference between the incoming and outgoing radiation in the planet.

Different gases in the atmosphere can have either a positive or negative RF resulting in warming or cooling of the climate system, respectively [8]. For instance, the average RF of all the aerosol type, like sulfur compounds and organic carbon (soot), is negative, hence it exerts a decrease in the Earth's surface temperature (described with blue bars in Fig. 1.3). As a result, in 2019 the mean human-caused RF was $2.72\,\mathrm{W\,m^{-2}}$, of which $0.34\,\mathrm{W\,m^{-2}}$ was related to an increase of GHG

concentration since 2011 [1].

Despite its definition and trustworthiness is recognized by the scientific community, radiative forcing is an instantaneous value that depicts the current atmospheric concentration of a gas, which results from its past emissions and life in the atmosphere. Therefore, it does not integrate the total impact over time of current emissions [9].

1.2.3 Global Warming Potential

To better estimate the complex phenomena responsible for the warming effect of a gas, further considerations on atmospheric chemistry should be taken into account. Anthropogenic GHGs exhibit different atmospheric concentrations, measured in part per million (ppm) and lifetimes, lasting up to tens of thousands of years for some halogenated gases. Over time, these substances in the atmosphere are removed (or "sequestrated") by chemical reactions or by emission sinks. In particular, carbon dioxide is subtracted and stored by vegetation through a natural process, therefore a fair management of the land use, land use-change and forestry (LULUCF) is essential to offset its emissions. Because of human activities, however, GHGs in general are being released in the atmosphere more quickly than they are being removed; as a result, quantities keep increasing [3].

With the aim of a more tangible, scientific approach, policymakers and climate organizations have developed several indexes to measure and compare the impact of chemicals, including the aforementioned factors: among all, *Global Warming Potential* (GWP) is widely adopted, and it estimate the amount of energy the emission of 1 ton of a gas will absorb over a given period of time, relative to the emission of 1 ton of CO_2. The reference period is usually of 100 years. Fundamentally, for each GHG the GWP reflects how long it remains in the atmosphere and how intensely it absorbs energy, on average [3], compared to CO_2. Therefore, the higher the GWP, the more climate-damaging the gas. In Table 1.1 the most relevant GHGs and relative warming potentials are listed.

For comparison purposes, CO_2 has a GWP of 1 (by definition) whereas hydrofluorocarbons (HFCs), perfluorocarbons (PFCs), sulfur hexafluoride (SF_6) and nitrogen trifluoride (NF_3) with the highest value are the most potent GHGs. These are the so-called "F-gases", a subgroup of halogenated gases where at least one atom is replaced by fluorine, and whose emissions in the atmosphere have significantly increased in the last decades [11], as shown in Fig. 1.4.

Commonly, the GWP is intended as "direct GWP", as it measures only the warming effect caused by the emissions of the gas itself. To also account for "the direct effects of degradation products or the radiative effects of changes in concentrations of greenhouse gases caused by the presence of the emitted gas or its degradation products," the "indirect GWP" is used [12].

Table 1.1: Global Warming Potential (100-year time horizon) [10].

Gas	**GWP_{100}**
CO_2	1
CH_4	27.9
N_2O	273
HFCs	up to 14,800
PFCs	up to 12,400
SF_6	25,200
NF_3	17,400

The indirect GWPs for most small hydrocarbon alkenes and olefins exceed their direct GWPs [13]. A recent paper [14] published updated values of indirect GWP for some hydrocarbons, but data for some other short-lived substances are still scarce and are currently estimated based on simulations [15]. Additionally, the former index is typically affected by a higher degree of uncertainty by means of the complex chemistry and physics of atmospheric phenomena, that in general are difficult to predict accurately [12].

1.3 Environmental commitments

1.3.1 Climate road map

F-gases have been widely used after the Montreal Protocol was adopted in 1987, aiming to phase-down around a hundred chemical compounds including chlorofluorocarbons (CFCs), hydrochlorofluorocarbons (HCFCs) and halons [11], that were identified as ozone-depleting substances or rather responsible for the reduction of the stratospheric ozone layer. Therefore, a higher, negative impact is associated to a greater *Ozone Depleting Potential* (ODP), which varies largely depending on the substance.

Further international negotiations for the climate have been signed since the early 1990s; nevertheless, only a few have been legally binding. These include the Kyoto Protocol (1997), which required developed countries to limit and cut GHG emissions in accordance with determined individual targets [16].

Successively, in 2015, the Paris Agreement was adopted by most Parties of United Nations (currently 193 out of 197), to set the challenging goal of keeping a maximum global surface temperature rise well below 2 °C above pre-industrial level, and pursuing efforts to limit it to 1.5 °C. According to the international treaty, the scope is also reaching global peaking of GHG emissions as soon as possible, to

become a climate neutral world by mid-century [16].

The very high warming potential of F-gases was internationally recognized as a threat to the climate later in 2016, by the Kigali Amendment of the Montreal Protocol, which established a progressive reduction and production of HFCs, still widely employed in a variety of application, such as: blowing agents for foams, aerosol propellants, solvent, and fire suppressants. Particularly, such substances are deployed as refrigerants in both stationary and mobile refrigeration, air-conditioners, and heat pump systems [11].

The European Union set an important milestone for containing GHG emissions with the F-Gas Regulation and the MAC Directive. The F-Gas was initially adopted in 2006 by Regulation (EC) 842/2006, and successively replaced by current Regulation (EU) 517/2014. It established multiple action pathways, including: preventing accidental emissions of F-Gases, limiting their total amount that can be sold in the EU, and banning their use in appliances where more sustainable options are applicable [17]. As a result, in 2020, EU consumption of HFCs was already 52% below the maximum, set by Kigali Amendment for the same year [18], if compared to the levels in 2014. Additional goals of the Regulation include further emission cut by two-thirds by 2030. The MAC Directive was also introduced in 2006, but addressed specifically the industry of Mobile Air-Conditioning Systems (MACs), with the imposition of a progressive ban in cars and vans for F-gases with GWP higher than 150 [17].

On 5th April 2022, the European Commission has proposed two new Regulations; one addresses ozone depleting substances (ODS), with the scopes of: further enforcing controls over their trade, committing their recycling from old foam construction materials, and including more substances. The other proposal is an update to current Regulation (EU) 517/2014, whose application would, for instance: speed up the phase down of HFCs, strengthen controls against illegal trade of fluorinated gases, and extend restrictions to more chemicals [19]. Overall, both measures would tighten up EU climate actions, with the attended results of saving emissions for around 490 Mt of CO_2 equivalent by 2050 [20], when "net-zero" emission target is expected to be reached.

1.3.2 Actions on HFCs

The latest report from EDGAR (Emissions Database for Global Atmospheric Research) states that, in 2019, F-gases emissions accounted for 3% of the total GHGs in the atmosphere, largest part of which (60%) consisted of HFCs [6], whereas, for the same year, IPCC AR6 claims F-gases had a share of 2% with an associated uncertainty of ±30% [21].

In particular, HFC-134a, HFC-143a and HFC-125 are the three different molecules that make up the most of HFCs (approximately 90%) [6], and they have

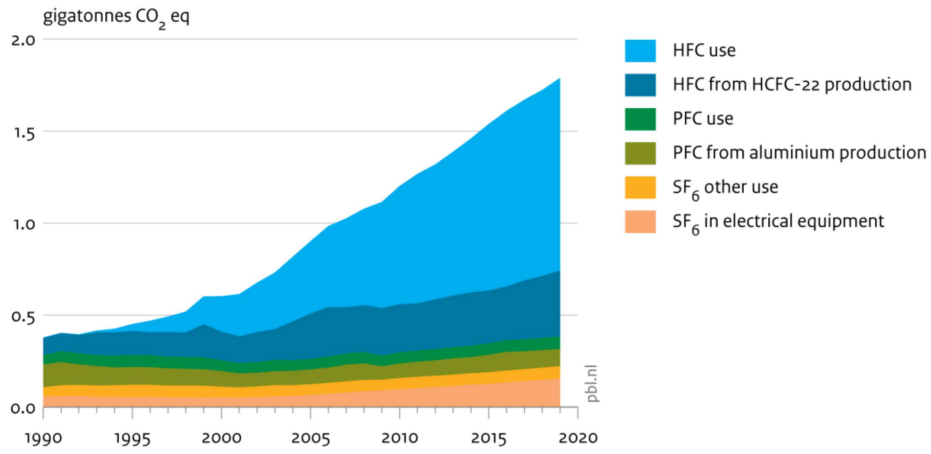

Figure 1.4: Global F-gas emissions, per main source [6].

been extensively produced and used mainly as refrigerants. Since 1990, these compounds underwent a massive production as a response of chemical industries to replace CFCs (see Figure 1.4), the first to be phased out by the Montreal Protocol, which not only has helped in safeguarding the ozone shield, but it also contributed significantly to limit global warming, with a calculated delay of 7–12 years [22]. Future scenarios, however, can be by far more meaningful to assess the impact of refrigerants on the climate, but also to introduce long-term solutions to mitigate the change. Particularly, in light of a warming world, far more air-conditioning and refrigerating equipment are expected to be used in the future, in both developed and developing countries worldwide: according to an estimate [23], up to 14 billion appliances will be necessary by 2050 to ensure the accessibility to cooling services for comfort and productivity in homes and workplaces, and to support the "cold chain", necessary for food safety and for storing and delivering vaccines. The Covid-19 pandemic, in this sense, has boosted the development of refrigerating systems, so that they could be both technically and economically feasible also in countries with low pro-capita incomes, especially for the most temperature-sensitive serums that need to be deployed quickly around the globe [23].

To further highlight the relevance of HFC phase down in mitigating the climate, an up-to-date report [24] estimates that shrinking their emissions, through an effective implementation of the Kigali Amendment, would potentially save from 0.3–0.5 °C in global temperature rise. The maximum 0.5 °C increase was predicted by Velders et al., in a 2009 in-depth paper [25], in which an exponential growth of HFCs was simulated for the forthcoming years.

1.3.3 Mitigating the impact on the environment

What makes reduction of HFCs emissions so crucial for safeguarding the climate is their relevant greenhouse effect, as they exhibit very high GWPs on average (see Table 1.1), but their atmospheric lifetime is considerably short: the weighted average value is around 15 years, whereas for CO_2 it varies from centuries to millennia [26]. However, their relatively low duration in the atmosphere points out an opportunity: if coordinated efforts were adopted in the near term to reduce the emissions, the climate would benefit from decreasing gas concentrations within some decades [27]. Therefore, it is decisive to investigate and prevent emissions from their potential sources.

HFC discharge occurs mainly as leakage — or fugitive emission — from both mobile and stationary cooling systems as a result of several causes, including [24]:

- wear,
- bad design and/or bad manufacturing, causing imperfectly sealed fittings,
- servicing operations and gas filling and/or replacements,
- disposal at end-of-life.

These situations are responsible for the "direct emissions", in contrast with the "indirect emissions" of carbon dioxide and other GHGs, that are poured in the atmosphere because of the energy consumption of the equipment all over its lifetime. Noteworthy, the latter makes up the largest part of GHG emissions in the refrigerant sector, with a share of 63% on the total [9]. Therefore, it is fundamental to consider both the direct and indirect contributes, i.e., accounting for the overall impact of the equipment over its lifetime, an approach that is often referred to as *life cycle assessment* (LCA).

In this regard, one of the most widely accepted indexes, developed in the 1990's, is the Total Equivalent Warming Impact (TEWI) , which can be calculated as [28]:

$$\begin{aligned} \text{TEWI (kg } CO_2) &= \text{(direct effect) + (indirect effect)} \\ &= (\text{GWP}mL + \text{GWP}m(1-\alpha)) + (E\beta n) \end{aligned} \tag{1.1}$$

where GWP is the 100-year GWP, L (kg) is the leakage rate per year, m (kg) is the refrigerant charge, α is the recycling/recovery factor (from 0 to 1), E (kWh/year) is the power consumed by the refrigeration system in a year, β is the indirect emission factor, and n is the system operating lifespan.

From Eq. (1.1) for TEWI, it can be seen that it is calculated for a particular refrigerant, and it depends on estimations of the aforementioned parameters, which are affected by uncertainty and changes, especially for the leakage rate in a year

and the values of GWP. These, in particular, have been updated from AR4 to AR6 of IPCC reports, as a result of advancements in calculation methods [29]. However, TEWI is a tool to effectively compare the environmental impact of similar refrigeration equipment, that can be used by designer, owners and policymakers. Interestingly, because TEWI considers system leakage, TEWI of a system using low-GWP refrigerants can be worse than traditional equipment relying on HFCs if it is not leak tight [28]. Moreover, the influence of a specific refrigerant to the calculation of TEWI is further remarked with the parameter E: as already mentioned, it measures the annual energy consumption of the system where such refrigerant is used, but it is also related to another index, namely the COP [30], which is one of the most relevant parameters to assess the performance of refrigerants, and it will be described in Section 2.3.1.

A more comprehensive approach is given by the Life Cycle Coefficient of Performance (LCCP), that specifically include some contributes not included in TEWI, that is, the direct fugitive emissions during the production of the equipment and of the refrigerants, and the greenhouse emissions related to their embodied energy [31]. LCCP is more complex to determine, but has already had successful applications. In particular, in 2009, LCCP was adopted by SAE International to approve the transition from HFC-134a to HFO-1234yf (a low-GWP fluid) in mobile air conditioning, rather than to other alternatives already available at that time [31, 32].

In addition to widely agreed standards and policies, to effectively prevent the emissions of HFCs in applications that still rely on these high-GWP operating fluids, it is fundamental to make a distinction between direct and indirect emissions, raising awareness on how innovative technical solutions for manufacturing refrigerating and heat pumping systems are able to boost the sustainability transition. Besides, proper recovery, recycling, and end-of-life disposal and destruction are the keystone to contain direct emissions, yet these are part of the weakest "link in the chain" as they are among the most difficult to manage [24]. Near-term solutions, however, need to be provided also to ensure the functioning of both the existing and the new equipment, that, as mentioned in Section 1.3.2, are expected to be produced and sold worldwide in quantities without precedent.

1.4 Refrigerants

1.4.1 Classification

From the first applications of mechanical refrigeration, a high number of different molecules have been developed and used as refrigerants. As a consequence, they have been conveniently named in accordance to a common nomenclature, and the

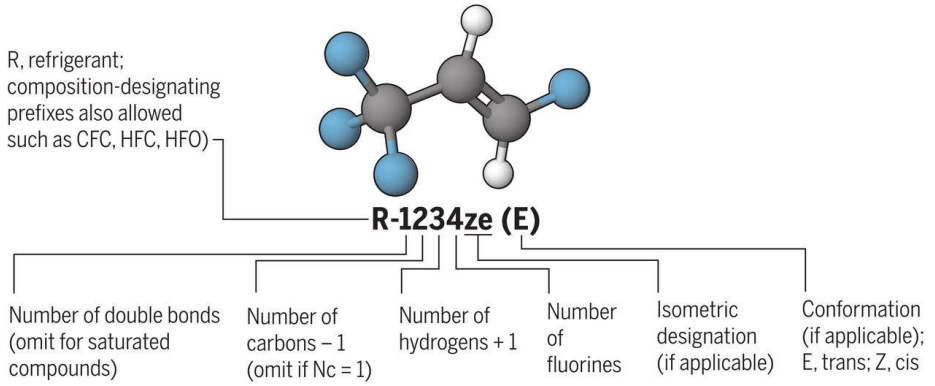

Figure 1.5: Refrigerant nomenclature based on ANSI/ASHRAE Standard 34 and ISO 817. From [33]. Reprinted with permission from AAAS.

most widely adopted is the one aligned with ANSI/ASHRAE Standard 34-2019 and ISO 817-2021, by which each commercial, pure substance or blend is identified with an alphanumeric code (see Fig. 1.5), that also provides additional chemical information.

Nearly all the refrigeration systems made use of a single chemical compound, that is, a pure refrigerant. In response to climate actions, chemical industries strove to come up with single-equivalent substances in place of CFCs and HCFCs, that have been progressively phased out, but it proved impossible to find substitutes that could match, for instance, the requirements and attributes of the widely used R-12 (CFC) and R-22 (HCFC) [34, 35]. Replacements have been mostly blends, i.e. a mixture of two or more compounds, whose components have been chosen based on the final desired properties [35], a part of which is regulated by law. In fact, refrigerants and the appliances they rely on are set out by international and local organizations, like the International Electrotechnical Commission (IEC) and the Underwriters' Laboratories (UL) which provide standards, i.e., definitions, guidelines and procedures broadly shared within the field of HVAC&R (standing for "Heating, Ventilation, Air Conditioning and Refrigeration"), or more commonly HVAC. Table 1.2 represents the most relevant ones in western countries. Usually, each nation adopts these standards as a basis for different, enforced local model codes (namely, laws) [34, 36].

1.4.2 Safety codes

The environmental footprint of refrigerants is indeed only one of the major issues that has been evaluated and regulated in relatively recent times. Other requirements, however, became relevant as new working fluids were progressively developed,

Table 1.2: Links between international, EU and US Standards [36, 37].

Standard type		**Global**	**EU**	**USA**
Refrigerant classification		ISO 817	Follows ISO 817	ASHRAE 34
Safety	**General**	ISO 5149	EN 378	ASHRAE 15
	Equipment specific	IEC 60335-2-24	EN 60335-2-24	UL 60335-2-24
		IEC 60335-2-40	EN 60335-2-40	UL 60335-2-40
		IEC 60335-2-89	EN 60335-2-89	UL 60335-2-89

commercialized, and as the equipment was consequently adapted.

During the operation of a typical refrigeration cycle, in fact, refrigerants are subjected to multiple interaction with different materials (elastomers, metals) and compressor lubricant, and must "resist" to intense frictional pressure drop, as well as temperature gradients, that alter the chemical stability of the molecule. Stability is typically considered the most important requirement for a refrigerant [34], because other attributes would be rather worthless if the fluid decomposed or reacted with system materials. These situations could potentially induce the malfunctioning of the equipment, but it is also likely to generate hazards for people, properties, and the environment.

Due to the considerable number of dangers, safety regulations have had an essential role in securing appropriate refrigerant handling, and in determining room conditions where the refrigerant is stored in case of accidental releases. Such circumstances determine risks that are mainly associated to chemical and physical properties of refrigerants, as well as to the temperature and system pressures involved in the refrigeration cycles [38]. For these reasons, standards including ISO 5149-2021 (equivalent to ASHRAE 15-2019) specify, as an example, the amount of refrigerant charge in relation to room dimensions and building occupancy (i.e. based on the different environments where the fluid operates), that could potentially create flammable mixtures with air and determine toxic hazard if at sufficient concentration. As an example, in a installed system, the total charge of R-32 divided by the room volume determines its concentration in case of a full discharge, and for occupied spaces this value should not exceed the "quantity limit with minimum ventilation" of $0.063\,\mathrm{kg\,m^{-3}}$, unless appropriate measures are taken [37]. ASHRAE Standard 34-2019 provides a similar parameter, the "refrigerant concentration limit" (RCL) which should not be greater than 25% of the "lower flammability level" (LFL), to be determined experimentally in accordance with ASTM E681 [34, 39]. Proper measures, otherwise, are to be taken, and these are primarily: ventilation (natural or mechanical), safety shut-off valves, alarms, and gas detection devices [38].

Toxicity and flammability are addressed specifically by ISO 817-2021 and equivalent ASHRAE Standard 34-2019, which classify refrigerants into eight "groups", as described in Table 1.3. Letters A and B refer to toxicity: respectively, they identify refrigerants with a lower chronic toxicity or with an occupational exposure limit (OEL) of 400 ppm or greater, and with an OEL lower than 400 ppm. The OEL can be estimated by different approaches [40].

Flammability is assessed through a series of different measurements, that overall place refrigerants into four classes. In particular, Class 2 identifies "lower flammability" refrigerants and refrigerant blends with the following criteria:

- exhibit flame propagation when tested at 60 °C and 101.3 kPa,
- have a LFL > 3.5% by volume,
- have a heat of combustion < 19 000 kJ/kg.

Class 2L was first introduced in 2010 by ASHRAE Standard 34, and it gathers fluids that, in addition to the aforementioned conditions, exhibit low burning velocity (thus the L) or less than 10 cm/s, when tested at 23 °C and 101.3 kPa [41, 42]. The aim was to allow the trade and usage of such pure and blend 2L substances, like R-32 (in class A2L) and R-717 or ammonia (which is B2L, due to its higher toxicity) as substitutes of the most intense, A1 greenhouse gases [41]. In fact, Class A1 (with "no flame propagation") includes widely used refrigerants such as R-22 and R-134a, whose fire-suppressant properties were specifically obtained by halogen atoms (in the example Chlorine and Fluorine, respectively). As a side effect, such chemical compositions involve an increased molecular stability, due to the strong carbon-halogen chemical bond, that translates to longer atmospheric lifetimes, therefore to higher GWPs. Thus, for most refrigerants there is a substantial trade-off between flammability and the warming impact [43]; actually, many low-GWP fluids are classified as highly flammable (A3/B3), flammable (A2/B2) or mildly flammable (A2L/B2L). A2Ls and B2Ls, however, prove much harder to ignite than A3s, that is, they exhibit a much higher "minimum ignition energy" and are rather less flammable than A3 substances [42].

To promote and accomplish a safe transition towards these substitutes, ASHRAE 15-2019 and the third edition of UL 60335-2-40 were updated with additional system requirements, including: the use of circulation and ventilation devices, leak detectors, ignition source protection, evaluation of the refrigerant charge, and training procedures for technicians [42].

Historically, the process of replacing CFCs and HCFCs required the introduction of refrigerant blends. In fact, finding pure fluids such as R-22 that could match its performance seemed to be a challenge. Additionally, blending has been considered strategic for other issues: in particular, it applies as a viable method to lower

Table 1.3: Safety group classification under ASHRAE Standard 15-2019 and ISO 817:2014 [34, 40].

	Safety group	
Higher flammability	A3	B3
Lower flammability	A2 A2L	B2 B2L
No flame propagation	A1	B1
	Lower toxicity	**Higher toxicity**

flammability for pure fluids, from Class 2L to Class 1. Mostly, R-134a and R-125 were added at substantial concentrations; however, by means of halogens, candidates resulted with GWP_{100} higher than 1000 in general [34, 38].

According to ISO 817-2021, blends should be assigned to a dual safety classification, as an expression of the different flammability that might occur as a result of a leakage. For instance, R-410A (consisting of R-32 and R-125 with 50/50 % composition in mass) is rated A1/A1. The two classes represent flammability and toxicity indexes for the "worst-case formulation" and the "worst-case fractionated formulation" of the refrigerant, where term "fractionation" refers to the change in composition of the components that is due to a preferential evaporation or condensation of the more volatile and the less volatile substance, respectively [40]. So, in the example of R-410A, flammability is assessed as even in both scenarios.

Safety is therefore fundamental to ensure a large-scale access to more sustainable refrigeration, air-conditioning and heat pumping (RACHP) equipment. To support a timely transition, other barriers have to be solved: primarily, weak points are in the funding, standards and regulations, and adequate training for technicians [17]. Despite the number of open issues, the volume of appliances that already rely on 2L fluids counts over 160 million units, manufactured by more than 40 companies worldwide [44].

1.4.3 Timeline of major changes

The search for the "ideal" refrigerants has occurred systematically multiple times from their very first use in the mechanical refrigeration, whose first applications were for the production of ice, after pioneer vapor-compression machines became commercially available, between 1850 and 1880 [45]. Nevertheless, the most significant advancements were achieved as a result of three major studies in the

1920s, 1980s, and 2010s, driven by [34]:

- new constraints and regulations (as discussed in Sections 1.3.1, 1.3.2 and 1.4.2),
- advancements in the tools and property models to identify new molecules,
- evolving equipment design.

Particularly, the introduction of CFCs was considered revolutionary if compared to natural refrigerants, widely used at that time, as they involved higher refrigeration cycle performances, and as they were thought (erroneously) to be completely safe and harmlessness to the environment [45].

Most of the "new" refrigerants, however, were included in the literature decades before they were deployed also as working fluids. A prime example is the synthesis of dichlorodifluoromethane, namely R-12, in 1931 by Thomas Midgley: the molecule was already listed in the chemical literature in 1907, but presumably Midgley was unaware of this, and no other citations of such chemical were found before in the SciFinder database [34].

Overall, the studies related to properties of refrigerants prompted their evolution through four "generations", ranging from "whatever worked" to the present zero or near-zero ODP, low-GWP alternatives. As represented in Figure 1.6, current requirements for RACHP are met with a limited set of pure refrigerants, especially by HFCs, hydrofluoroolefins (HFOs) and their mixtures (blend) and some natural compounds [34]. At present, however, the majority of global vapor compression RACHP systems relies predominantly on fluorocarbons (83%), whereas inorganic fluids (such as ammonia and carbon dioxide) and hydrocarbons have a low share, of 11% and 6%, respectively [46].

1.4.4 Natural refrigerants

Since the early applications of mechanical refrigeration, at the end of the 19th century, some fluids have been employed as "natural" refrigerants, so called because occurring also naturally in the environment (as mentioned in Section 1.2.1). These include:

- carbon dioxide (CO_2),
- ammonia (NH_3),
- hydrocarbons, especially propane (C_3H_8),
- water,

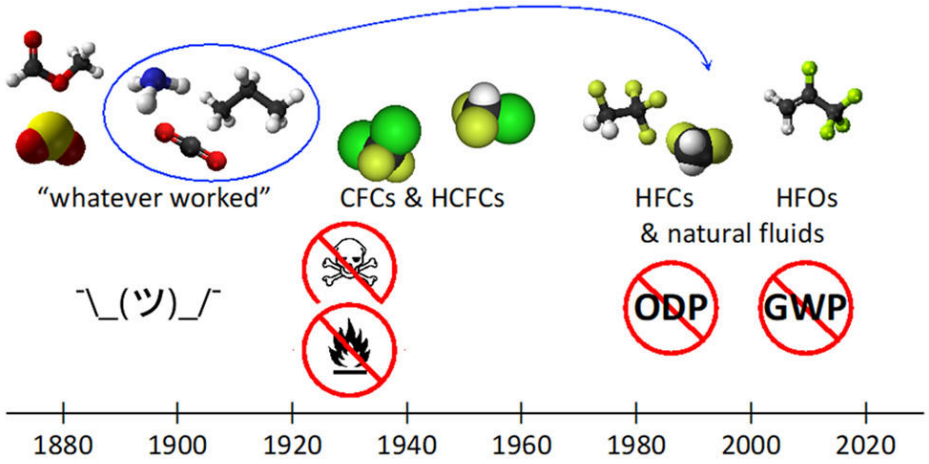

Figure 1.6: Evolution of refrigerants [34].

- air.

Although their anthropocentric emissions could cause lower, negative impact on the climate, in general such alternatives are not free of concern (see Table 1.4).

Ammonia has been one of the most longstanding, widespread refrigerants for food and beverage preservation and treatment. It exhibits excellent thermodynamic properties, high heat transfer coefficient and remarkable energy performances of the refrigeration cycle. Despite being highly available, its low cost is compensated by the need to use expensive, corrosion-proof, welded steel piping, as ammonia lacks material compatibility with copper and its alloys [17].

Particularly, due to its high toxicity at relatively high concentrations, ammonia refrigerating systems are in some countries subjected to regulations and standards that might discourage plant implementation in public buildings. For this reason, it is used mainly as a primary refrigerant in indirect refrigeration systems, where ammonia is kept isolated into designed machine rooms, while secondary coolants (such as glycols and salt brines) circulate inside public spaces [17]. Nevertheless, if compared to other refrigerants, ammonia can be detected by its characteristic smell at very low concentrations, allowing an early warning signal of its accidental release. Recently, ammonia has gained adoption also in chillers for air conditioning equipment in commercial and public buildings [48].

Another relevant refrigerant is carbon dioxide, that initially has been broadly employed in ice manufacturing and refrigerating systems, from the late 19th century to the 1930s. When synthetic working fluids were introduced, however, carbon dioxide was rapidly abandoned, since with standard technologies available at that time it provided mostly low efficiencies, but also because its cooling capacity proved to be highly penalized by an increase of the ambient temperature [49]. However, in

Table 1.4: Key characteristics for common natural refrigerants [17, 47]. The COP (coefficient of performance) and the Q_{vol} (volumetric heat capacity) are two key parameters discussed in Chapter 2.

Refrigerant	Safety class	Advantages	Issues
R-717 (ammonia)	B2L	Excellent efficiency (COP) for low temperature applications (well below 0°C)	Toxic
		Easy to operate and maintain Low operating pressures	High discharge temperatures
		Low operating pressure	
R-744 (carbon dioxide)	A1	High temperature fluid for heat recovery	High discharge pressures
		Compact system design due to high Q_{vol}	Very low critical temp. (31 °C)
		Non-toxic and non-corrosive Low maintenance systems	More complex systems
R-290, R-1270, R-600a (hydrocarbons)	A3	High efficiency (COP)	Highly flammable
		Availability	Restricted application areas due to low charge limits
		High Q_{vol}	

the last decades, there has been a renovated interest for research on carbon dioxide, in light of the low toxicity, non-flammability zero ODP and negligible GWP [48], that would inherently outreach other candidates. Besides, there have already been successful commercial applications in the full range of compression systems, from high temperature heat pumps [49] to low temperature freezers [48].

Hydrocarbons like propane (R-290), isobutane (R-600a) and propylene (R-1270) are widely used in all commercial and industrial RACHP systems as both pure refrigerants and blends thereof, to take advantage of their excellent environmental properties and performances [48]. They also benefit from similar operating pressure to systems using HFCs, and the compatibility with most equipment materials and compressor lubricants. The major issue is related to their high flammability, that requires specific system adjustments, and that mostly involve charge limits in compliance with safety codes.

Evolving standards and constraints are therefore essential in order to leapfrog these barriers, and smooth the path to such potential refrigerants [17]. There is an expectation that the approval of the new edition of IEC 60335-2-40, on 29th April 2022, "will enable R-290 to be used in many A/C and heat pump systems which were previously blocked from using this refrigerant by the outdated version." According to the new standard, up to 988 g of propane will be allowed in new typical split air-conditioning systems, provided the equipment satisfies additional safety requirements [50].

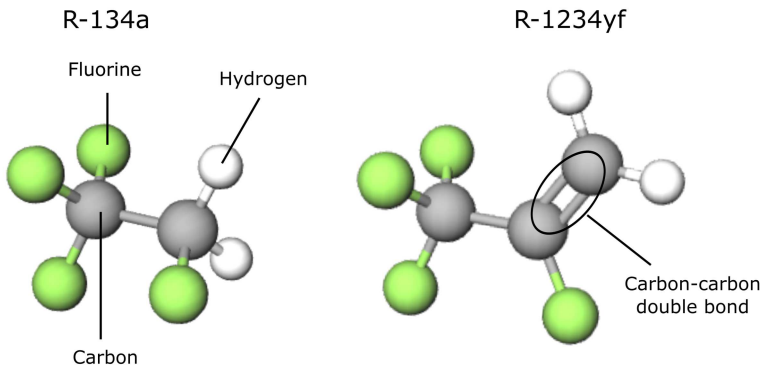

Figure 1.7: A comparison between the molecular structure of HFCs and HFOs. 3D models from Molview [52].

1.4.5 Synthetic, low-GWP alternatives

Since 2012, suitable potential substitute to HFCs have been extensively investigated by McLinden, Domanski, Kazakov, and coworkers at NIST. They extended previous searches to a database of around 60 million compounds in the PubChem database, which provided a final list of 29 pure fluids, including both natural and synthetic molecules [34]. Nevertheless, as international treats for the climate apply restrictions to HFC deployment and usage, the number of compliant replacements is progressively reducing to a few groups of "low-GWP" substances. Currently, in reference to the medium-long term goals of F-Gas (GWP < 150), potential synthetic substitutes include: hydrofluoroolefins (HFOs), hydrochloroolefins (HCOs), hydrochlorofluoroolefins (HCFOs), hydrofluoroethers (HFEs) and blends thereof [31, 51]. These sets of candidates have had an increased interest in all application sectors, since not only do they exhibit a substantially reduced direct effect on global warming, but their use can also further improve the performance of refrigeration and heat pump systems.

Most widespread, low-GWP refrigerants are HFOs, which derive from alkenes (also called olefins) or unsaturated hydrocarbons with a carbon-carbon double bond, where one or more hydrogen atoms are replaced with halogens. The double bond between carbon atoms is responsible for a high reactivity of the molecule with OH radical in the troposphere, that translates into shorter atmospheric lifetimes and into lower GWP than that of HFCs, for instance, which instead have a single carbon-carbon bond (see Fig. 1.7) [53]. Another key characteristic of halogenated olefins is the presence of residual hydrogen atoms in the molecule, that also increase its reactivity with radical species; again, the effect is a shorter molecular lifespan, once the gas is emitted in the atmosphere. A higher number of hydrogens, however, causes greater interaction with oxygen so that the molecule exhibits higher

flammability, which is one of the major hurdles to the widespread adoption of these novel fluids, even though other relevant issues have arisen so far.

Recently, some low-GWP refrigerants containing a functional group -CF_3 such as R-1234yf, have been addressed as a source of acid trifluoroacetic (TFA), a breakdown substance that is argued as harmful to the environment and for organisms in aquatic ecosystems [31, 54]. It is noteworthy, however, that TFA is commonly used in research laboratories and in industry. Additionally, it is a degradation product of other fluorinated and perfluorinated compounds, plus it occurs naturally from geochemical sources [54]. Although there is conflicting evidence as to whether TFA is primarily from either anthropogenic or natural causes [54], concentrations of this substance are regarded as too low to harm humans and the biosphere [55]. Furthermore, some EU countries are requesting to broaden the European REACH restriction proposal to prohibit PFAS substances, which are chemicals "that contain at least one fully fluorinated methyl (CF_3) or methylene (CF_2) group not directly attached to any hydrogen, chlorine, bromine or iodine atom." [56] This definition addresses also refrigerants such as high-GWP R-134a, as well as low-GWP R-1234yf and R1234ze(E). The ban of some of most promising novel refrigerants, however, is supposed to have a heavy impact on the HVAC&R sector that, besides, has to be aligned also to other challenging, forthcoming goals by international regulations, such as the F-Gas and the MAC Directive, as discussed in Section 1.3.1.

Apart from safety and environmental issues, most halogenated olefins has already proved technically suitable for many refrigeration and heat pump applications, both as pure refrigerants and as blends. Blends among different halogenated olefins, as well as with other classes of fluids (e.g. hydrocarbons and HFCs) are of a major interest, for instance, to reduce flammability or to match the properties of the fluids they will likely replace. To assess the qualities of a refrigerant as an alternative fluid, one of the most crucial steps is to estimate and measure its performance in a specific equipment and under a variety of operating condition, as that contributes to the determination of the overall power consumption. However, although some low-GWP refrigerants have been thoroughly investigated, there are still scarce data for other pure substances and blends, in particular, for the intrinsic properties of the fluids [30, 54]. Properties of refrigerants are essential for building reliable models for engineering design of HVAC&R systems, and for boosting the transition to new generations of more sustainable refrigerants. In this regard, the following chapter focuses on the role of refrigerants, and on the influence of their properties for the key elements of a refrigeration cycle.

Chapter 2

The importance of refrigerants

2.1 The vapor-compression cycle

Modern refrigeration and heat pump technologies have come a long way since the very first attempts to build a machine that, according to the second law of thermodynamics, could reverse the natural direction of heat flow from a hot medium source to a cold one [57]. Through the years, due to a wider scientific understanding and fast technological changes, equipment performances and reliability have had significant improvements, but at the core of their functioning there are the same principles that date back to the onset of mechanical refrigeration, when in 1834 Jacob Perkins filed the patent of the first vapor-compression system, which is regarded as one of the world's most revolutionary engineering innovations [57]. In fact, if compared to other compressor-free refrigerating technologies such as the thermoelectrics, thermoionics and thermoacustics, vapor-compression systems have seen a widespread due to their mature technology, but also for their relatively ease of manufacturing and scalability, from small consumer appliances to large-scale industrial systems [31, 33].

Nearly all modern air-conditioners, refrigerators as well as most heat-pumping systems, base their functioning on the vapor-compression cycle [58], where a refrigerant is used to absorb heat from a low temperature heat source and to release it to a higher temperature heat sink, as represented by the thermodynamic system in Fig. 2.1a. Practically, a basic, single-stage vapor-compression system consists of four major components: a compressor, an expansion device (typically a valve) and two heat exchangers, working as a condenser and as an evaporator, as described in Fig. 2.1b. Pipelines connects the components together in order to create a closed circuit, within which the refrigerant is cycled indefinitely. Such components compose the ideal vapor-compression cycle, which is based on the Carnot refrigeration cycle (or "reverse Carnot cycle") [59] and it consists of four

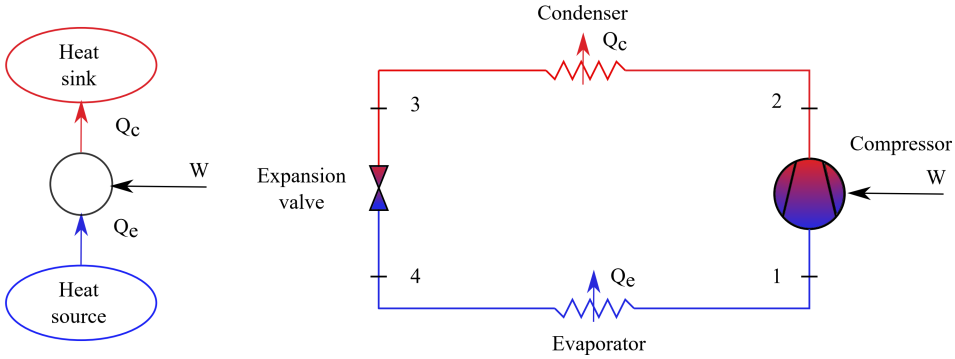

Figure 2.1: Thermodynamic system for a basic vapor-compression cycle (a) and its schematic representation (b).

major thermodynamic processes, as follows [58]:

- reversible adiabatic (i.e. isentropic) compression (1–2), where the refrigerant at the suction line (1) as dry saturated vapor is compressed from pressure P_e to P_c in the discharge line (2); as a result of the compression, the gas temperature is also raised. The process requires the mechanical work W.

- reversible condensation at constant pressure P_c (2–3), because of a heat rejection (Q_c) from the high-pressure, high-temperature fluid to the heat sink. Through phase changes, the super-heated vapor returns to the liquid form (3).

- irreversible isenthalpic expansion (3–4), through which the fluid pressure and temperature are reduced to P_e and T_e, respectively. Some of the liquid is flashed during the expansion, so that not all the refrigerant is available to vaporize in the evaporator. Therefore, at the end of the expansion (4), the fluid is in the two-phase state.

- reversible evaporation at constant pressure (4–1), during which the refrigerant evaporates by means of a heat absorption from the heat source, thus providing the intended refrigeration effect.

Additionally, the ideal cycle is characterized by other assumptions: the cycle has zero approach temperatures between evaporating line and the heat source, as well as between the condensing line and the heat sink; there is minimum or no pressure drop in the same heat exchangers; there is neither a subcooling nor a

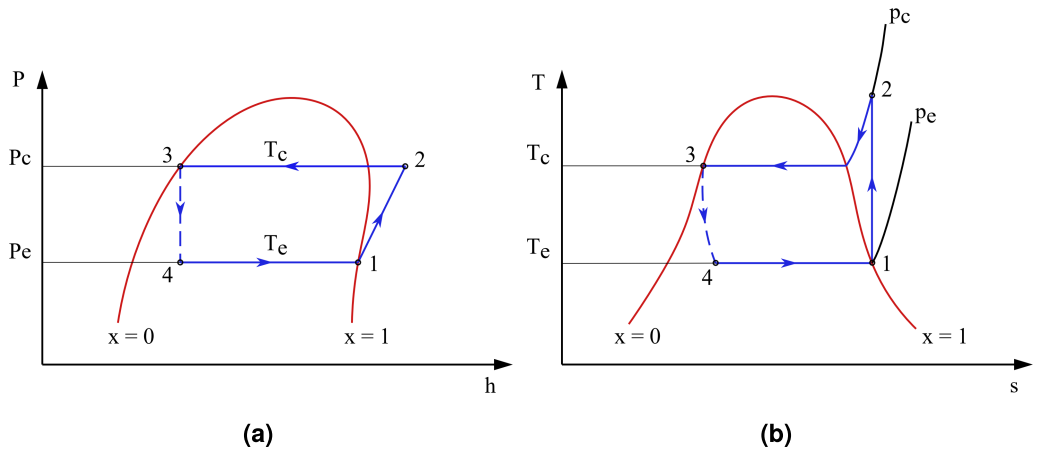

Figure 2.2: *P-h* (a) and *T-s* (b) diagrams for a basic, (single stage) ideal vapor-compression refrigeration cycle.

suction superheating [60]. In this regard, it is important to notice that for an actual refrigerating cycle a slightly superheated gas may be preferred, in order to avoid a wet compression that would endanger the system reliability. Particularly, if a wet compression occurred unintentionally, liquid droplets remaining by means of an incomplete evaporation might damage the compressor head and cylinders and its valves.

The refrigeration cycle is typically represented by the pressure-enthalpy (*p-h*) and temperature-entropy (*T-s*) diagrams (see Figs. 2.2a and 2.2b), which depict the evolution of the aggregate states of the fluid by means of thermodynamic state variables pressure and enthalpy, and temperature and entropy, respectively. These properties are used for calculations and analyses of heat and work transfers and to evaluate the performance of a refrigeration cycle for a specific refrigerant. Each working fluid exhibits different *P-h* and *T-s* curves, although these have a similar dome-like shape, as shown for a comparison in Figs. 2.3a and 2.3b.

As to blends, they can be zeotropes (in the 400 series by ASHRAE classification), azeotropes and near-azeotropes (in the 500 series). Zeotropes exhibit temperature glides (variations) during the phase change at constant pressure, between the inlet and the outlet of the heat exchangers. This effect is due a to change in composition of the vapor phase and liquid phase that happens while both exist. In this sense, zeotropes differ from the behaviour of a single-compound refrigerant. Zeotropic refrigerants have an impact on the cycle efficiency as well as on the system design, typically by introducing additional challenges in the optimization of heat exchangers, especially when glides are relatively high [62, 63], that is, more than 4–7 K [31]. The temperature glide, however, is low or negligible in the case

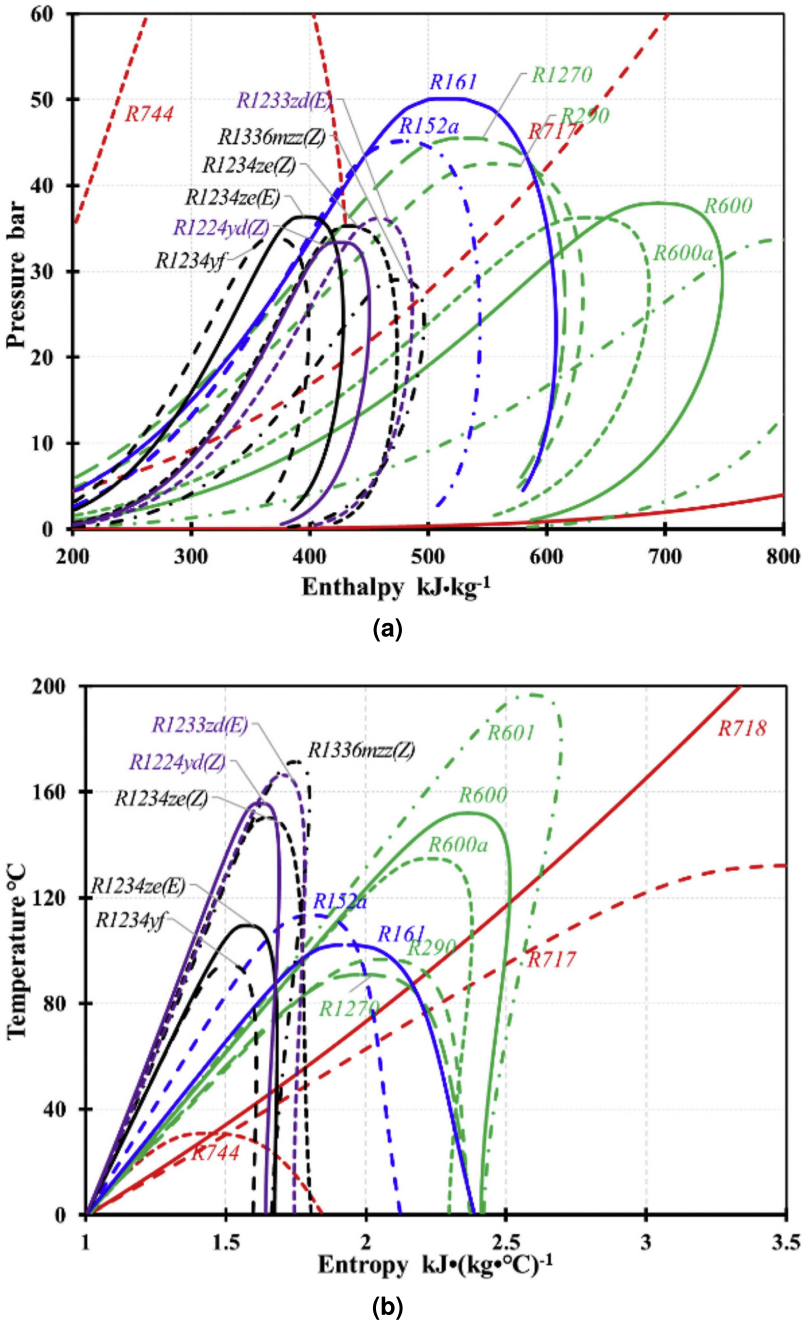

Figure 2.3: *P-h* (a) and *T-s* diagrams for some pure low-GWP refrigerants. Reprinted with permission from [61].

Table 2.1: Main desirable properties and parameters of refrigerants [34, 64].

Category	Characteristics
Environmental, health and safety	Low ODP, low GWP and short atmospheric lifetime
	Non-toxic, non-flammable
Chemical	Chemically stable
	Non-corrosive
Thermophysical	Critical temperature suitable for the application
	Boiling point suitable for the application
	High thermal conductivity
	Low viscosity
	Positive but not excessive pressures at evaporating and condensing conditions
	High vapor density at suction line
	High enthalpy of vaporization
	Low specific heat of the vapor
Miscellaneous	Compatibility with equipment materials
	Miscible with compressor lubricants
	High dielectric strength of the vapor
	Ease of leakage detection
	Low freezing point
	High efficiency (COP) and capacity (Q_{vol})
	Availability
	Low costs of the refrigerant, equipment operating and maintenance

of near-azeotropes and azeotropes, respectively. In general, azeotropic mixtures are of a greater interest, as at certain pressure and temperature they behave like a pure substance [58].

2.2 Properties of refrigerants

As mentioned in Chapter 1, there is no single ideal refrigerant that can stand out from others in any of its characteristics, and that can suit equally regardless the applications. In fact, when selecting a working fluid, multiple considerations are to be made: the choice typically responds to an acceptable compromise in terms of, mostly, economical, environmental, technical and safety criteria. Overall, for conventional refrigeration and air-conditioning applications the most relevant requirements for a refrigerant are listed in Table 2.1, from which it is possible to conclude that is rather difficult to satisfy all of them, and thus a trade-off

must somehow be accepted. Refrigeration cycles, however, rely essentially on thermodynamics and on properties of the working fluids [33]. Among others, *thermophysical properties* of refrigerants are fundamental for developing reliable equations of state (EoS), but also for estimating the performance of refrigerants in RACHP systems in terms of energy efficiency and capacity [65], as well as for the design and manufacturing process of refrigeration equipment.

The most common thermophysical properties relate to the changes between to two states of thermodynamic equilibrium, that occur, for instance, when a mass of fluid changes its temperature by means of a heat exchange; in this case, these are known as *thermodynamic properties*. Differently, the properties that address the rate at which a fluid in a non-equilibrium state changes its state because of evolving external conditions, or by means of the transport of mass, momentum or energy among different portions of the fluid, are known as *transport properties* [66].

For the refrigeration cycle, the most relevant properties of the working fluids are [65]:

- the thermodynamic properties at the boundaries of the thermodynamic space (critical pressure and temperature, vapor pressure, saturation densities), the speed of sound, the specific heat capacity and the PvT properties in the single-phase regions. Other essential properties such as enthalpy, entropy as well as the Helmholtz and Gibbs energies, may be derived from the PvT correlations through appropriate EoS.

- the transport properties thermal conductivity, viscosity and surface tension.

Most common HVAC systems typically requires a critical temperature falling in the range from 300–400 K; different critical temperatures would otherwise require major modification to the design of the equipment. Primarily, the reason is because the critical temperature of the refrigerant was confirmed as the most dominant parameter in influencing the trade-off that occurs between the COP and the Q_{vol} for an ideal refrigerating cycle [67]: refrigerant with a high critical temperature exhibits high efficiency (COP), but low capacity (Q_{vol}), and vice versa. In particular, a low-critical-temperature fluid (such as CO_2) often determines a transcritical cycle and higher expansion losses [43]. For the most common air-conditioning and refrigeration equipment, suitable critical temperatures are in the range between 300 K and 400 K [43]. The benefit of a high critical point (CP) , however, is reduced by means of a consequent lower density at state 1 (see Figs. 2.2a and 2.2b). In fact, assuming that the compressor runs at constant speed, or rather that the rate at which the refrigerant volume is being compressed is constant, a lower density at the suction line translates to a lower mass flow rate, and thus a decreased volumetric heat capacity. Consequently, for a new equipment design, in order to obtain the

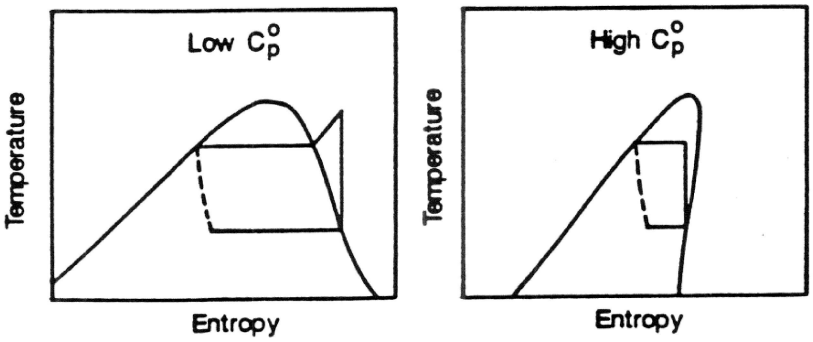

Figure 2.4: The effect of the vapor heat capacity (in the limit of zero pressure) on the shape of the vapor dome in the *T*-*s* diagram [58].

same capacity, a refrigerant with a higher CP will require an increase compressor pumping displacement [58].

The molar heat capacity of an ideal gas (i.e., of the vapor phase of the refrigerant in the limit of zero pressure), often referred to as "ideal-gas specific heat capacity", has a lower influence on performance than that of the critical temperature for an ideal cycle, but it is still relevant: it modifies the shape of the *T*-*s* curve, so that a relatively low specific heat allows the compression process to end in the superheated region, thus avoiding the problems related to wet compression [68]. New synthetic refrigerants exhibit in general more complex molecular structure than that of traditional working fluids, and for the former this translates into higher values of molar heat capacity at constant pressure of the vapor phase. In turn, a greater molar heat capacity is linked to a bending of the vapor saturation line, so that its slope is negative at low pressures and positive at the higher pressures (for reference, see Figs. 2.3b and 2.4). The saturated liquid line is also influenced; regardless, its slope always remains positive [58]. Despite the impact of properties on thermodynamic diagrams, in actual compressors for refrigeration units wet compression is typically avoided, since the refrigerant at the compressor inlet is already slightly superheated, and the compression is non-isentropic [69]. Moreover, according to a study by McLinden et al [43], the optimal value for the ideal-gas specific heat capacity depends on the cycle: low values are preferable with a simple cycle, whereas configurations with a liquid-line/suction line heat exchanger perform better with higher values of specific heat. Low values of specific heat are preferred, in any case, to minimize the entropy change that occurs by means of the expansion process [68]. The normal boiling point (NBP) of the refrigerant (or bubble point, for blends [63]), i.e., the temperature at which the vapor pressure equals the atmospheric pressure so that the liquid refrigerant starts to boil [68], must be appropriate for a given application, so that the refrigerant is volatile enough to provide the cooling effect. This requisite is typically met by small molecules

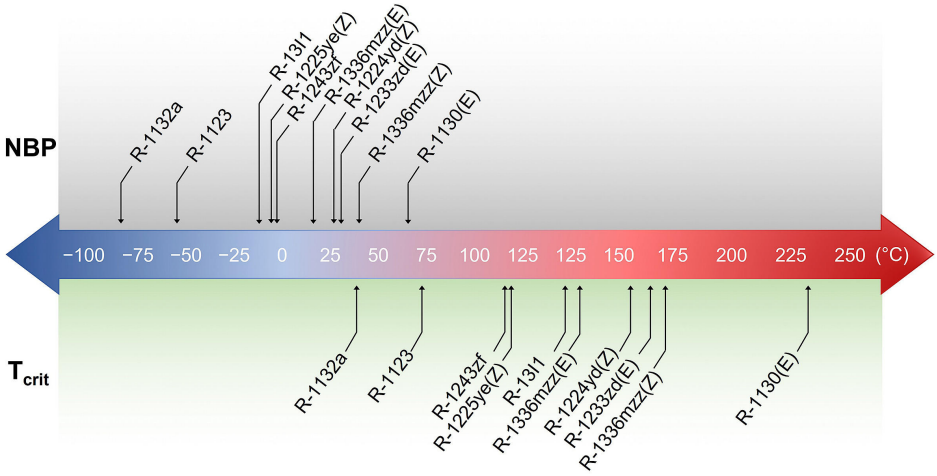

Figure 2.5: Normal boiling point and critical temperature for the main low-GWP refrigerants [70].

(based on one to four carbons), with NBP generally between −50 °C and 30 °C [33]. NBP is useful also when looking for a substitute fluid in place of a previous one with similar thermodynamic properties, as it is a first-order estimate of suitability. In fact, the industry preference is to find a single-component replacement with a comparable value of NBP, since such a refrigerant change would require fewer product redesign and retooling of the manufacturing plant [63]. Figure x depicts the normal boiling point and the critical temperature for some

Viscosity is another important parameter that ultimately affects the performance of the systems: in general, low dynamic viscosity is desirable in order to minimize the frictional pressure drops, but also to attain a higher coefficient of convective heat transfer, both in the evaporator and the condenser [71].

The pressure in the system should be neither too high or too low: values below atmospheric are undesirable, especially at the evaporator where the lowest pressure occurs, to prevent any air from entering into the refrigeration system [72, 73]. The co-presence of non-condensable gas negatively affects the performance of the system, as even in low quantities it increases the thermal resistance at the condenser, causing the heat transfer coefficient to diminish [74].

One of the most important properties for refrigerants and its performance is the thermal conductivity: high values are required in order to improve the fluid heat transfer coefficient, thus, to maximise the heat exchange in the evaporator and the condenser. Especially in a two-phase flow, the liquid conductivity is the most influential parameter for the heat transfer coefficient, whereas the vapor conductivity has a relatively negligible effect [75].

Other important properties concerned with the equipment functioning include,

for instance, the refrigerant miscibility with compressor lubricant. In fact, in most vapor-compression HVAC systems the working fluid is a mixture consisting of the refrigerant and the compressor lubricant, essential for lubricating moving parts of compressors. Consequently, both must be circulated throughout the equipment simultaneously, so the lubricant must be miscible with the refrigerant.

A rather large number of factors are therefore to be considered when choosing a refrigerant for a specific application. In particular, the technical interest of thermophysical properties and their relevance are further covered in Section 2.4.3.

2.3 Performance of refrigeration systems

2.3.1 Analysis of an ideal basic vapor-compression cycle

According to the first law of thermodynamics and assuming a steady-state refrigerant flow, as regard to the basic vapor compression cycle (see Figs. 2.2a and 2.2b), the specific compression work w and the refrigeration effect q_e can be determined as [62]:

$$w = h_2 - h_1 \quad [\text{kJ/kg}] \tag{2.1}$$

$$q_e = h_1 - h_4 \quad [\text{kJ/kg}] \tag{2.2}$$

These parameters allow an evaluation of the COP (Coefficient of Performance) of the refrigerating system, given by the formula:

$$\text{COP} = \frac{q_e}{w} = \frac{h_1 - h_4}{h_2 - h_1} \tag{2.3}$$

and the volumetric heat capacity Q_{vol}, defined as:

$$\text{Q}_{\text{vol}} = \rho_1 q_e \quad [\text{kJ/m}^3] \tag{2.4}$$

where the indexes 1, 2, 3, and 4 refer to properties of the fluid in the respective four states in Figs. 2.2a and 2.2b. The coefficient of performance (COP) and volumetric capacity are two parameters that stem from thermodynamic properties [76]: COP determines the energy efficiency of the system, therefore it reflects its operating cost, whereas Q_{vol}, particularly when volumetric compressors are involved, influences the physical size of the equipment, with implication on the plant cost [69]. High values of both COP and Q_{vol} are sought in general but, as previously mentioned, one must consider that a compromise between the two is observed when referring to an ideal cycle, that suggests an inevitable compromise in terms of efficiency and size of the refrigerating equipment [58]. A representative example of the trade-off is depicted in Fig. 2.6, concerning a simple vapor-compression cycle and working

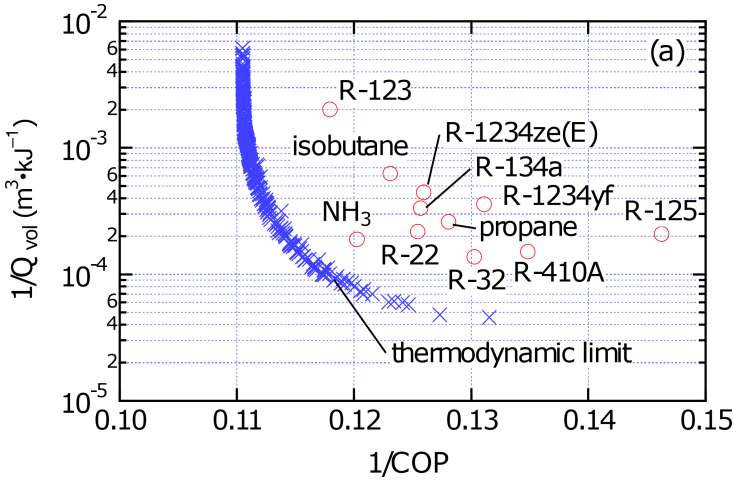

Figure 2.6: Pareto front (x) and selected refrigerants (o) for the simple vapor compression cycle with temperatures representative of an air-conditioning application (T_e = 10 °C, T_c = 40 °C). Reprinted with permission from [43].

conditions that are representative for air conditioning applications. The "best" refrigerants, i.e., the ones showing the most favorable compromise between the COP and the Q_{vol}, lie closer to the Pareto front, which expresses the thermodynamic limit to performance for the cycle [43]. Significantly, Fig. 2.6 also reveals that the refrigerants involved in the study [77] were far from the Pareto front, implying that better fluids could at least be allowed by thermodynamics.

The refrigerant mass flow rate $\dot{m}$ can be determined from the relation between the refrigeration capacity $\dot{Q}_e$ and the refrigeration effect q_e as:

$$\dot{m} = \frac{\dot{Q}_e}{q_e} \quad \text{[kg/s]} \tag{2.5}$$

whereas the power required for the isentropic compression P_{is} is given by the following:

$$P_{is} = \dot{m} w \quad \text{[kW]} \tag{2.6}$$

The non-isentropic compression process involved in actual compressors is considered by means of the isentropic efficiency η_{is}, therefore the effective power P_{ef} on the compressor shaft is higher and may be calculated as.

$$P_{ef} = \frac{P_{is}}{\eta_{is}} \quad \text{[kW]} \tag{2.7}$$

2.3.2 Efficiency and capacity for different refrigerants

Various cycle performance can be achieved using different refrigerants within their working conditions and based on their thermophysical properties. Table 2.2

illustrates an example. Among the other traditional refrigerants, at fixed condensing temperature and evaporating temperature, two exhibits rather different characteristics. One is R-717, being one of the fluids showing better efficiency, but as a drawback it has a very high discharge temperature, which is attributable to the low molecular mass of ammonia. Indeed, high discharge temperature should be limited in order to avoid, primarily, the deterioration of lubricant properties or even lubricant burnout, that can ultimately affect the system reliability [62].

The other peculiar working fluid is R-744, which exhibits the highest volumetric capacity, that is more than six times higher than that for R-12. Volumetric capacity, in general, should be as high as possible in order to benefit from the use of compressors with reduced displacement. Due to the high vapor density at the suction side of the compressor, necessary pipe dimensions can be very small, and the mass flow rate reduced, with equal refrigeration capacity. Additionally, due to the high operating pressure, pressure drops occuring within the system are relatively low, which translates into less required pumping work [78]. However, for such working conditions, i.e., with a condensing temperature approaching the critical temperature, the COP for R-744 is very low if compared to that for other working fluids, as a result of non-optimal thermodynamic properties for usual applications in refrigeration and air conditioning [78]. Furthermore, the pressure at the condenser p_c is relatively very high, which technically involves thicker piping wall, appropriate brazing methods, equipment materials [17], and compressors, that overall cause higher equipment costs [78]. Economically feasible and efficient solutions for carbon dioxide typically requires transcritical or subcritical cascade plants: in the latter, R-744 is used as a secondary fluid at significantly lower condensing and evaporating temperatures, so as to achieve higher performance [78].

2.3.3 Thermodynamic irreversibilities

As mentioned in Section 2.1, the basic ideal vapor-compression cycle is based on the reverse Carnot cycle. However, the first differs from the latter as a result of two, principal causes of performance detriment or irreversibilities: the isenthalpic expansion, and the superheating of the refrigerant vapor during compression [79]. An actual refrigeration system, however, exhibits additional phenomena responsible for a decrease of capacity and efficiency, which are mainly [80, 81]:

- heat transfer in the pipeline and in the compressor,
- frictional pressure drops along the circuit and pressure drops at the suction and discharge line of the compressor, at the inlet/outlet of headers, manifolds, tanks and so on,
- heat transfer and pressure drops in the heat exchangers.

Table 2.2: Performance comparison of an ideal, single stage, basic vapor-compression cycle for different refrigerants, assuming t_e of −15 °C and t_c of 30 °C [62].

Refrigerant	P_c (bar)	P_e (bar)	P_c/P_e	Q_{vol} (kJ/kg)	COP	t_2 (°C)
R-717	11.672	2.362	4.942	2167.6	4.76	99.08
R-744	72.1	22.9	3.149	7979	2.69	69.5
R-12	7.437	1.823	4.079	1273.4	4.70	37.81
R-22	11.919	2.962	4.024	2096.9	4.66	52.95
R-32	19.275	4.881	3.949	3420.0	4.52	68.54
R-134A	7.702	1.639	4.698	1225.7	4.60	36.61
R-404A	14.283	3.610	3.956	2099.1	4.16	36.01
R-507	14.60	3.773	3.870	2163.2	4.18	35.25
R-290	10.79	2.916	3.700	1814.5	4.55	36.60

For these reasons, ideal COP and Q_{vol} are not representative of an actual system [64]. Several models, however, have been developed to describe the real performance under specified conditions that account for cycle penalties. A prime example is given in the study by Domanski et al. [77], who carried out "optimized" simulations that included forced-convection, air-to-refrigerant heat exchangers as well as a refrigerant-dependent isentropic efficiency of the compressor and the effect of pressure drops, for a typical air-conditioning application; Fig. 2.7 shows that, once a more realistic system is considered, the trade-off between COP and Q_{vol} vanishes. In this case, higher efficiencies were obtained at relatively high volumetric heat capacities, approximately from 60–110 % to that of R-410A, that was set for a common reference [82].

2.4 Heat exchangers

To reduce the footprint of refrigerants on the environment, a transition to low-GWP alternatives has been under way in the RACHP sector as a reaction to regulatory changes worldwide. Nevertheless, the latest key outcomes from the International Institute of Refrigeration (IIR) [63] underline how the selection of a new refrigerant should be weighed and accomplished with a comprehensive approach. In fact, in addition to considerations on the value of GWP, other potential opportunities for mitigating global warming can be drawn, for instance, from the paramount terms in the expression of TEWI (see Eq. (1.1) on Page 10), and particularly from the refrigerant charge, whose reduction in a refrigerating system implies a substantial decrease of the direct effect of TEWI. To provide an insight, nowadays

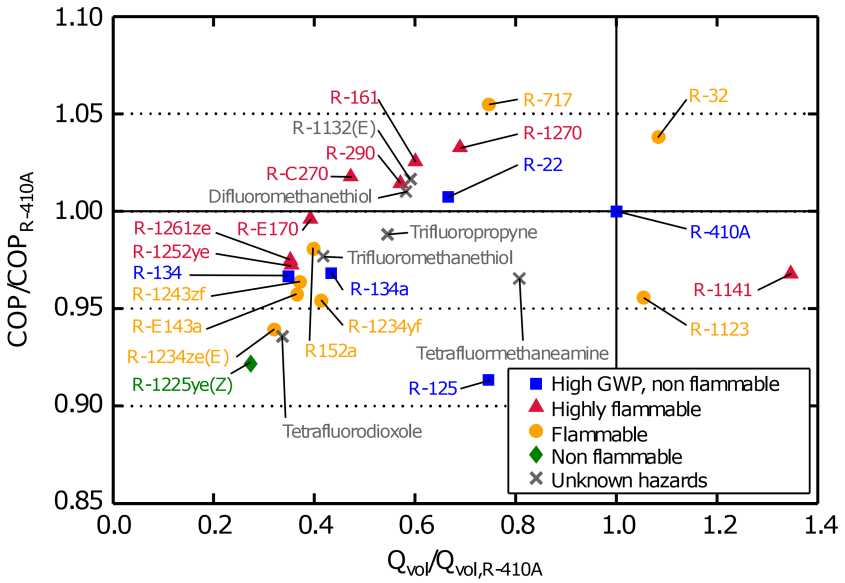

Figure 2.7: Coefficient of performance and volumetric capacity of selected low-global-warming-potential fluids, calculated with an "optimized" model for the basic vapor compression cycle, in the study by Domanski et al. [77]. Values are relative to those for R-410A [82].

the RACHP sector encompasses a wide range of systems in temperature levels and sizes. For instance, domestic refrigerators typically rely on a refrigerant charge in the range from 30–150 g, with power consumption from 50–250 W, depending mainly on refrigerant type and size of the appliance. Differently, the industrial cold chain for standard applications involves temperatures from −10–−40 °C; in this case, the refrigerant content may be of several hundreds of kilograms and the maximum electrical power consumption reaches is in the order of megawatts [31]. Air conditioning, that include also reversible air heat pumps — or "reversible heat pumps" — encompasses units with power mostly in the range from 1–1.100 kW, the majority of which are less than 70 kW. The refrigerant charge may vary greatly, depending on the system and of the specific installation [31]: indicatively, a small, self-contained air conditioner has a minimum charge of around 0.3 g, whereas a ducted commercial split could contain up to 300 kg of refrigerant.

The reduction of the refrigerant charge can then be accomplished through indirect refrigeration systems that use lower-GWP, secondary refrigerants, such as the traditional glycols and salt brines as well as CO_2 [48], but another relevant option is in the careful design of key, refrigeration components [48], especially of heat exchangers, where the heat transfer process also very often represents the bottleneck on improving the equipment efficiency and capacity [48, 83]. Proper design techniques, therefore, are relevant also for the indirect effect of TEWI, as a

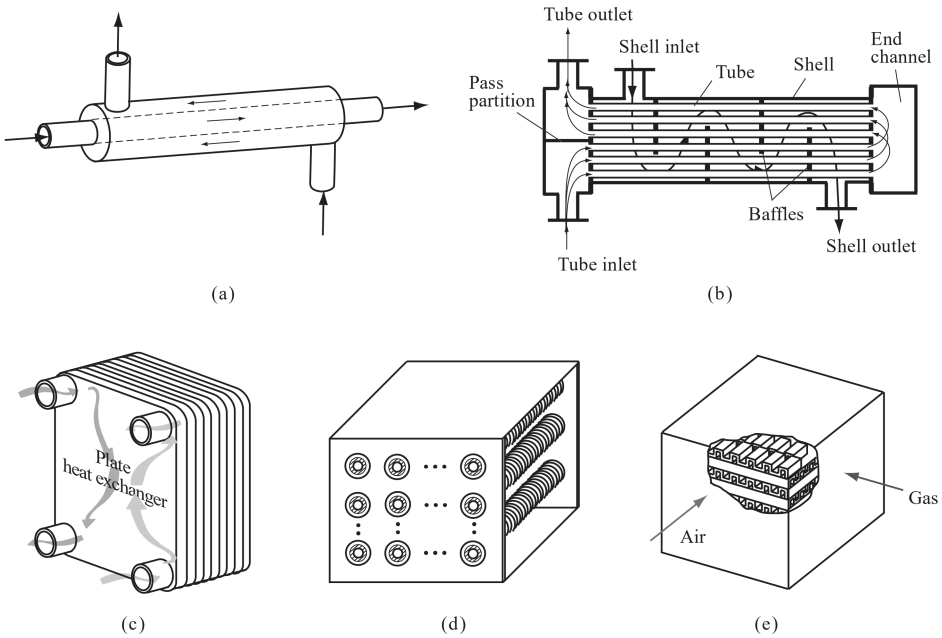

Figure 2.8: Common heat exchangers: (a) double-pipe heat exchanger, (b) shell-and-tube heat exchanger, (c) brazed plate heat exchanger, (d) circular-finned tube heat exchanger and (e) plate-fin heat exchanger. Reprinted with permission from [84].

contribute to the reduction of power consumption in the system.

2.4.1 Design methods

Heat exchangers are devices that are used to transfer thermal energy in the process of heating, cooling, heat recovery and heat rejection, typically between two or (less often) more fluids, but also between a solid surface and a fluid, as well as between solid particulates and a fluid, that are each at different temperatures and in thermal contact. In most heat exchangers, the heat transfer occurs between two fluids through a separating wall, whose surfaces are fundamental for the heat transfer. They are custom designed for virtually any refrigeration capacity and operating conditions, and there is a wide variety of sizes and geometries, ranging from the double-pipe and shell-in-tube heat exchanger to the more compact plate heat exchanger, and heat exchangers with surface enhancements (see Fig. 2.8).

The process of manufacturing a heat exchanger involves several considerations, which can be collected and structured in a framework, as the one represented in Fig. 2.9.

Complex analyses are carried out in the thermal and hydraulic design, and these primarily pertain to the determination of heat transfer and pressure drop (in transient

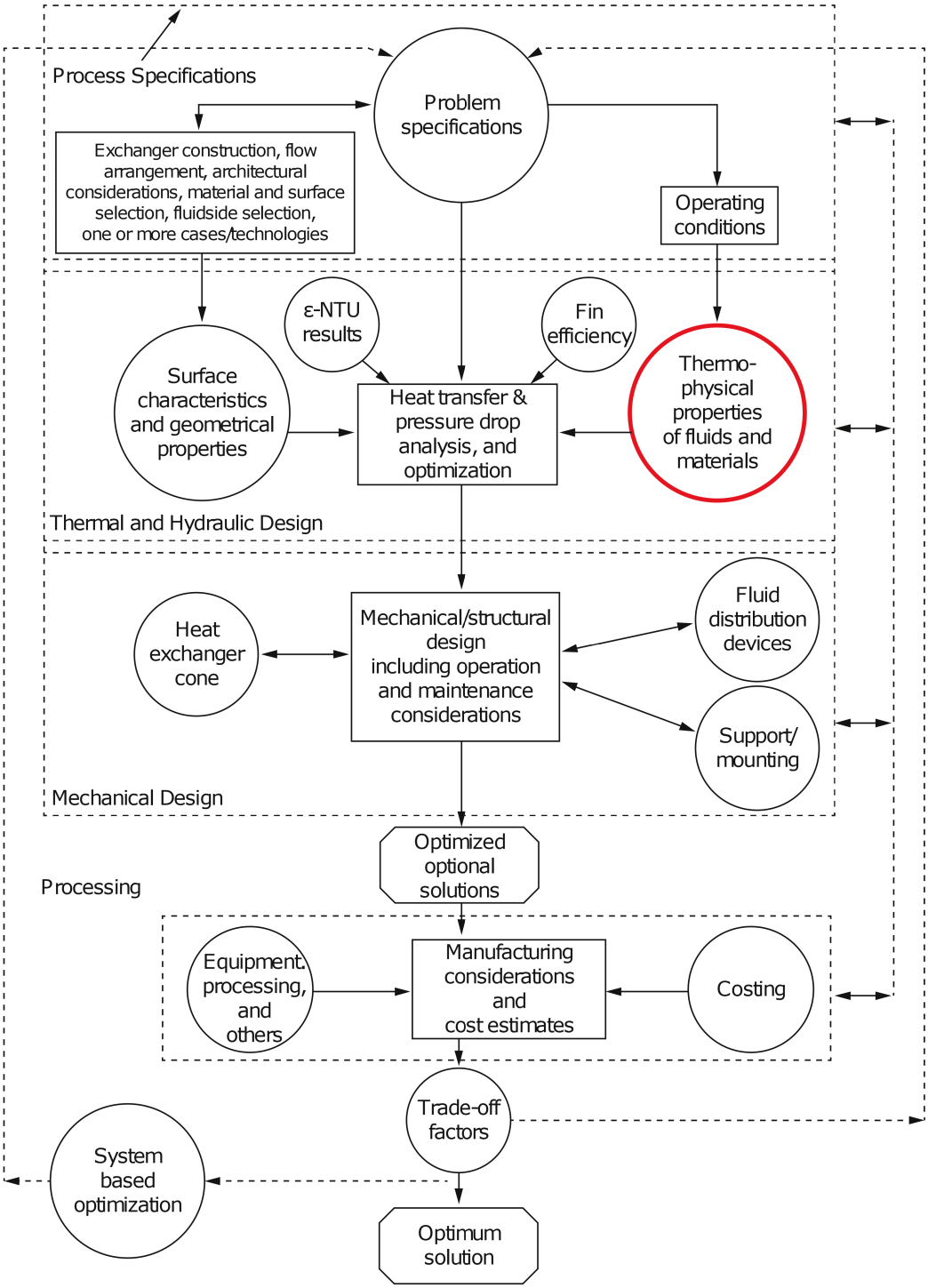

Figure 2.9: Design methodology for heat exchangers. Modified from Shah (1982), Taborek (1988), and Kays and London (1998). Adapted with permission from [85].

state rather than in steady state), and to the sizing of heat exchangers. Especially, if phase transitions are involved, such as in most common heat exchangers for refrigerating units, the uncertainties that arise to the complex behavior of multi-phase flow may significantly affect the design of the refrigerating system [83], so in today's scope of design optimization, the analyses typically involve advanced modeling with Computational Fluid Dynamics (CFD), but, at the core of the heat exchange process, fundamental relations are applied regardless the specific design method (such as the LMTD and the ε-NTU). Ultimately, as highlighted in Fig. 2.9, thermophysical properties of the working fluids play a major role in the thermal and hydraulic design, and they possess multiple interdependencies with other key aspects, including the equipment sizing and cost estimation [85].

2.4.2 Fundamental equations

The effects of thermophysical properties can be found in the heat transfer theory applied to heat exchangers, that provides two important relationships for the entire thermal design procedure. Concerning the most common two-fluid heat exchangers relying on the heat transfer mechanism of convection and conduction (when radiation can be negligible), and based on a series of assumptions [81], the relations are the *enthalpy rate equation*, expressed as:

$$\dot{Q} = \dot{Q}_j = \dot{m}_j \Delta h_j \tag{2.8}$$

for each working fluid ($j = 1, 2$) involved in the heat exchange, and the *heat transfer rate equation*, given by the following:

$$\dot{Q} = UA\Delta T_m \tag{2.9}$$

where Eq. (2.8) relates the heat transfer rate $\dot{Q}$ to the mass flow rate $\dot{m}_j$ and the specific enthalpy change Δh_j occurring in a heat exchanger at constant pressure, whereas Eq. (2.9) expresses the same quantity in a heat transfer phenomenon involving convection and conduction. U is the overall heat transfer coefficient, A is the heat transfer surface and ΔT_m is a mean temperature difference, calculated from the inlet and outlet temperatures of both fluids, and it can be a log-mean temperature difference (for counter-flow and parallel-flow heat exchangers), or related to it so that the terminal temperature differences between the fluids are accounted for [81]. The heat transfer rate equation can be used, for instance, to calculate the required heat transfer area with different fluids, for certain inlet and outlet temperatures as well as for different types and arrangements of heat exchangers.

The expression of U varies with different geometries of heat exchangers, but its general form allows a distinction among each contribute to the global heat transfer coefficient. Considering the heat transfer between a hot and a cold fluid separated

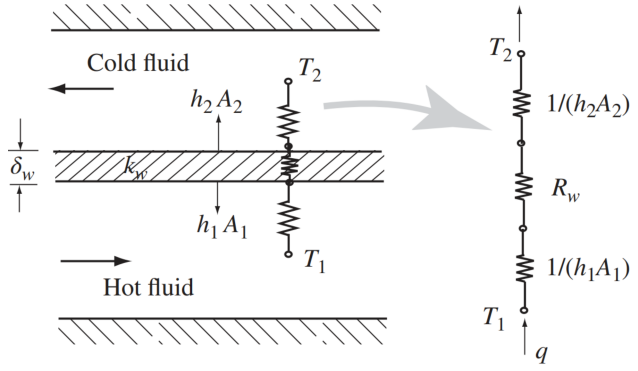

Figure 2.10: Typical configuration of a heat transfer process and its equivalent thermal circuit. Reprinted with permission from [84].

by a wall (as shown in Fig. 2.10), U can be referred either to the surface A_1 at the hot side (U_1) to or the surface A_2 at the cold side (U_2) of the same separating wall. In the latter case, the expression is the following [84]:

$$U_2 = \frac{1/A_2}{\frac{1}{h_1A_1} + R_w + \frac{1}{h_2A_2}} \tag{2.10}$$

where h_1 and h_2 are the convective heat transfer coefficient of the hot and the cold fluids, respectively. The terms $1/(h_1A_1)$, $1/(h_2A_2)$ and R_w represent the thermal resistances to the heat flow offered by the two fluids and the separating wall, respectively. The higher their values the lower the heat transfer rate coefficient will result. It is important to notice that the thermal resistance R_w, that depends on the sizes and the thermal conductivity of the wall (which is mostly made of metallic materials), is generally low so that it can often be considered negligible if compared to those given by the fluids [86], which therefore are the ones exerting a major influence on the heat transfer process.

2.4.3 Effects of thermophysical properties

The convective heat transfer coefficients (h) is affected by a number of factors, including the flow rate, the flow geometry and particularly by the fluid properties; the existing relations are mostly in terms of empirical equations, some of which make use of several dimensionless numbers. In particular, these are:
the Reynolds number:

$$\mathrm{Re} = \frac{\rho \overline{w} L}{\mu} \tag{2.11}$$

the Prandtl number:

$$\mathrm{Pr} = \frac{c_p \mu}{\lambda} \tag{2.12}$$

and the Nusselt number:

$$\mathrm{Nu} = \frac{hL}{\lambda} \tag{2.13}$$

where ρ, $\overline{w}$, μ and λ are the density, mean velocity, dynamic viscosity and thermal conductivity of the fluid, respectively; L is a characteristic length that depends on the heat exchanger geometry (for instance, for a flow in a circular pipe, L is the pipe diameter). The three dimensionless numbers, which may have different expressions for single- or two-phase flow and for different flow arrangements (such as counter flow and cross flow), can be found in equations in the following form:

$$\mathrm{Nu} = C\mathrm{Re}^m\mathrm{Pr}^n \tag{2.14}$$

which is a generalized, empirical correlation between h and the aforementioned properties involved in a single-phase, forced convection heat transfer. The coefficient C, m and n are determined experimentally [69]. Equivalently, to explicit the convective heat transfer coefficient as a function of the properties in the dimensionless numbers, Eq. (2.14) can be written as:

$$h = C\left(\frac{\rho\overline{w}L}{\mu}\right)^m\left(\frac{c_p\mu}{\lambda}\right)^n\frac{\lambda}{L} \tag{2.15}$$

For the condensation and evaporation in a heat exchanger, the thermophysical properties of the fluids that influence the heat transfer coefficient h and the pressure drops are [75]:

- liquid thermal conductivity,
- liquid and vapor density,
- liquid and vapor viscosity,
- liquid specific heat at constant pressure,
- surface tension (only for evaporation).

The surface tension affects the nucleate boiling phase during evaporation: a low surface tension leads to a higher h but, overall, its effect is secondary to that of other properties. In fact, a forced-convection heat transfer with two-phase flow (the type of flow that often occurs in common heat exchangers) is governed primarily by the liquid conductivity and the vapor density: the higher their value, the higher the two-phase heat transfer coefficient is. In general, pressure drop increases as the vapor density decreases and as vapor and liquid viscosity increase. The effect of liquid viscosity depends on the refrigerant and operating conditions, whereas the contribute of vapor viscosity is small [75].

The evaluation of pressure drops is addressed specifically in the hydraulic design of a heat exchanger and it is of great interest, for instance, to adequately sustain the fluid flow in the desired working conditions, but ultimately it affects other key aspects, such as the compressor power requirements, that in turn impacts on the overall performance of the refrigerating system. Additionally, pressure drops influence the heat transfer rate for a condensing/evaporating fluid: the saturation temperature changes with shifts in saturation pressure, therefore, differently from an ideal cycle where the two-phase heat transfer is assumed to be isobaric, pressure drops cause the saturation temperature to diminish. That, in turn, influences the mean temperature difference ΔT_m, with a consequent effect on the heat transfer rate. Moreover, the saturation temperature drop in the condenser and in the evaporator results in a greater pressure lift seen by the compressor, so that a higher pumping power is required at the expense of the COP [77].

A primary objective, therefore, is often the maximization of the heat transfer while maintaining low pressure drops. Equivalently, the goal can be translated into the minimization of entropy generation that arises by means of the heat transfer and pressure drop. With thermal performance and geometry fixed in an actual heat exchanger, a design choice could be modifying the overall heat transfer coefficient and the driving temperature difference between the two fluids. In general, however, the larger the temperature difference the more irreversible the heat transfer process is. Therefore, to limit the entropy generation while using the same heat exchanger and providing the desired thermal performance, the driving temperature difference should be kept low, while the overall heat transfer coefficient should be maximized; this can be achieved mainly through a proper control over the refrigerant mass velocity, and with fluids with suitable thermophysical properties [79].

2.4.4 Compact heat exchangers

Research is working on the development of advanced heat exchangers with more complex surfaces for the intensification of the heat transfer, some of which in recent years have been developed by virtue of the rise of topology optimization and additive manufacturing techniques. The most traditional compact heat exchangers, such as circular-finned tubes heat exchangers and plate-fin heat exchangers are developed and used to provide a very large heat transfer area per volume, as well as to achieve high overall heat transfer coefficients. Their implementation is a key to reduce the refrigerant charge, which is an effective approach to curb global warming, but the design may often require modifications in order to achieve optimum performance; especially, with some low-GWP refrigerants is currently not well grasped. For instance, this was observed in a study [87] that investigated the capacity and pressure drop of two ultra-low-GWP HFOs, namely R-1234yf and R-1234ze(E) in finned-tube heat exchangers originally designed for R-410A.

The results showed that, in comparison to the design with R-410A, to increase the cooling capacity and decrease the pressure drop at the refrigerant side, the tube diameter should be decreased, whereas the fin density, and the number of tubes should be increased.

The design and the performance of the refrigeration equipment are therefore closely linked to that of their working fluids. As discussed in Chapter 1, regulatory changes on global scale are calling for air conditioning and heat pump equipment manufactures to switch refrigerants to alternatives with reduced GWP; hence, in order to hold up the ongoing transition to low-GWP alternatives, it is crucial to widen the knowledge of their thermophysical properties and their behavior in applications where they could potentially be used. In light of this, the next chapter focuses on the equations of state, the fundamental tools that to calculate properties of refrigerants and predict the energy performance of refrigeration and air-conditioning equipment.

Chapter 3

Equations of state

3.1 Introduction

In the previous chapter, the prominent thermophysical properties of refrigerants have been discussed in relation to their impact on the basic refrigeration cycle. Accurate property measurements of fluids are essential, in general, for many industrial and natural processes, to develop consistent models capable to assess the functioning of energy systems. However, the availability of properties over a wide range of operating conditions would require sampling of likewise amounts of data, that is either impossible or too time-consuming and expensive [66, 88]. In the past, once thermophysical properties were measured for a specific fluid, the data were processed with early computers and provided in the forms of tables and charts, from which engineers had to interpolate data to obtain needed missing values. As the number of pure fluids started to increase, and more sophisticated numerical methods became available, this traditional approach progressively proved inconvenient and thus was later superseded [34].

The breakthrough of modern computers was revolutionary also in this field: far more flexible and faster implementation of mathematical expressions for correlating and predicting fluid properties was possible, yielding to higher accuracy, consistency, computational speed, and robustness. Properties could be extracted directly from equations, and this introduced also better predictive abilities, so that required values can be estimated from a limited set of fitted, directly measured data [88]. Among all mathematical formulations, equations of state (EOSs) have been the typical method to correlate and calculate all thermodynamic properties of fluids, that, as mentioned in Section 2.2, refer to the properties that characterize a fluid in its state of thermodynamic equilibrium. More in general, an equation of state is intended as any mathematical relation among the pressure, the volume, and the temperature of a thermodynamic system (e.g., represented by a mass of fluid inside

an enclosed vessel) [89], and, as mentioned before, it has been preferred over the traditional charts and tables because it can be implemented in computer programs and employed directly to extract fluid properties; this is fundamental, especially for those properties that cannot be obtained directly with measuring instruments, such as for the internal energy, enthalpy and entropy, which are essential information for the analyses of refrigeration cycles [89, 90]. In any case, a specific process simulation, such as for a two-phase heat transfer in heat exchangers, can be highly influenced by the qualities of such relations [88]; therefore, among other requisites, the models must be able to represent measured data within their experimental uncertainties [90].

A lot of different EOSs have appeared in the literature: some apply to pure fluids, whereas others extend to mixtures; nevertheless, in general, none is able to represent equivalently any substance or is adequate for all applications [91]. Furthermore, even though the vast majority of correlations is developed from solid theoretical principles, modern EOSs are empirical or semi-empirical, based on available data. As a consequence, typically the effectiveness of a specific EOS diminishes when properties of the fluids are computed outside the domain of temperatures and pressures where the behavior of the fluid has been investigated [92]. To highlight the importance of equations of state for HVAC&R equipment design and simulation, in the present chapter the prominent models for pure fluids will be discussed in relation to their applications; additionally, their impact on the estimation of performance indicators for equipment relying on the vapor-compression cycle will be presented.

3.1.1 The ideal gas law

The evolution of mathematical equations for the correlation of thermodynamic equilibrium properties started with Boyle's studies, who first noted that, at a specific temperature, the volume of a certain mass of gas is inversely proportional to its pressure; afterward, in 1802, its linear dependence in temperature at a fixed pressure was postulated by Gay-Lussac. By bridging the previous outcomes with Dalton's law of partial pressure, the first EOS was postulated for an ideal gas, and thus it is known as the *ideal gas law*, which can be written as [93]:

$$PV_m = RT \tag{3.1}$$

where P, V_m, and T are the pressure, molar volume (given by the ratio between the gas volume and its number of moles), and absolute (or thermodynamic) temperature of the ideal gas, respectively, whereas R is the universal gas constant.

Eq. (3.1) provides the simplest form for an EOS. Although it has been widely employed for several practical applications, for instance, with air and hydrogen, it

has significant shortcomings: it can be representative of the PvT correlation only for gases, whose behavior closely reflects that of an ideal gas. In general, this occurs the lower the pressure and molecular mass are, and the higher the temperature (in relation to the critical temperature) is [94]. As a result, to describe the properties of a fluid when its thermodynamic state is far from the conditions of an ideal gas, other relations are needed.

3.1.2 The virial equation of state

As mentioned before, a wide number of EOS have been developed in the last decades. Actually, the ideal gas law can be seen as a specific form of a more general equation: the virial equation of state. The relation can be written as follows [94]:

$$PV_m = A\left(1 + \frac{B}{V_m} + \frac{C}{V_m^2} + \frac{D}{V_m^3} + \dots\right) \tag{3.2}$$

where $A = RT$ and B, C, ... are the *virial coefficients*, which depend on the temperature and composition of the fluid. Consistently, in the limit of zero pressure P, the molar volume V_m in Eq. (3.2) approaches infinity, and the virial equation can be reduced to the ideal gas law [94].

The virial equation of state is one of the several generalized equations that have been proposed in order to represent the thermodynamic properties of real gases, i.e., of gases that do not follow the conditions of an ideal gas, over a greater domain of P and T. For the purpose, a substantial database of virial coefficients, determined both experimentally and analytically, has been attained to accurately estimate the thermodynamic properties of pure substances and mixtures [95]. In broad terms, the high relevance the virial equation has had is due to its sound theoretical basis, that grants exact analytical relations to describe the behavior of a thermodynamic system [95]. Besides, many common EOSs can be expressed as specific developments of the virial equation, but in general, each EOS includes, with a specific degree of complexity, the effects that distinguish a real gas from an ideal one. These will be discussed for some of the prominent EOS in the following section.

3.2 Cubic equations of state

3.2.1 Van der Waals equation

In real gases at high pressure and in liquids, both the volume of molecules and the intermolecular forces are no longer negligible; consequently, in such circumstances the model of an ideal gas cannot be representative, and other mathematical relations

historically had to be used [89]. Initially, a solution came when J.D. van der Waals proposed the idea of continuity between the vapor and the liquid phases, and suggested that the PvT properties of fluids could be described by a single semi-empirical EOS. In 1873, he formulated his renowned EOS, that is commonly expressed as follows [89, 96]:

$$P = \frac{RT}{V_m - b} - \frac{a}{V_m^2} \tag{3.3}$$

According to van der Waals, molecules could be represented by hard spheres with finite dimensions, and that overall occupy the volume b (called "covolume"), causing the reduction of space $(V_m - b)$ available to molecular motion; differently, a is a temperature-dependent parameter to include the contribute of attractive forces between molecules, which are assumed to be inversely proportional to v^2 [89]. Actually, the two constants a and b, which can be obtained by the properties of the fluid at its critical point, allow to formulate a pressure-explicit EOS made of two distinct terms: the ratios $RT/(V_m - b)$ and $-a/V_m^2$, which express the repulsive and attractive effects of intermolecular forces, respectively, that collectively contribute to the pressure P [97, 98].

A remarkable fact is that the van der Waals equation was the first cubic EOS (i.e., equations that can be written as an explicit function that is cubic in volume) able to qualitatively characterize the liquid and the vapor phase as well as the phase transition of a fluid, although it fails in estimating quantitatively the saturation and single-phase properties, especially with polar substances. Consequently, the equation was later superseded by other, more advanced PvT correlations, although many of these stemmed from the van der Waals model in terms of modifications to its expression [97].

3.2.2 Modern cubic formulations

Substantial enhancements to the van der Waals EOS were introduced 1949, when the Redlich-Kwong model [99] was made available. The equation, still cubic in volume and consisting in a two-parameter (a and b) formulation, retained the same repulsive term of the van der Waals equation, but introduced a temperature-dependent modification to the attractive expression so that the PvT correlation could be stated as:

$$P = \frac{RT}{V_m - b} - \frac{a}{T^{0.5} V_m (V_m + b)} \tag{3.4}$$

where constant a and b are again related to the fluid critical temperature and pressure [89]. Noteworthy, the Redlich-Kwong EOS has been used to calculate the vapor-phase enthalpies for a multitude of substances, including polar and

non-spherically simmetric molecules, overcoming some major issues of the van der Waals EOS. Additionally, it can also extend to mixtures by applying proper mixing rules [97].

The achievements the Redlich-Kwong model has had fostered plenty of empirical advancements for EOS. Afterwards, in the 1970s, especially the oil and gas industry often made use of the Soave-Redlich-Kwong equation of state [100], which is a modification to the Redlich-Kwong model that specifically addresses the parameter a [34, 89]. Soave calculated parameter a in Eq. (3.4) for several pure fluids and related it to an additional parameter: the acentric factor, that is representative of the fluid molecular complexity [89] and is related to the slope of the vapor saturation curve on the T-S diagram [101]. Overall, the Soave-Redlich-Kwong proved good capabilities in estimating vapor-liquid equilibrium properties, but as a drawback it heavily underestimates liquid densities [89].

In 1974 Peng and Robinson [102] developed a new EOS (known as the Peng-Robinson EOS), still widely used in the refrigeration industry and for research purposes [103]. The two-constant EOS was proposed in the following form [102]:

$$P = \frac{RT}{V_m - b} - \frac{a}{V_m(V_m + b) + b(V_m - b)} \tag{3.5}$$

where constants a and b are obtained similarly to the Soave-Redlich-Kwong EOS. The intention that took to the development of the Peng-Robinson EOS was to enhance the estimating capabilities of the liquid density [89]. However, although it proves better results for medium-size hydrocarbons and with substances with intermediate values of the acentric factor, its accuracy for substances with small acentric factors is lower than that provided by Soave-Redlich-Kwong [98].

The strengths and weaknesses of each EOS discussed so far further highlight the need of specific equations of state to predict and verify fluid properties. Cubic equations of state, in general, are not the most accurate models to represent thermodynamic properties of fluids, but because of their convenient compromise in terms of reliability, simplicity and computational speed, they are still among the most widely used in practical applications, such as in semi-quantitative predictions of equilibrium states, as well as in process design and in simulations [98, 104].

3.3 Multiparameter equations of state

3.3.1 Pressure-explicit relations

If the prediction accuracy of thermodynamic properties has a priority over the model ease, other approaches have to be pursued. These include the use of more sophisticated, empirical multiparameter EOSs, most of which became available

in the 1970s. All of these equations are non-cubic, and are formulated with up to 60 or even more parameters to be calculated [104]. Additionally, they typically require numerous datasets of low-uncertainty experimental data in order to compute fluid properties accurately [105]. The Martin-Hou equation of state, in particular, falls into this category; the EOS, which has frequently been used to correlate the thermodynamic properties especially of halogenated refrigerants, has the following general form [106]:

$$P = \frac{RT}{V_m - b} + \sum_{i=2}^{5} \frac{A_i + B_i T + C_i \exp(-KT/T_c)}{(V_m - b)^i} \tag{3.6}$$

As it can be seen from Eq. (3.6), the repulsive term is kept from the van der Waals equation, whereas the more advanced attractive contribute relies on fitted parameters A_i, B_i, C_i, and K, where T_c is the fluid critical temperature. Differently from the cubic EOS, the Martin-Hou model lacks the ability to compute fluid properties in the liquid region and requires auxiliary equations to obtain saturated pressure and saturated liquid density [34].

Before moving to another category of EOS, two more correlations are mentioned. These are the Carnahan-Starling-DeSantis [107] and the modified Bennedict-Webb-Rubin EOS [108]. The first is a successful six-parameter equation that is able to represent both the liquid and vapor phases, and because it has a solid theoretical basis it proves a reliable model to predict the thermodynamic properties even when experimental data are scarce. The second, as the name suggests, is a modification to the earlier Bennedict-Webb-Rubin EOS: this consists of a more advanced 32-parameter expression, that came into use when research focused on alternative refrigerants in place of CFCs and HCFCs. Significantly, it improved the fitting of experimental data for properties of more polar substances, such as R-134a, for which the Carnahan-Starling-DeSantis showed hindrances [34].

3.3.2 Models based on Helmholtz energy

Traditionally, equations of state have been developed in a form so that the thermodynamic variables pressure, volume (or density) and temperature could be related to each other implicitly or explicitly, such as for the aforementioned van der Waals-based formulations. In fact, the pressure (P) and temperature (T), primarily, are those properties that can be measured directly and with relative ease in a thermodynamic system, and that constitute the most accessible variables representing the operating conditions in refrigeration and air-conditioning systems [34]. Nevertheless, as discussed in Section 2.2, in evaluating the performance of these thermal equipment, other properties are required, and these include the entropy (s) and enthalpy (h) of the refrigerants, which according to the theory can be obtained

in any thermodynamic state as a function of two independent variables pressure P and density ρ of the fluid, by the followings [90]:

$$s(T,\rho) = s^0_{T_0} + \int_{T_0}^{T} \left(\frac{c_p^0}{T}\right) dT - R\ln(RT\rho) + \int_0^{\rho} \left[\frac{R}{\rho} - \left(\frac{1}{\rho^2}\right)\left(\frac{\partial P}{\partial T}\right)_\rho\right]_T d\rho$$

$$h(T,\rho) = h^0_{T_0} + T\int_0^{\rho} \left[\left(\frac{P}{T\rho^2}\right) - \left(\frac{1}{\rho^2}\right)\left(\frac{\partial P}{\partial T}\right)_\rho\right]_T d\rho + \left(\frac{P-\rho RT}{\rho}\right) + \int_{T_0}^{T} c_p^0\, dT$$

where terms $s^0_{T_0}$ and $h^0_{T_0}$ are the reference values of entropy and enthalpy of the gas under ideal conditions at temperature T_0 and pressure P_0, that must be defined for the specific refrigerant. From the expressions above of s and T, it can be noticed that the relation for the ideal-gas specific heat capacity c_P^0 is required, and this in turn make use of a specific auxiliary equation.

To overcome the limits of such approach, a new class of EOSs have been developed. These are referred to as *fundamental equations*, which include c_P^0 and fluid reference information, so that absolute values of all thermodynamic properties can be computed without the need of additional sources and from a single mathematical correlation [90, 109]. The fundamental equations may have different forms, but the only able to represent the fluid over the whole domain of pressures and temperatures are the ones based on the Helmholtz free energy (or Helmholtz energy), whose development started in the 1940s [90]. In particular, nowadays the most accurate thermodynamic properties are computed using multiparameter Helmholtz-energy equations explicit in fluid properties P, ρ and T [53].

The Helmholtz energy is one of the four thermodynamic potential along with the internal energy, enthalpy, and entropy, that allows to express a fundamental EOS in the following form [110]:

$$a(\rho,T) = a^0(\rho,T) + a^r(\rho,T) \tag{3.7}$$

for which the molar Helmholtz energy $a(\rho,T)$ of a real gas is obtained by the sum of the ideal gas $a^0(\rho,T)$ contribution, and a residual term $a^r(\rho,T)$, which accounts for the effects of intermolecular forces. In other words, this formulation allows a real gas to be described as the sum of its ideal behavior and what distinguishes it from an ideal gas. The expression for a in Eq. (3.7) is often non-dimensionalized by the product of the universal gas constant R and gas temperature T, yielding the relation:

$$\frac{a(\rho,T)}{RT} = \alpha(\delta,\tau) = \alpha^0(\delta,\tau) + \alpha^r(\delta,\tau) \tag{3.8}$$

where the independent variables are non-dimensionalized as well, and expressed as the reduced density $\delta = \rho/\rho^*$ and temperature $\tau = T/T^*$ [105]. Properties ρ^* and

T^* are typically determined as part of the data fitting procedure, but for pure fluids they correspond mostly to the critical density and temperature, respectively [111].

As a result of such formulation, thermodynamic properties can be obtained conveniently taking analytic derivatives of the α^0 and α^r functions [111]. For instance, the pressure can be obtained as [110]:

$$P = \rho^2 \left(\frac{\partial a}{\partial \rho} \right)_T \tag{3.9}$$

or in reduced form [105]:

$$\frac{P}{\rho RT} = 1 + \delta \left(\frac{\partial \alpha^r}{\partial \delta} \right)_\tau \tag{3.10}$$

whereas the enthalpy h and entropy s can be obtained by the followings [105]:

$$\frac{h}{RT} = \tau \left[\left(\frac{\partial \alpha^0}{\partial \tau} \right)_\delta + \left(\frac{\partial \alpha^r}{\partial \tau} \right)_\delta \right] + \delta \left(\frac{\partial \alpha^r}{\partial \delta} \right)_\tau + 1 \tag{3.11}$$

$$\frac{s}{R} = \tau \left[\left(\frac{\partial \alpha^0}{\partial \tau} \right)_\delta + \left(\frac{\partial \alpha^r}{\partial \tau} \right)_\delta \right] - \alpha^0 - \alpha^r \tag{3.12}$$

Similarly, all the other thermodynamic properties can be obtained analytically [111], once the expressions for α^0 and α^r are defined. The availability of enough accurate data for the ideal-gas isobaric specific heat capacity $c_P^0(T)$, which are obtained experimentally, allow to formulate a correlation for $c_P^0(T)$ and derive the ideal-gas contribution (α^0) quite simply [92]; this can be expressed by the following:

$$\alpha^0 = -1 + \ln \frac{\rho T}{\rho_0 T_0} + \frac{h_0^0}{RT} - \frac{s_0^0}{R} + \frac{1}{T} \int_{T_0}^{T} \frac{c_P^0(T)}{R} \, dT - \int_{T_0}^{T} \frac{c_P^0(T)}{RT} \, dT \tag{3.13}$$

where ρ_0, T_0, h_0^0 and s_0^0 are parameters to be defined in order to set the desired values of enthalpy and entropy at the gas reference state [111].

The most demanding correlative process is instead for the residual term of the reduced Helmholtz energy [92], which is mostly formulated as a sum of contributes having different forms [111]; a meaningful example of the residual term formulation may be presented in relation for a low-GWP refrigerant, such as R-1234ze(E), for

which Akasaka and Lemmon [112] provide the following expression:

$$\alpha^r(\delta,\tau) = \underbrace{\sum_{i=1}^{K_1} n_i \tau^{t_i} \delta^{d_i}}_{\text{polynomial}} + \underbrace{\sum_{i=K_1+1}^{K_2} n_i \tau^{t_i} \delta^{d_i} \exp(-\delta^{e_i})}_{\text{exponential}} + \underbrace{\sum_{i=K_2+1}^{K_3} n_i \tau^{t_i} \delta^{d_i} \exp[-\eta_i(\delta-\varepsilon_i)^2 - \beta_i(\tau-\gamma_i)^2]}_{\text{Gaussian}} \quad (3.14)$$

where each type of term composing $\alpha^r(\delta,\tau)$ is identified. The number of terms K_1, K_2, K_3, coefficients n_i as well as exponents t_i, d_i, e_i, η_i, ε_i, β_i and γ_i are ascertained by fitting experimental data, typically using linear and non-linear least-squares fitting algorithms. The polynomial and exponential terms in Eq. (3.14) compose the conventional expression of modern fundamental EOSs that apply also to other fluids [112]; instead, the Gaussian bell-shaped (or Gaussian) term was introduced to better represent the region around the critical point, where the singularity of the fluid behavior is generally a concern for users of property correlations [90]; nevertheless, this class of equations is able to represent critical properties within the experimental uncertainties of most accurate experimental data [92].

In general, several different properties are fitted, including the vapor pressure, liquid and vapor density, speed of sound, heat capacities and critical parameters [90]. The selected data by the correlator to formulate the EOS, however, is a subset of the available experimental data for the specific refrigerant, which is identified for each property in the sets of values showing the lowest experimental uncertainty [110].

3.4 Equations of state and equipment simulation

3.4.1 Program software accounting for refrigerant properties

In the previous Section, the Helmholtz energy-based EOSs were discussed and said to be the most accurate models to calculate refrigerant properties. Because of the success of these methods, nowadays the most common libraries for thermophysical properties of fluids and fluid mixtures rely especially on this type of equations. Noteworthy, it is the case of REFPROP (acronym for "reference fluid properties"), a program developed by NIST [113], and the open-source software CoolProp [111]. The software can be queried by the user to obtain fluid properties, that are computed by the program with a specific EOS, for instance, at certain conditions of pressures

2: R1243zf: V/L sat. T=210, to 370, K

	Temperature (K)	Pressure (MPa)	Liquid Density (kg/m³)	Vapor Density (kg/m³)	Liquid Enthalpy (kJ/kg)	Vapor Enthalpy (kJ/kg)	Liquid Entropy (kJ/kg-K)	Vapor Entropy (kJ/kg-K)
1	210,00	0,014227	1189,3	0,79134	120,67	358,18	0,67200	1,8030
2	215,00	0,019325	1179,1	1,0529	126,42	361,44	0,69905	1,7922
3	220,00	0,025832	1168,7	1,3799	132,26	364,73	0,72588	1,7826
4	225,00	0,034019	1158,2	1,7836	138,19	368,06	0,75249	1,7741
5	230,00	0,044187	1147,6	2,2762	144,21	371,42	0,77890	1,7668
6	235,00	0,056664	1136,7	2,8710	150,32	374,79	0,80512	1,7603
7	240,00	0,071803	1125,7	3,5821	156,51	378,19	0,83116	1,7548
8	245,00	0,089985	1114,6	4,4249	162,80	381,59	0,85703	1,7500
9	250,00	0,11161	1103,1	5,4161	169,18	385,00	0,88274	1,7460
10	255,00	0,13712	1091,5	6,5735	175,66	388,41	0,90830	1,7426
11	260,00	0,16694	1079,6	7,9162	182,24	391,82	0,93372	1,7398
12	265,00	0,20156	1067,5	9,4651	188,91	395,22	0,95901	1,7376

(a)

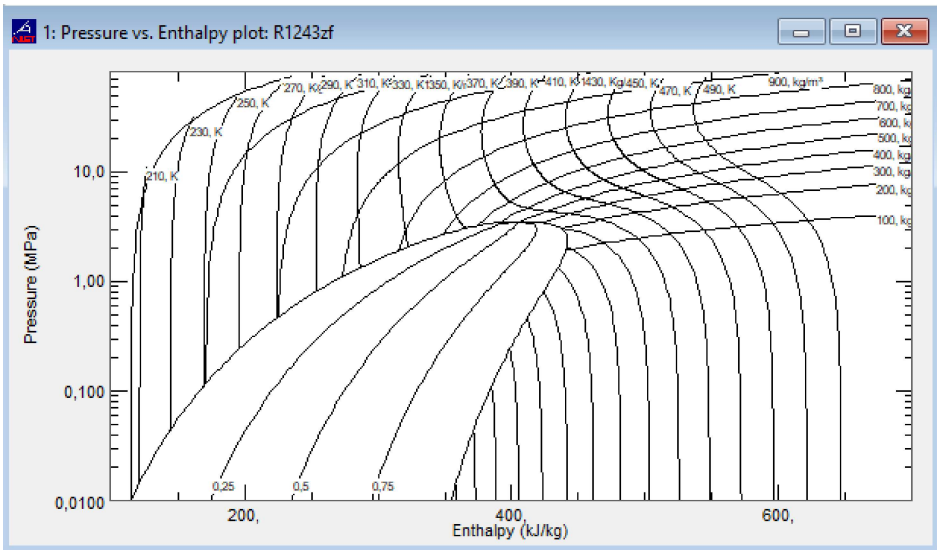

(b)

Figure 3.1: An example of refrigerant thermodynamic properties computed with REFPROP 10.0 in table (a) and plot (b) output.

and temperatures, and display them in tables and plots (see Figs. 3.1a and 3.1b). In other words, they do not collect datasets of fluid properties, but rather they include the most updated, reliable models to correlate and compute the properties that are available in the literature. Nowadays, a variety of applications including the chemical process industry and the RACHP sector rely heavily on these databases to perform cycle modeling and simulations, from the specific design optimization of components (for instance, in CFD simulation to optimize heat exchangers) to the overall process design. For this purpose, in particular, a number of simulation tools is available: as an example, the software provided by the NIST (called "CYCLE_D-HX" [114], whose GUI is depicted in Figs. 3.2a and 3.2b) is a semi-theoretical model for a vapor-compression cycle, that make use of REFPROP database to include the thermophysical properties of refrigerants within the simulation. The software allows to simulate the performance of a system with either pure refrigerants or refrigerant mixtures based on user-defined parameters, so that it is possible to evaluate an ample variety of operating conditions, from a single-stage vapor-compression cycle to multistage configurations, as well as to consider intermediate heat exchangers, economizers, pressure drops and compressor efficiencies, heat exchanger features and flow arrangements, etc. Indeed, this approach is fundamental for fine-tuning the design and the functioning of air conditioners, heat pumps and refrigerators, especially to maximize their energy efficiency and reduce their power consumption [115]. Other prominent program software with additional advanced features are Simulink® [116] and the tools provided by Modelica® [117].

3.4.2 The influence of equations of state on equipment design

Accurate refrigerant property measurements, advanced mathematical property correlations and process simulation have been discussed so far as a fundamental prerequisite for today's product innovation in the HVAC&R sector. While the accountancy of the effects thermophysical properties have in the design process is quite straightforward, and (as seen in Chapter 2) it is regularly included in the design methodology of key components such as heat exchangers, the use of different models to correlate and compute fluid properties has an impact on the equipment sizing and features that is still not thoroughly investigated.

Concerning this fact, in a recent study [118] the main performance indicators (COP, compressor displacement and heat exchanger capacity) of a hypothetical equipment based on a basic vapor-compression cycle and with refrigerant mixtures were calculated; the parameters were computed with fluid properties obtained with different EOSs and through specific mixture models. For the purpose, a fundamental multiparameter EOS in the Helmholtz energy formulation was used as a benchmark to compare the predictive accuracy of the different models (including the Soave-Redlich-Kwong and Peng-Robinson EOSs), that are expressed in terms

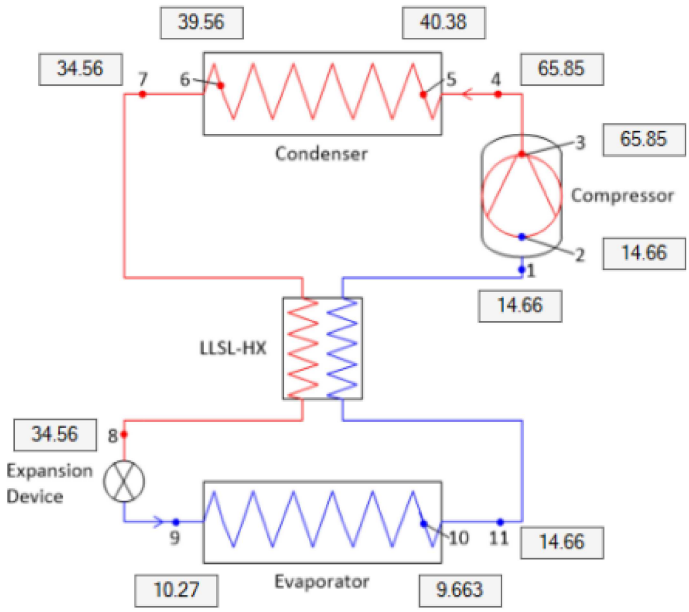

(a)

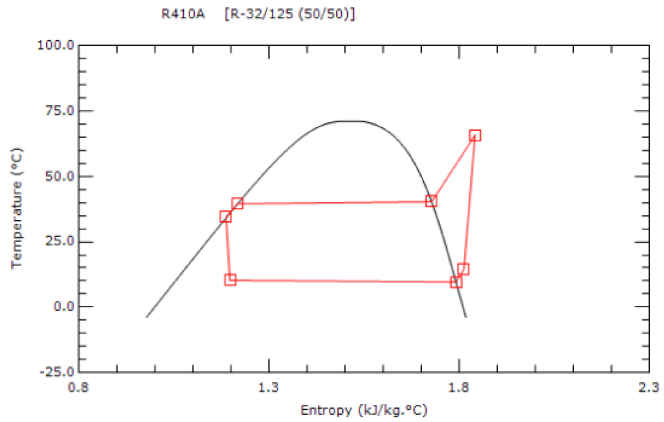

(b)

Figure 3.2: Simulation of a vapor-compression cycle with "CYCLE_D-HX", a program software developed by NIST, where Figure (a) shows a schematic representation of the equiment and Figure (b) depicts the simulated cycle on the T-s diagram.

of absolute average relative deviation (AARD):

$$AARD = \sum_{i}^{n} \frac{U_i}{n} \tag{3.15}$$

where n is the number of the refrigerant mixtures considered in the survey, whereas U_i is calculated as:

$$U_i = \frac{|Y_{\text{Ref}} - Y|}{Y_{\text{Ref}}} \cdot 100\% \tag{3.16}$$

that represents the relative deviation between the calculated parameter or thermodynamic property Y_i with different EOSs and the reference value Y_{Ref} computed with the reference EOS. Some results of the study are shown in Fig. 3.3a, Fig. 3.3b and Fig. 3.3c. In regard to the COP (Fig. 3.3a), the study showed that the highest AARD (AARD = 3.56%) (representing the worst property prediction) is achieved with cubic EOS (the "SRK;COS" model), whereas the better estimation is obtained with the "SAFT;SAFT" case, with AARD = 0.05%. The authors of the study point out that, despite the absolute deviations among all EOSs are relatively small, an improvement in COP estimation, even for a couple of percentage points, can be attributed to the choice of the model to compute the properties and parameters. For the UA-coefficient, useful in the design process of heat exchangers, Fig. 3.3b shows that large deviations among different models occur, with a maximum AARD of 14.31 %. In particular, it was found the EOS being the main reason for such deviations. In the case of the volumetric heat capacity (Q_{vol}), the choice of the EOS turned out to have a lower impact than that of the mixture model on the AARDs. These outcomes report that in the procedure of refrigerant screening to find the best alternative for a specific application, the EOS used to predict the refrigerant properties differently estimate key cycle parameters, and, as a consequence, the design of the equipment might be affected notably [118].

In summary, the availability of mathematical correlations for predicting thermophysical properties of refrigerants is of a great importance for engineering, but, although the state-of-the-art of property modeling is believed to be quite mature [111], new correlations are continuously being proposed and the existing ones are updated as soon as more accurate data are available. From the standpoint of transport properties, modeling is instead less developed, and the reasons are several: among all thermophysical properties, thermal conductivity, viscosity, and surface tension are affected by the largest uncertainties [70], in addition to the fact that typically there are less quality data for transport properties than for thermodynamic ones [34]; moreover, there is a lack of theory that is able to quantitatively represent transport properties of fluids over a full domain of temperatures and pressures, so the available tools for property prediction are empirical correlations or semi-empirical models [34]. Among others, the extended corresponding states (ECS) model has

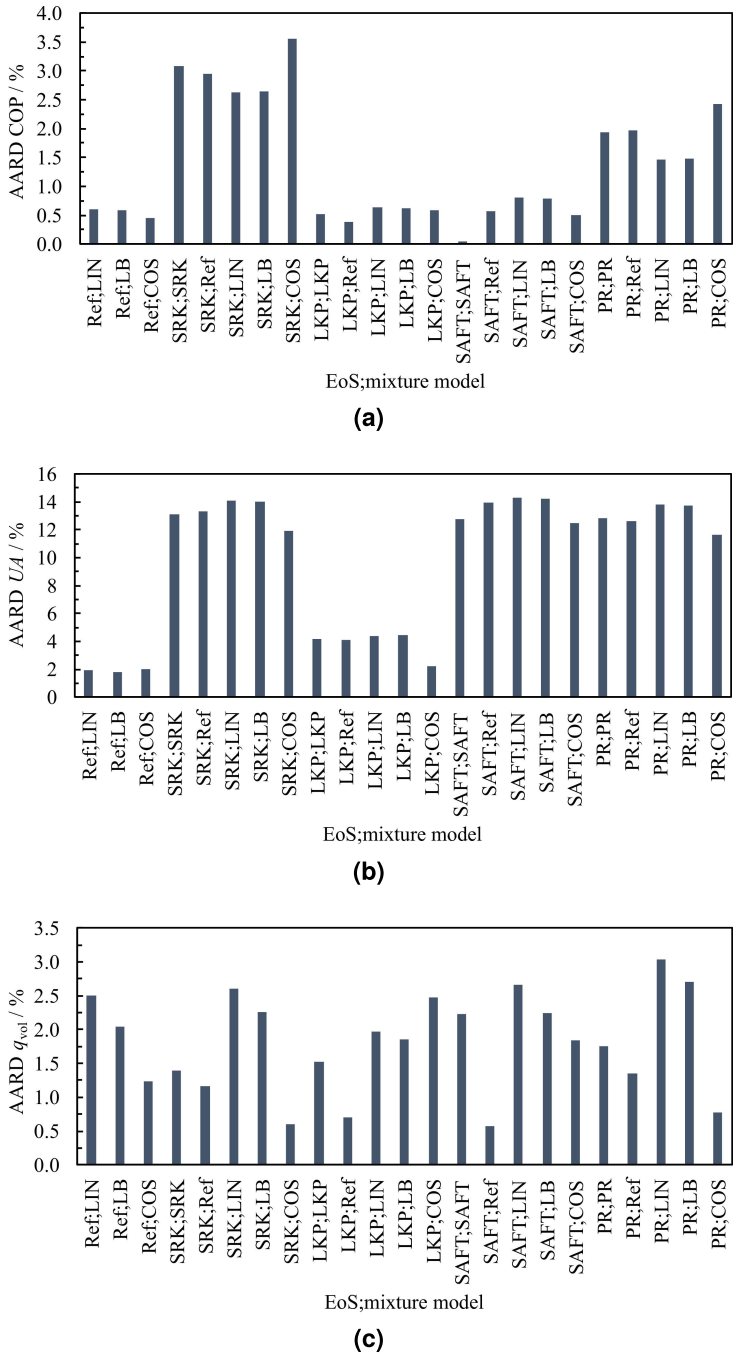

Figure 3.3: AARDs for the COP (a), UA-coefficient (b), and Q_{vol} for all considered EOS and mixture models, that are specified in the x-axis labels in the form "EOS;mixture model". Reprinted with permission from [118].

been successfully applied to pure fluids and mixture, but to formulate accurate equations for transport properties, the ECS model requires reliable correlations of thermodynamic properties (in particular, for temperature and density), i.e., equations of state [34, 111].

Chapter 4

Methods for measuring refrigerant properties

In the previous chapter, the categories of most widely adopted correlations for properties of refrigerants have been discussed, as well as their importance for the HVAC sector. The accuracy, consistency, and robustness of mathematical models are important to reliably correlate available data and make prediction of missing values, but these characteristics are affected to a great extent by the quality of experimental measurements: systematical errors in the measuring process propagate across the data fitting algorithms, and thus the final mathematical correlations implemented in simulation software will also be influenced [90].

Laboratories and companies all over the world have developed several different apparatus for measuring refrigerant properties. This chapter will review the state-of-the-art methodologies for measuring the main thermophysical properties of pure refrigerants, focusing primarily on the methods adopted at the Thermodynamic Properties Laboratory of ITC-CNR.

4.1 PvT properties

Among all properties of refrigerants that are required for building accurate property correlations, density is a key information for HVAC&R engineering. Density is generally required at different *P-T* coordinates in the subcooled (compressed) liquid, saturated vapor and superheated regions of the phase diagram. For this reason, density measurements are often referred to as "PvT properties measurements", or equivalently as $P\rho T$ properties measurements", where v refers to the specific volume and ρ to the density of the refrigerant. In particular, as discussed in Chapter 2, refrigerant density affects the pressure drop as well as the heat transfer process in vapor-compression systems, but its data are necessary also to implement

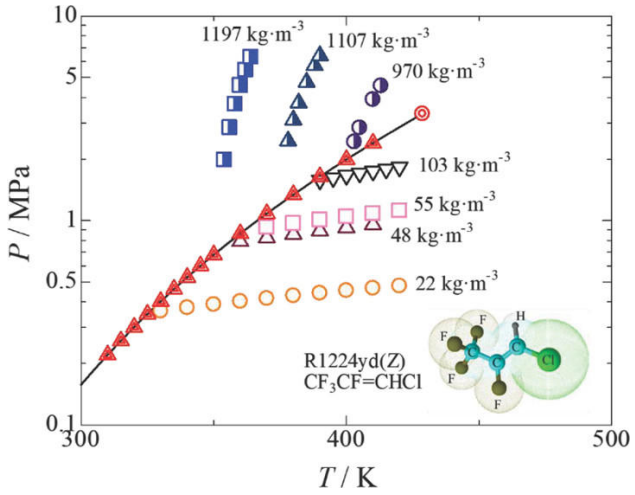

Figure 4.1: *PvT* property data for R-1224yd(Z): the red marks represents the experimental measurements of density along the liquid-vapor saturation curve (in black), whereas the data above and below the curve are the densities in the compressed liquid and superheated vapor region, respectively; the red mark at the top end of the curve depicts the data at the critical point. In the figure, different colors and signs are used to group the data based on the distinct isochores (or equivalently, constant density) along which the measurements are performed. Reprinted with permission from [119].

correlations for other important properties, including the viscosity and thermal conductivity [115]. In order to have a quick overview of the amount of experimental measurements and the fluid domain in which studies have been performed, available *PvT* data for a specific refrigerant are typically represented in *P-T* diagrams, such as the one depicted in Fig. 4.1.

4.1.1 Vibrating-tube densimeter

Density is an intrinsic properties of matter that is usually measured by densimeters of based on different techniques. For refrigerants in the liquid, vapor, and supercritical states it can be measured with a vibrating-tube densimeter. The working principle of this instrument lies on a constant relation, at fixed pressures P and temperatures T, between the density ρ of the fluid contained inside of a hollow, stainless-steel, U-shaped tube, and the vibration period π of the tube filled with the fluid, that acts as a mass-spring oscillator. A representation of the setup for the vibrating-tube densimeter available at ITC-CNR is provided in Fig. 4.2. A refrigerant sample is charged in the densimeter through a circuit of stainless-steel tubes from an external refrigerant cylinder.

Inside the densimeter, the U-shaped tube is supported at each of its ends, and it

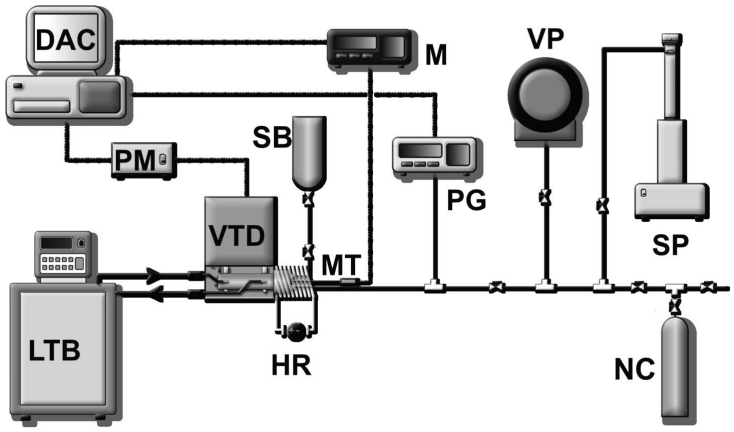

Figure 4.2: A scheme of the vibrating-tube densimeter apparatus used at ITC-CNR. VTD, vibrating tube densimeter; PM, frequency meter; DAC, data acquisition and control; MT, temperature measurement sensor; M, multimeter; LTB, liquid thermostatic bath; HR, heating resistance; SB, sample bottle; PG, pressure gauge; VP, vacuum pump; SP, syringe pump; NC nitrogen cylinder. Reprinted with permission from [120].

is "excited" mechanically so that the system, consisting of the tube and the liquid contained therein, vibrates at its natural frequency [121]. A preliminary calibration, however, is needed to determine the natural frequency of the hollow tube under vacuum conditions, and the relation between the resonance frequency and the known density of a reference fluids, such as water, in a range of temperatures and pressures that will encompass that of the investigated refrigerant. In the case of the setup depicted in Fig. 4.2, the pressure is measured by a differential pressure gauge, whereas the temperature is tested with a PT 100 Ω resistance thermometer (MT). The pressure is controlled by means of a syringe pump, whereas the temperature is reached and maintained at the desired value with an external thermostatic bath, but it can be more finely adjusted by an electric heating resistance. Overall, the temperature is controlled by means of a Proportional-Integral-Derivative (PID) control system. The densimeter is connected to a device for measuring the oscillating period; this, along with the temperature and pressure, is acquired with a dedicated program software in the computer (DAC). The experimental density ρ of the fluid is then obtained by the following calibration equation:

$$\pi^2 = (aP^2 + bP + c)\rho + B \tag{4.1}$$

where π is the measured oscillation period and P is the pressure. Parameters a, b, c, and B are determined through the preliminary calibration phase. In particular, a, b, c are regressed by correlating the known density of water at different pressures and temperatures with the measured oscillating period π, whilst B depends only on the experimental oscillating period measured when the instrument is under vacuum

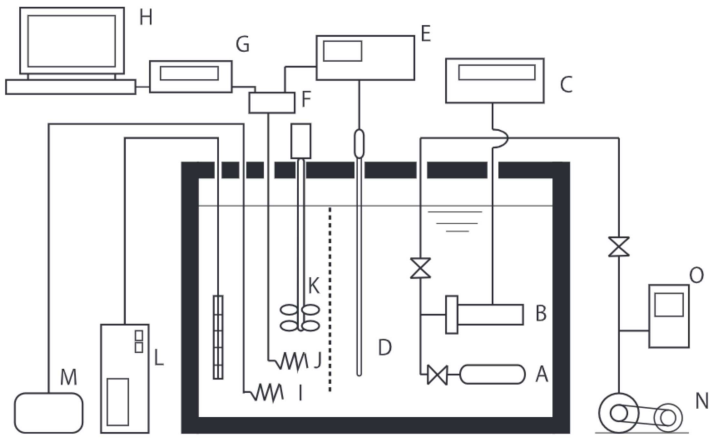

Figure 4.3: A schematic representation of the experimental isochoric apparatus. (A) sample vessel; (B) pressure transducer; (C) pressure indicator; (D) 25 Ω standard platinum resistance thermometer; (E) thermometer bridge; (F) PID controller; (G) digital multi meter; (H) computer; (I) main heater; (J) sub heater; (K) stirrer; (L) cooler; (M) voltage transformer; (N) vacuum pump; (O) vacuum indicator. Reprinted with permission from [123].

conditions [120, 122].

4.1.2 Isochoric apparatus

In order to measure the $P\rho T$ properties by fixing the density (or equivalently, the specific volume) and varying the P-T coordinates, other methods are adopted. Among others, the isochoric method is widely employed for measuring single phase density correlations. The setup used by Higashi et. al [123] (represented in Fig. 4.3) will be here discussed.

A definite mass of a refrigerant sample is charged in a stainless-steel pressure vessel, that is immersed in a thermostatic bath containing a silicon oil. A resistance thermometer is placed in proximity of the steel vessel to test the fluid temperature (when in thermal equilibrium), whereas a pressure transducer is connected directly to the vessel inlet. Both the pressure and temperature sensors are connected to external signal acquisition units. The bath temperature is maintained at the desired value by means of a stirrer, two heaters, a cooler, and a PID system. Prior to the measurements with the fluid under investigation, the inner volume of the vessel, the volume of the pressure transducer as well as that of the tubing are evaluated with a reference fluid in a range of temperatures, that allows to express the volume as function of the temperature. Therefore, because the refrigerant mass is constant, and the volume undergoes minor changes only, overall the density (or the specific volume) is maintained approximately constant. As a consequence, by varying the

temperature, the pressure changes along a specific isochoric curve.

The experimental measurements of the refrigerant density in the liquid or vapor phase are therefore obtained at various temperatures and pressures of the refrigerant by calculating the ratio between the known refrigerant mass and the total inner vessel volume, dedicated tubing included [123, 124].

4.2 Saturated densities and critical properties

The measurements of saturated liquid and vapor densities are typically determined through different procedures. In general, the densities along the saturation curve can be obtained graphically from the intersection of the vapor pressure curve and the isochores of $P\rho T$ for available experimental data [123] (for reference, see Fig. 4.1): specifically, the break point of both the liquid phase and vapor phase isochores on the vapor pressure curve provides the saturated liquid and vapor densities, as shown in Fig. 4.4. Differently, as it is generally too complicated to distinguish the break points of isochores near the critical point, in this region the density measurements can be performed with the equipment represented in Fig. 4.5, through the technique referred to as the "visual observation of the liquid-vapor meniscus disappearance". In the apparatus, three stainless-steel, high-pressure vessels are installed inside of a thermostatted silicone-oil bath. The optical cell, whose inner volume is measured by charging a reference fluid (such as water) at room temperature, has two windows that allows to observe the refrigerant behavior contained therein. The expansion vessel and the supplying vessel are used to modify the refrigerant density being studied in the optical cell without charging further refrigerant. The temperature of the sample is measured by a platinum resistance thermometer in the vicinity of the optical cell, and it is controlled by means of two heaters, linked to an external PID system. The refrigerant density can thus be computed from the sample mass and the inner volume of the three vessels for each measurement [123, 125]. The meniscus position is then observed at different temperature and pressure: by means of the phenomena of the meniscus appearance and disappearance, it is possible to known whether the fluid is in the liquid, vapor, or in saturation state, and thus to calculate the density in that conditions. The critical parameters (temperature, pressure, and density) can also be determined by the visual observation of the liquid-vapor meniscus disappearance [119, 123, 125]. For the critical region, in particular, property modeling might often experience difficulties in representing data accurately, due to the fact that there the fluid density varies much more intensely by the temperature and pressure than elsewhere. Experimental measurements of critical properties, therefore, may overcome that issue, providing in general more reliable data than that predicted with property models [126].

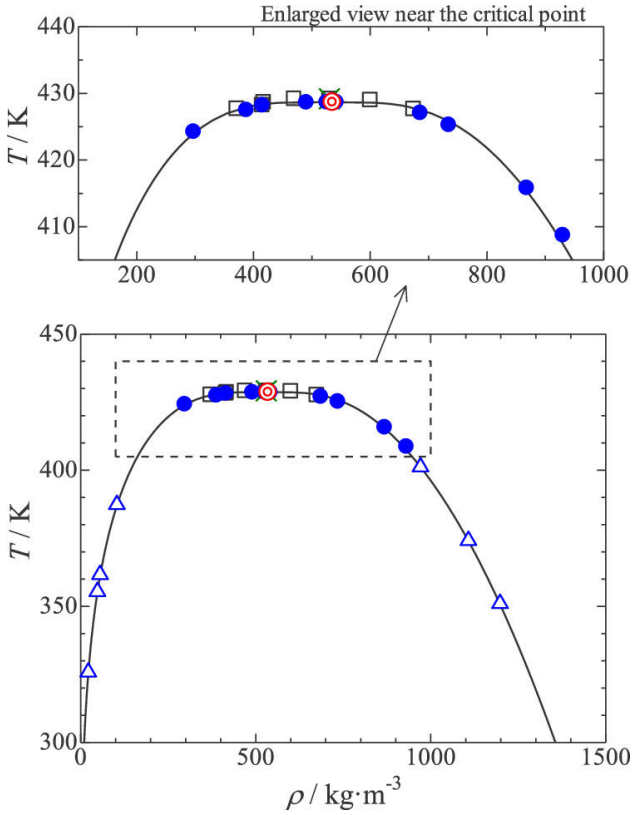

Figure 4.4: Saturated vapor and liquid densities for R1224yd(Z). Data outside the dashed-line box are obtained by the intersections of the liquid-vapor coexistence curve and the isochores of the $P\rho T$ data, whilst properties inside the box are mostly measured by the visual observation of the meniscus disappearance. Red symbol ◎ is the critical point. Reprinted with permission from [119].

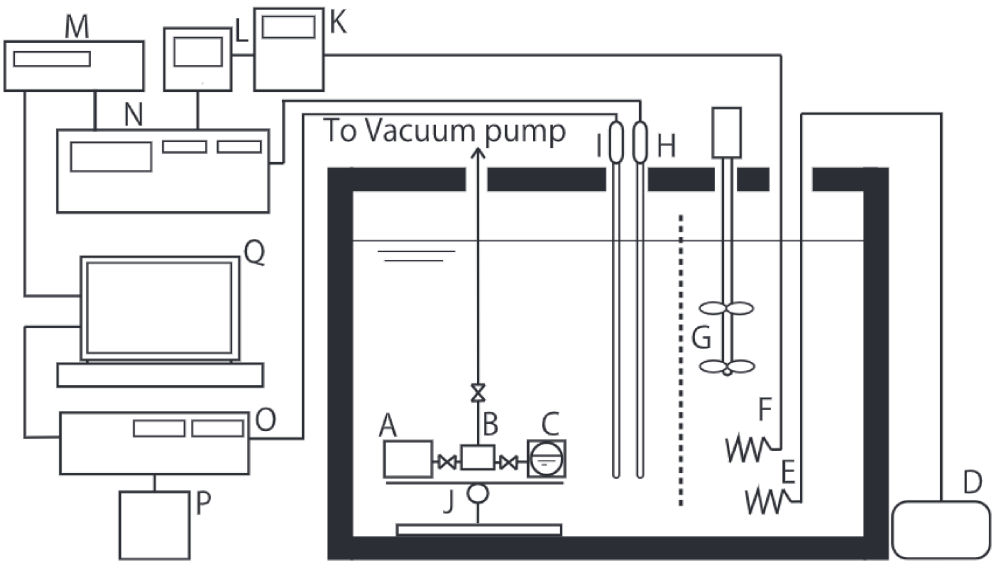

Figure 4.5: An experimental equipment for measuring saturated densities and the density at the critical point: (A) supplying vessel; (B) expansion vessel; (C) optical cell; (D) voltage transformer; (E) main heater; (F) sub heater; (G) stirrer; (H, I) 25 Ω standard platinum resistance thermometer; (J) rocking unit; (K) PID controller; (L) voltage output setting unit; (M) digital multi meter; (N, O) thermometer bridge; (P) 25 Ω standard resistance; (q) computer; (v) high-pressure valves. Reprinted with permission from [123].

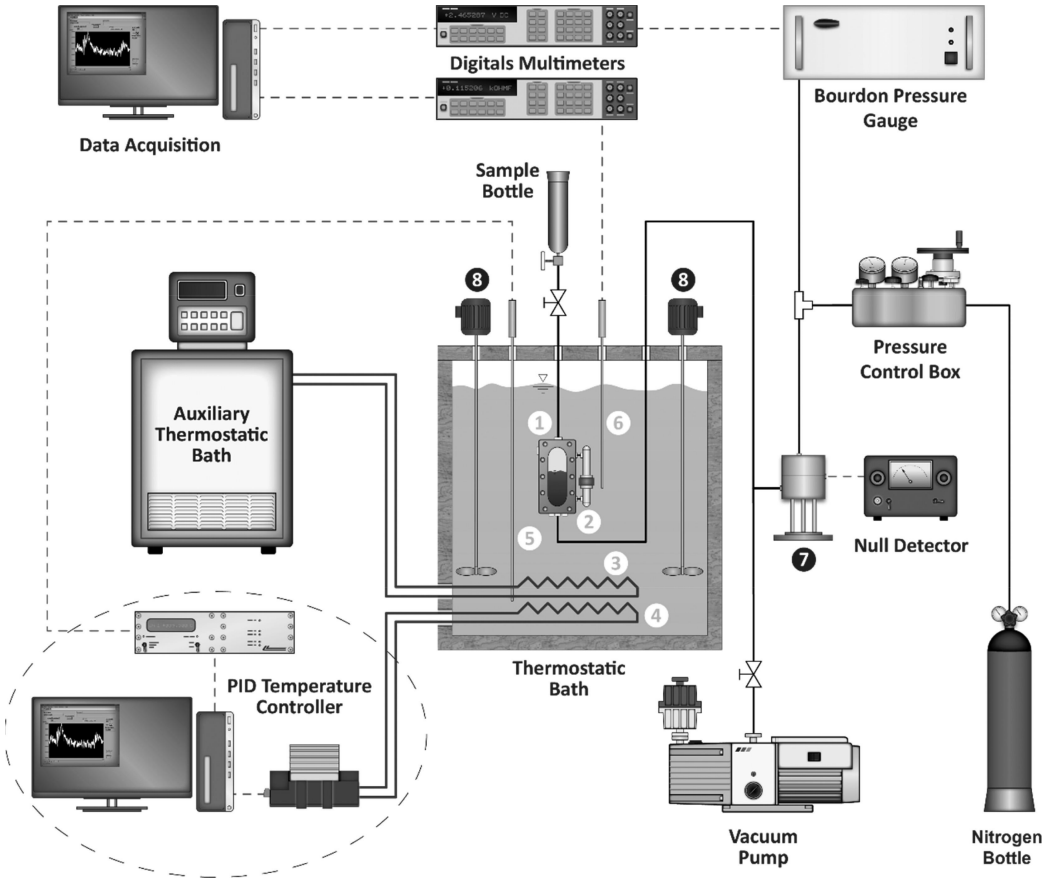

Figure 4.6: Schematic representation of the VLE apparatus in use at the Thermodynamic Properties Laboratory of ITC-CNR: 1, equilibrium cell; 2, magnetic pump; 3, cooler; 4, ohmic heater; 5, temperature control sensor; 6, measurements thermometer; 7, diaphragm; 8, stirrers. Reprinted with permission from [127].

4.3 Saturated vapor pressure

The formulation of equations of state and other property models requires another refrigerant property: the saturated vapor pressure (or vapor pressure) [54].

At ITC-CNR, experimental vapor pressure measurements are conducted with a vapor-liquid equilibrium (VLE) apparatus, represented in Fig. 4.6. The equipment consists of a windowed, stainless-steel cell, with an inner volume of around 50 cm^3. Connected to the cell, a magnetic pump allows the vapor to flow through the liquid, so as to speed up the reaching of the equilibrium. Both the cell and the pump are installed inside of a thermostatic bath, whose inner volume is of about 0.1 m^3, ensuring a thermal stability of ± 1 mK. Two stirrers are adopted to promote temperature uniformity throughout the thermostatic bath. The temperature is

measured with a 100 Ω platinum resistance thermometer, whereas for pressure a pressure controller based on a quartz bourdon tube reference sensor is used. Both the temperature sensor and the pressure controller are connected to two digital multimeters, that sample the temperature and pressure, and send the data to an external acquisition unit [127].

Prior to the experimental measurements, the cell and the piping are purged with nitrogen, and put under vacuum to remove any undesired leftovers. Successively, the cell is charged with the refrigerant sample for the experimental measurements. The system is controlled in temperature by means of two heaters: one is powered by a fluid, that is heated or cooled by an additional, external thermostatic bath, whereas the other is an electrical resistance. The pressure gauge senses the pressure at one side of a diaphragm, whilst the other side is connected to the cell. In this way, the pressure controller is kept isolated from the refrigerant. When the temperature proves stable for sufficient period of time, the pressure at the nitrogen side is adjusted to counterbalance the pressure at the refrigerant side. A pressure control box and a null detector are used for the purpose. As soon as the pressure also stabilizes, multiple vapor pressure measurements are performed with time. The value of vapor pressure for a specific temperature is then considered to be the average of multiple vapor pressure measurements [127].

4.4 Specific heat capacity

Different types of calorimeters are commonly used to measure the isobaric heat capacity and the isobaric heat capacity, both essential properties for evaluating the accuracy of an equation of state, and for calculating the enthalpy and entropy, that are fundamental in engineering calculations and system simulations [128].

4.4.1 Isobaric specific heat capacity

For the experimental measurements of the constant-pressure specific heat capacity, the adiabatic steady-flow calorimeter is among the most employed techniques [128]. In the apparatus used by Sheng et al. [129], represented in Fig. 4.7, the main components are a thermostatted liquid bath, a calorimetric cell, a flow system, and a data acquisition unit. Noteworthy, apparatus has been built to measure the liquid specific heat capacity, but similar flow calorimeters has been used to measure the c_p also in the vapor phase as well as in the supercritical region [129].

The experimental procedure consists on a refrigerant sample flowing with a constant mass flow rate inside the thermostatic bath, so as to reach the desired temperature at a target pressure. Successively, the refrigerant enters the calorimetric cell at an inlet temperature and exits with an outlet temperature. Between the inlet

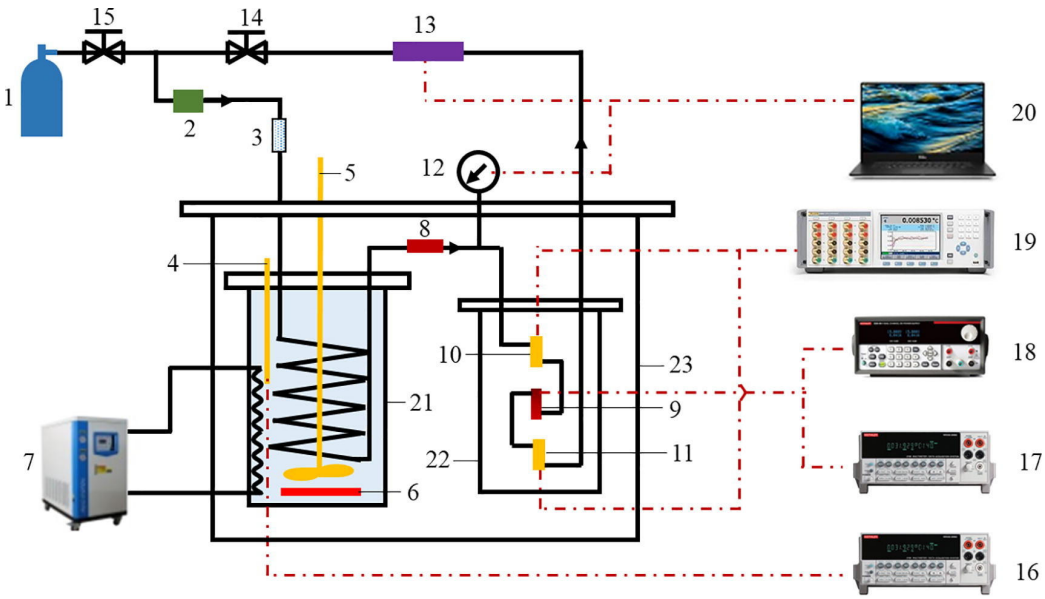

Figure 4.7: Schematic diagram of the apparatus for the adiabatic steady-flow calorimeter: 1, sample bottle; 2, double plunger-type pump; 3, filter; 4, 100 Ω platinum resistance thermometer; 5, magnetic stirrer; 6, heater; 7, refrigerator; 8–9 microheater; 10–11, 1000 Ω platinum resistance thermometer; 12, digital pressure transducer; 13, mass flow meter; 14–15, needle valve; 16–17, Keithley 2002 multimeter; 18, DC power supply; 19, Fluke 1594A super thermometer; 20, computer; 21, thermostatic bath; 22, calorimetric cell; 23, vacuum cylinder. Reprinted with permission from [129].

and the outlet, the fluid temperature slightly increases due to a microheater. The mass flow rate, the heating voltage, the pressure, and the two temperatures are then acquired.

The experimental isobaric specific heat capacity c_p is calculated with the relation:

$$c_p = \frac{P_1}{q_m \cdot \Delta T} = \frac{\alpha P}{q_m \cdot (\Delta T_h - \Delta T_b)} \tag{4.2}$$

where P_1 is the actual thermal power absorbed by the fluid, that differs from the electric power P provided by the microheater; coefficient α accounts for such temperature-dependent deviation, and it is measured beforehand with reference fluids; q_m is the refrigerant mass flow rate; ΔT_b is calculated as the temperature difference the fluid experiences without heating in a preliminary test, whereas ΔT_h is the temperature rise measured between the inlet and the outlet of the calorimetric cell for the actual experimental measurements [129].

4.4.2 Isochoric specific heat capacity

Experimental constant-volume specific heat capacity of refrigerants is typically determined with an adiabatic calorimeter with intermittent heating [129]. Fig. 4.8 depicts an apparatus used by Zhong et al. [128] to implement the experimental method. A cell (called "bomb") contains a determined mass of refrigerant sample, and it is installed inside a chamber (inner), in turn displaced inside another chamber (outer). By evacuting the chambers, in addition to the use of two adiabatic shields, internal heat losses are minimized. Similarly to the determination of the isobaric specific heat capacity, the principle is to measure the temperature lift the fluid undergoes by means of a heat absorption; in this case, however, the fluid is not continuously circulated, but rather confined within the bomb, whose volume has to be measured, and expressed as a function of temperature and pressure to account for slight expansions.

The experimental isochoric specific heat capacity is calculated as:

$$c_v = \frac{Q - Q_0 - W_{Pv}}{m \cdot \Delta T} \tag{4.3}$$

where Q is the electric energy provided for a certain amount of time to the bomb by the DC power unit, with an electrical resistances applied to the outer side of the cell; Q_0 is the thermal energy supplied to the empty bomb, that is determined prior to the c_v measurements of the investigated fluid; m is the refrigerant sample mass, and ΔT is the temperature difference measured by the thermometer; W_{Pv} is the work related to the cell expansion, calculated separately by a function that consider the temperature and pressure contributes [128].

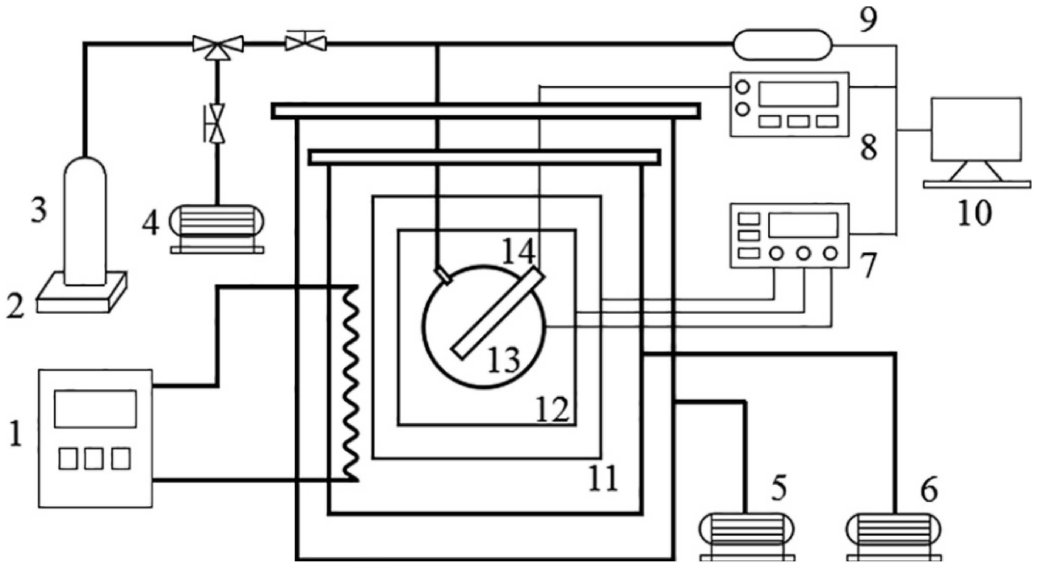

Figure 4.8: Representation of an equipment for measuring the isochoric specific heat capacity: 1, refrigerating machine; 2, scale; 3, gas cylinder; 4–6, vacuum pump; 7, DC power system; 8, multimeter; 9, pressure transducer; 10, computer; 11, outer adiabatic shield; 12, inner adiabatic shield; 13, bomb; 14, thermometer. Reprinted with permission from [128].

4.5 Speed of sound

Amid other thermophysical properties, sound speed of refrigerants is essential for the development and verification of equations of state. The ability to experimentally determine the speed of sound with high accuracy is also fundamental to derive those properties that cannot be measured directly, especially the ideal-gas specific heat capacity [90, 130].

Sound speed of fluids has been mostly measured with the method of acoustic resonators, which may typically be implemented with two different shapes: spherical, that boast precise measurement capabilities, and cylindrical. The latter exhibits lower qualities overall, but are easier to fabricate and assemble [131].

The apparatus used in a study by Peng et al. [130] for measuring speed of sound is depicted in Fig. 4.9. It consists mainly of a cylindrical resonator, a frequency measurement unit, a thermostatic bath, measurement systems for pressure and temperature, a vacuum system, and a data acquisition unit. The cylindrical resonator has a specific inner length and radius. Overall, the cavity dimension is related to the temperature and pressure variables, based on preliminary tests conducted with reference fluids, for which accurate sound speed data are available. Both heads of the cylinder consist of thin diaphragms, on each of which a sonic generator and a

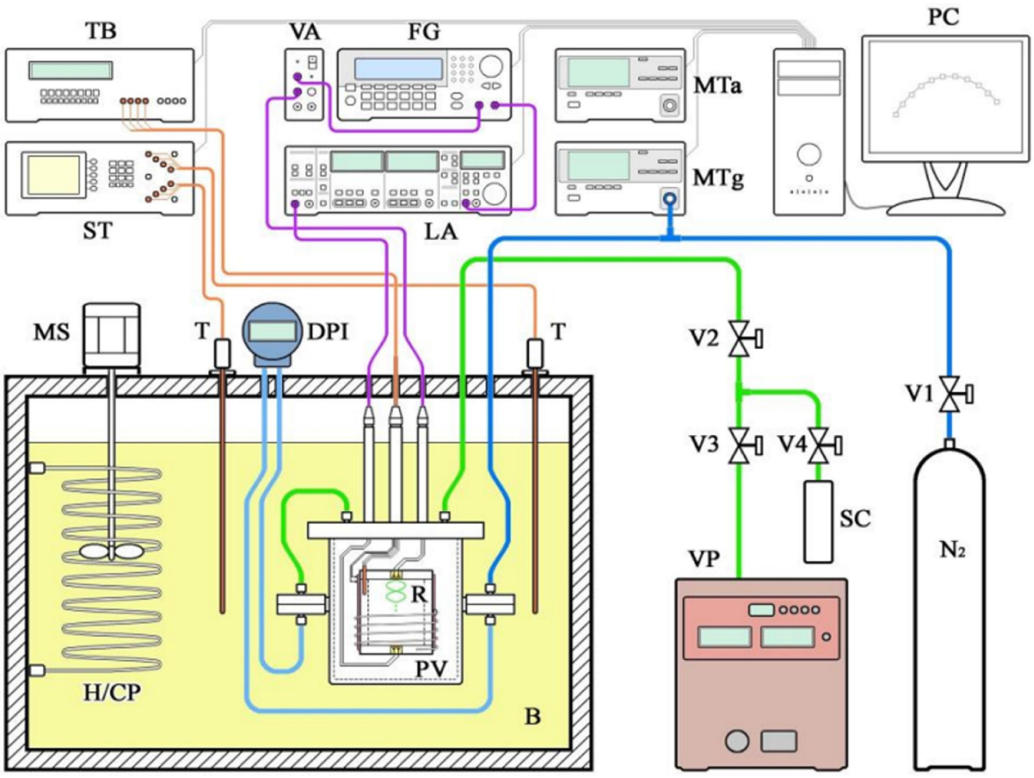

Figure 4.9: An equipment for the acoustic cylindrical resonator: B, thermostatic bath; DPI, differential pressure transducer; FG, function generator; H/CP, heater/cooler; LA, lock-in amplifier; MS, mechanical stirrer; MTa, absolute pressure digital manometer; MTg, gauge pressure digital manometer; PC, personal computer; PV, pressure vessel; R, resonator; SC, sample cylinder; ST, super thermometer; T, platinum resistance thermometer; TB, thermometer bridge; VA, voltage amplifier; VP, vacuum pump; V1 to V4, valves. Adapted with permission from [130].

sensor are connected.

For the measurements of resonance frequencies, a standard sinusoidal wave is generated by the function generator, and transmitted to the sonic generator applied to the upper diaphragm of the resonator. That produces a mechanical vibration, that in turn generates a sound wave within the fluid. To the other side of the resonator, the sound wave is detected and converted back to a mechanical vibration by the diaphragm, whose frequency is measured by the sensor, processed by an amplifier, and acquired by the data acquisition unit. The speed of sound is then calculated using an expression that considers the sampled resonance frequency, and other parameters, including characteristics of the waves and the resonator length and inner radius [130, 131].

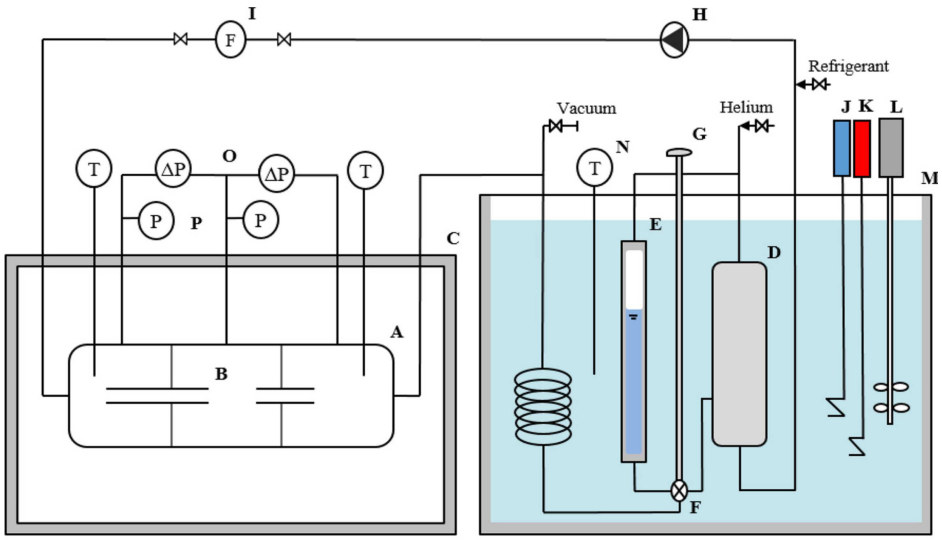

Figure 4.10: Schematic representation of a tandem capillary tube viscometer: A, viscometer vessel; B, capillary tube; C, electric heater; D, pressure vessel; E, sight glass; F, 3-way valve; G, knob of 3-way valve; H, nonpulsation pump; I, Coriolis flowmeter; J, cooler; K, heater; L, stirrer; M, thermostatic bath; N, thermometer; O, differential pressure gauge; P, pressure gauge. Adapted with permission from [133].

4.6 Viscosity

Another important transport property of refrigerant for the design process of HVAC systems is viscosity. As discussed in Chapter 2, it relates to the refrigerant flow behavior by contributing to the pressure drop, but it also influences the convective heat transfer, thus the overall heat exchange in the equipment.

Different methods are currently employed to measure viscosity of refrigerants, that include vibrating-wire viscometer, rotating viscometer, surface light scattering viscometer, and tandem capillary tube viscometer. The tandem capillary tube is used to measure dynamic viscosity of refrigerants either in the liquid or vapor state, and it is among the most accustomed techniques based upon Hagen-Poiseuille theory [132]. An illustrative example of this apparatus, sourced from a study by Alam et al. [133], is represented in Fig. 4.10. In this setup, a mass of refrigerant sample is charged within a closed circuit, and circulated by a nonpulsation pump with a low flow rate, measured by a flowmeter, so that the fluid exhibits a laminar flow. In vessel A, the refrigerant flows in two different-length capillaries, connected in series. By means of the thermostatted bath, the experimental temperature is controlled and maintained at the desired value, whereas a helium cylinder connected to the piping allow to set the pressure. For measuring the temperature, a PT 100 Ω resistance thermometer is employed, while pressure transducers are used to obtain

pressure measurements. Because of the fluid passing through the capillary tubes, a pressure drop will occur in each. These pressure drops are measured by a differential pressure gauge. Therefore, given the mass flow rate q, the inner radiuses a_s and a_l, lengths L_s and L_l, pressure drops ΔP_s and ΔP_l for the shorter (s) and longer (l) capillary tube, the experimental (dynamic) viscosity is determined by the following:

$$\mu = \frac{\pi(a_l^4 \Delta P_l - a_s^4 \Delta P_s)}{8q(L_l - L_s)} \tag{4.4}$$

As seen with the appartus for other thermopysical properties, preliminary measurements are performed with a reference fluid to verify the reliability and stability of the experimental equipment [133].

4.7 Surface tension

In Chapter 2, surface tension is discussed as a property of refrigerants that affects the phase change processes, and thus influences the heat exchange phenomena.

A conventional approach for measuring the surface tension is the differential capillary rise method, that can be executed with an apparatus such as the one represented in Fig. 4.11, sourced from a study by Liu et al. [134]. The key components in the equipment are three glass capillaries, with different inner diameter, installed vertically inside a pressure vessel, wherein the liquid refrigerant is charged. The pressure vessel is placed inside a thermostatic bath, filled with a propylene glycol aqueous solution, to set the system at the desired temperature and control the thermal stability. For the purpose, a chiller and an electric heater are employed to control the solution temperature through a PID controller, whereas the temperature is measured in the vicinity of the pressure vessel by means of a PT 100 Ω resistance thermometer. Additionally, in order to maintain an uniform temperature throughout the thermostatted bath, three stirrers are used.

Surface tension is determined experimentally under saturation conditions by measuring the differential capillary heights, using a microscope and a CCD camera (an image example taken by the camera is represented in Fig. 4.11). The meniscus bottom is considered as the reference point for experimental measurements; therefore, the differential height between two meniscus bottoms is referred to as Δh_m. By using the methodology of Rayleigh, Δh_m is corrected, resulting in the following:

$$\Delta h_c \approx \Delta h_m + \frac{(r_2 - r_1)}{3} \tag{4.5}$$

where r_2 and r_1 are the inner radiuses of two capillaries among the three available (assuming $r_2 > r_1$), as described in Fig. 4.11. The corrected differential height Δh_c

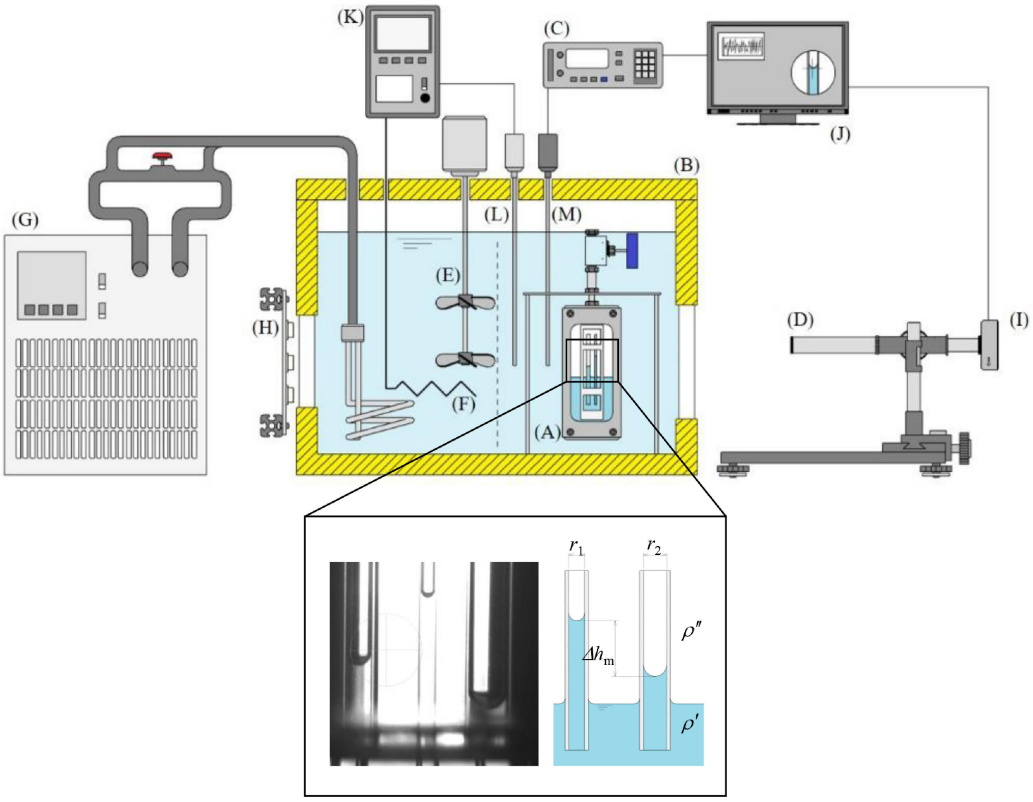

Figure 4.11: A schematic view of experimental setup for the differential capillary rise technique, and a typical CCD image to determine the differential capillary height. The equipment consists of: A, pressure vessel; B, thermostatic bath; C, thermometer bridge; D, traveling microscope; E, stirrers; F, electric heater; G, chiller; H, LED illumination; I, CCD camera; J, computer; K, PID temperature control system; L, sheathed thermocouple; M, PT 100 Ω resistance thermometer. Reprinted with permission from [134].

is used to calculate the capillary constant a^2 as follows:

$$a^2 = \frac{g\Delta h_c}{g_n(1/r_1 - 1/r_2)} \tag{4.6}$$

where g is the local gravitational acceleration (that is, the gravitational acceleration where surface tension is measured) and g_n is the normal gravitational acceleration ($g_n = 9.806\,65\,\mathrm{ms}^{-2}$). The experimental surface tension measurements are then provided by the relation:

$$\sigma = \frac{g_n(\rho_L - \rho_V)a^2}{2} \tag{4.7}$$

that requires the data for the saturated liquid and vapor densities ρ_L and ρ_V. The use of three capillaries allow to calculate an average value of surface tension obtained by three, different combinations of capillaries [134].

4.8 Thermal conductivity

Heat transfer capabilities of refrigerants are closely related to their thermal conductivity, as described in Chapter 2. Therefore, quality data of the property are fundamental to accurately simulate heat exchange phenomena involved in the vapor-compression cycle, and optimize the design of components.

A conventional approach to measure the thermal conductivity of refrigerants is the transient hot-wire method (THW). It is a common belief that first applications of this technique began in 1931, with studies by Stâlhane and Pyk [135] on thermal conductivity of solids, powders, and some liquids. However, according to Assael et al. [136], pioneer implementations of this technique can be dated back to 1780, at a time when gas capabilities to conduct heat was still controversial. Nowadays, the transient hot-wire method finds widespread use for measuring thermal conductivity of liquid and gases, as well as nanofluids, melts, and solids. In addition to such an ample variety of applications, the strength of this technique lies in its very low experimental uncertainty, that apart from the troublesome critical region and low pressure region of gases, can be well below 1 % for thermal conductivity measurements for gases and liquids [136].

In the Thermodynamic Properties Laboratory at ITC-CNR, the transient hot-wire technique is used with the equipment represented in Fig. 4.12a. For measuring the thermal conductivity of a refrigerant, a sample of the same fluid is charged in a stainless-steel pressure vessel, so that the wires are completely in contact with the fluid, whether it is in the vapor or liquid state. The pressure vessel is installed inside another vessel; the latter is filled with a liquid, that is maintained at a desired temperature (with maximum fluctuation of 0.02 K) by means of an external thermostatic bath. It is important for the refrigerant sample to reach and maintain

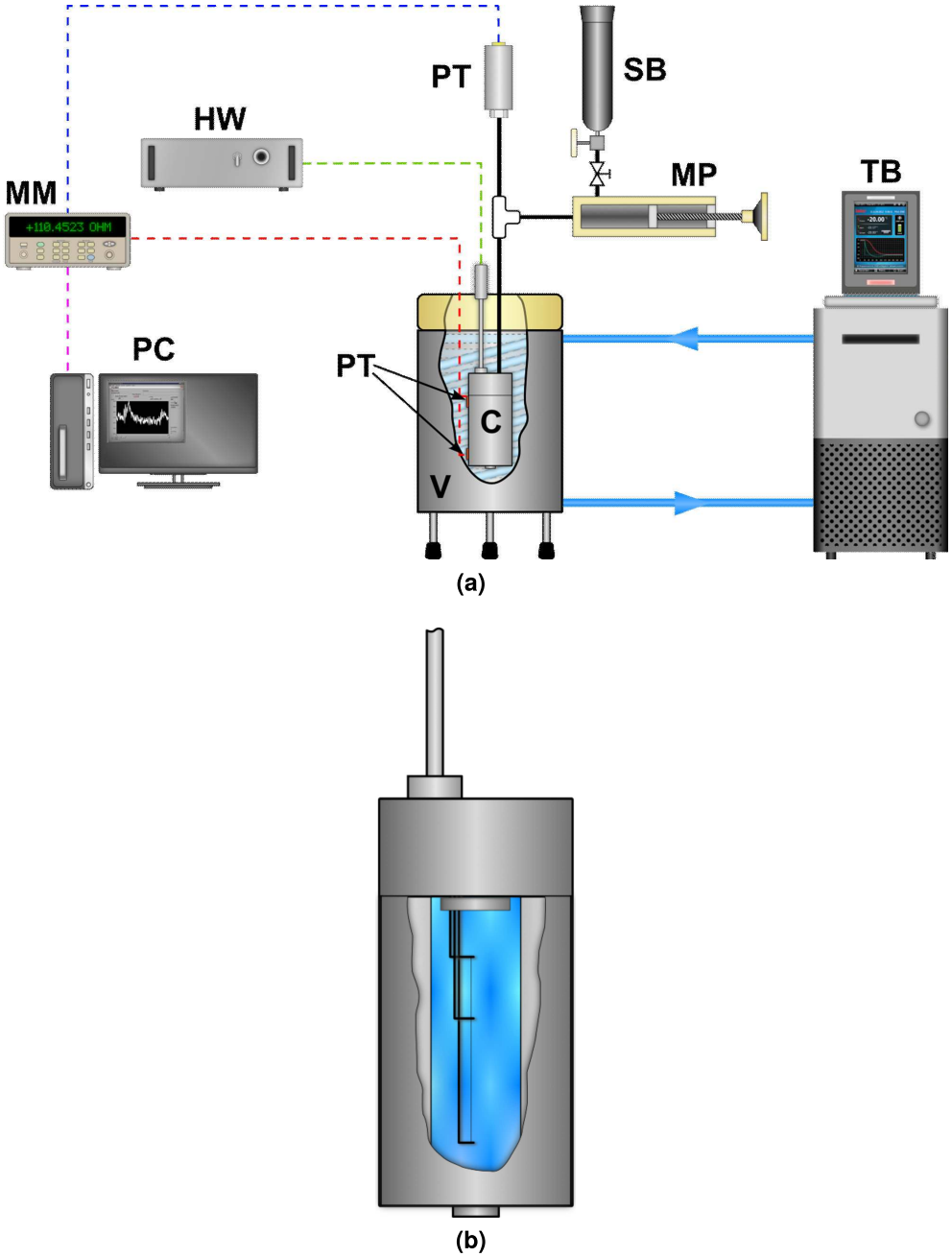

Figure 4.12: The THW apparatus (a) in use at ITC-CNR, and a close-up of the hot-wire sensor in cutaway view (b) [137]: MM, multimeter; HW, Hot Wire instrument, PC, personal computer; C, pressure cell; TS, PT 100 Ω thermometers; V, pressure vessel; SB, sample bottle; MP, manual press; TB, thermostatic bath.

an uniform temperature all across the pressure vessel. For the purpose, two PT 100 Ω resistance thermometers are in contact with the pressure vessel, and measure the temperature at the top and the bottom of it, respectively; the experimental temperature value is then given by the average of the two temperatures. A manual press is connected with piping to the upper side of the pressure vessel, to set the pressure at the desired value, measured by a pressure transducer connected to the same piping. Therefore, thermal conductivity is measured for a fixed temperature and pressure by the how-wire sensor, the key component of the apparatus (Fig. 4.12b). It consists of two Tanatalum wires having same diameter (25 µm) but different length, and its function is twofold: the two wires serve as a line source of heat flux to determine a temperature rise in the fluid, but at the same time they are used as a thermometer by correlating the temperature to their electric resistance. The different lengths are set to exclude the end effects a finite section of wire exhibits in the determination of the electric resistance. Consequently, if the difference of the two resistances is measured with time, that value will correspond to the resistance variation of an infinite wire, as the end effects of the two finite-length sections, being approximately the same, will be subtracted. Such resistance difference is then measured by a Wheatstone bridge, implemented in a dedicated instrument, that in turn provides the thermal conductivity measurements to the computer. Differently, pressure and temperature signals are first gathered by a multimeter, and then processed by the computer [136, 137].

Chapter 5

Thermophysical properties analysis for novel low-GWP refrigerants

In light of the relevance of reliable refrigerant properties models for the effective functioning of HVAC equipment, in this thesis the properties of some of the most promising pure fluids as low-GWP refrigerants have been investigated. The work that is being presented in this chapter develops from two previous studies: a detailed examination of publicly available data for refrigerant properties up to 2018, conducted by Bobbo et al. [65], followed by the recent work by Fedele et al. [138], an extensive update in the period 2018–2021 to the properties of the most considered low-GWP refrigerants as well as for the least surveyed.

As outlined by the aforementioned studies, current pure-fluid alternatives to the most potent climate-harming substances are restricted to a handful of candidates, most of which are unsaturated HFC, i.e., organic compounds with a carbon-carbon double bond, as discussed in Chapter 1. This characteristic is essential for synthetic molecules to limit their atmospheric lifetime, and thus to match the requirements of low GWP and ODP set by the international regulations to curb the climate change, and power energy-efficient equipment in the mid-long term.

In particular, in the study by Bobbo et al. [65], a total of 17 pure substances were considered as potential candidates in a number of applications, including heat-pumping, air-conditioning, refrigeration, and ORC systems. Based on the new studies appeared in the literature since 2018, the work in this thesis intentionally include most of these fluids in the broader domain of refrigerants for which to perform the analysis, to be described in this chapter.

5.1 Literature review

To widen the analysis of experimentally determined thermophysical properties to the most recent publications (articles, conference proceedings, technical reports, etc.), a preliminary phase consisted in exploring the literature and retrieve the data sets for the properties of technical interest, that have been made publicly available. This search added to the literature review for low-GWP refrigerant properties initiated previously at ITC-CNR during 2022.

5.1.1 Methodology

To collect new data sets of relevant thermophysical properties, online journals were accessed from the web by means of specific keywords addressing the refrigerants with their conventional name, such as "R1233zd(E)", or with their IUPAC nomenclature (for instance, "trans-1-Chloro-3,3,3-trifluoropropene" in the case of R1233zd(E)) in order to broaden the search, and include studies for the intended refrigerants that were published before ASHRAE Standard 34 became the ordinary designation system. To refine the queries, words such as "viscosity", "PvT", "thermal conductivity" were mostly included in the search to look for the availability of studies addressing particular properties. Web search engine Google Scholar and IIR database Fridoc were used largely to look for useful publications, but also authors referencing for previous articles proved effective in obtaining sets of data for the considered properties, especially for studies that did not include the typical keywords in the title or in the abstract, and thus that very likely otherwise would not have been identified.

Although a variety of studies reporting thermophysical properties of refrigerants can be found in the literature, for instance, concerning the investigation of the Vapor-Liquid Equilibrium (VLE) for refrigerant mixtures, the survey in this work deliberately focused on publications reporting properties for pure fluid only.

The thermophysical properties that are considered in this work are the main involved in the formulation of properties models and equations of state. For the thermodynamic properties, these are: the PvT properties, saturated pressure (P_{sat}), specific heat capacities (c_p and c_v), and speed of sound (w). The investigated transport properties are: viscosities (μ, dynamic and ν, kinematic), thermal conductivity (λ), and surface tension (σ).

5.1.2 Update on available studies

The search started from a subset of pure refrigerants that have been issued in the last years for potential technical applications, as replacements with low GWP (< 150) for traditional working fluids. These were selected among the pure fluids

identified in the study by Bobbo et al. [65] and in the subsequent update by Fedele et al. [138], whereas other two molecules, namely, R-13I1 and R-1130(E) were added to the scope.

The categories of reviewed fluids primarily include hydrofluoroolefins (HFOs) and hydrochlorooffluorolefins (HCFOs). Comprehensively, a total of 21 pure refrigerants were initially involved in the search. Each is listed in Table 5.1, with its main inherent properties (if available). Actually, several fluids have not been added yet to ASHRAE Standard 34; consequently, their safety class is not currently available, an thus has not been reported. Similarly for the experimental normal boiling points and critical temperatures for some relatively new refrigerants, whose data still have not been found in the literature.

Refrigerants R-1132(Z), R-1141, R-1225ye(E), and R-1234ye(E) have been issued in recent studies as low-GWP candidates [54]; however, to date no experimental data for thermophysical properties among the aforementioned have been found in the literature.

A similar situation is for R-1354mzy(E), R-1354mfy(E), and R-1225ye(Z): new experimental data have not been found in the literature since the latest search [138] for the period 2018–2021. Moreover, available data for these fluids to date are rather scarce: for studies on thermodynamic properties, R-1354mzy(E) is the one that presents the most, with only 5 data sets, whilst for transport properties, none of these refrigerant have been investigated so far.

As a result of the search, at present the studies reporting experimental data for the investigated thermophysical properties relate to 17 of the 21 refrigerants. The updated number of literature references for each refrigerant is provided in Table 5.2.

Overall, the most investigated fluids are still (as it was observed in the 2018's review [65]) R-1234ze(E) and R-1234yf, with 53 and 51 sets of experimental properties, respectively.

For the period 2021–2022, in particular, the newly identified studies are presented as follows:

- new experimental specific heat capacity measurements for R-1234yf are reported by Sheng et al. [129], consisting of 33 data, whereas Liu et al. [134] reported 66 saturated density measurements and 33 data for surface tension.

- R-1234ze(E) exhibits 57 new specific heat measurements by Sheng et al. [142], and 51 data of thermal conductivity by Scattolini et al. [137].

- new data for R-1234ze(Z) consist of 58 sound speed measurements by Peng et al. [130], and 90 viscosity data by Alam et al. [143].

- new data sets for R-1336mzz(E) have been introduced for viscosity (Mondal et al. [144], Zhang et al. [145], and Xu et al. [146], with 124 new experimental

Table 5.1: Overview of the refrigerants considered in the search. Entries are referred from [65], unless noted otherwise.

ASHRAE/ISO designation	Refrigerant category	NBP (K)	T_{crit} (K)	Safety class [b]	GWP_{100}
R-1141	HFO	209.71	327.2		0.024[a]
R-1132(E)	HFO	220.51	348.82		1
R-1234yf	HFO	243.7	367.85	A2L	0.501[a]
R-1243zf	HFO	247.7	376.93		0.261[a]
R-1234ye(E)	HFO	252.39	382.66		2.3
R-1234ze(E)	HFO	254.18	382.51	A2L	1.37[a]
R-1225ye(Z)	HFO	255.44	383.97		0.344[a]
R-1132(Z)	HFO	259.8	405.77		1
R-1225ye(E)	HFO	259.89	390.83		0.118[a]
R-1336mzz(E)	HFO	280.58	403.37	A1	17.9[a]
R-1234ze(Z)	HFO	282.9	423.27		0.315[a]
R-1233zd(E)	HCFO	291.41	438.86[e]	A1	3.88[a]
R-1336mzz(Z)	HFO	306.6	444.5	A1	2.08[a]
RE-356mmz	HFE	323.99[d]	459.58[d]		8.13[a]
R-1123	HFO	214.06	331.73		0.005[a]
R-13I1	other	251.29[c]	396.44[c]	A1	1
R-1224yd(Z)	HCFO	287.77[c]	428.69[c]	A1	0.88[a]
R-1354mzy(E)	HFO	289–291	424.73		
R-1132a	HFO		302.81	A2	0.052[a]
R-1130(E)	HCO			B2	5
R-1354myf(E)	HFO				

[a] AR6 by IPCC WGI [139]
[b] ISO 5149 [38]
[c] REFPROP 10.0 [113]
[d] Sako et al. [140]
[e] Tanaka and Akasaka [141]

Table 5.2: Updated number of literature references reporting experimental measurements for the considered thermophysical properties of low-GWP refrigerants.

Refrigerant	**Thermodynamic properties**					**Transport properties**		
	CP	P_{sat}	PVT	c_P	w	λ	μ/ν	σ
R-1141								
R-1132(E)	1	1	1					
R-1234yf	2	12	13	9	5	1	7	2
R-1243zf	2	4	3	2	1	1	1	2
R-1234ye(E)								
R-1234ze(E)	2	13	15	9	4	3	4	3
R-1225ye(Z)		1	1					
R-1132(Z)								
R-1225ye(E)								
R-1336mzz(E)	2	2	2		1	2	3	1
R-1234ze(Z)	2	9	7		3	1	3	1
R-1233zd(E)	2	8	7	2	5	2	5	4
R-1336mzz(Z)	1	7	3		2	2	3	1
RE-356mmz	1	1	3	1	1	1	1	
R-1123	2	3	4		1			2
R-13I1	2	2	4	1	1			1
R-1224yd(Z)	2	3	3		1	1	2	2
R-1354mzy(E)	1	1	3					
R-1132a	1	1		1				
R-1130(E)		2	1					1
R-1354myf(E)			1					

measurements in total), speed of sound (Peng et al. [147], 98 measurements), surface tension (Zhang et al. [145], 22 experimental data), and thermal conductivity (Mondal et al. [148] and Haowen et al. [149], with a total of 263 experimental measurements). Sakoda et al. [150] reported 60 PvT properties, 26 vapor pressure, and measurements of the critical parameters.

- for R-1132(E), Sakoda et al. [124] published new PvT measurements (58 experimental densities) and saturated densities (18 data) as well as measurements for the critical parameters, whereas Perera et al. [151] reported novel measurements for vapor pressure (24 experimental data).
- R-1130(E) provides new data sets by Tanaka et al. [152]: 73 PvT properties, 14 vapor pressure and 14 saturated densities, and 38 experimental measurements for surface tension.
- R-13I1 exhibits new data sets by Perera et al. [153], that report 47 PvT measurements, 37 experimental vapor pressures, 24 saturated densities and the measurements for the critical parameters.
- for R-1123, Liu et al. [134] reported 28 surface tension measurements.
- R-1233zd(E) exhibits novel studies for sound speed (Peng et al. [147] and Kano [154], with 128 measurements overall), and for the critical parameters (Tanaka and Akasaka [141]).
- for R-1224yd(Z), new measurements were published for the critical parameters (Tanaka et al [141]), vapor pressure (Beltramino et al. [155], 66 data), and PvT properties (Lago et al., to be published, 80 measurements).
- R-1336mzz(Z) presents a new study by Zhang et al. [145], reporting experimental measurements of kinematic viscosity (20 data) and surface tension (20 data).
- R-1243zf provided new references for specific heat capacity (Sheng et al. [156], 64 data, and Ding et al. [157], 86 measurements), speed of sound (Chen et al. [158], 92 data), and thermal conductivity (Kim et al. [159]).

Notably, for the same period 2021–2022, R-1336mzz(E) and R-1243zf present the highest number of new studies overall (7 and 4, respectively). For refrigerants R-1233zd(E), R-1224yd(Z), R-1336mzz(Z), and R-1243zf a significant number of references reporting experimental measurements have appeared in the literature since 2018. Besides, these refrigerant have already been implemented into REFPROP, which allows to make a comparison between the collected experimental data and the EOS and models/correlations implemented in the NIST software. These four refrigerants were therefore involved in a more detailed examination.

5.1.3 Overview of the selected refrigerant

R-1233zd(E) has been studied as a suitable low-GWP refrigerant in chillers, ORC systems, and it is already in use in commercial high-temperature heat pumps [160], due to its relatively high NBP (291.41 K), as a drop-in replacement for R-245fa [147], an HFC molecule [160]. Particularly, it is classified in safety class A1 [38], and because of its very low GWP and close-to-zero ODP, it is considered a safe next generation fluid [54].

R-1224yd(Z) is an HFCO molecule containing a chlorine atom, which is harmful for the stratospheric ozone. However, due to the short lifetime in the atmosphere, the ODP is very limited and near zero, whereas the GWP is also very low (0.88). By showing similar properties to that of R-245fa and R-123, it is considered as a valid alternative for centrifugal chillers, heat pumps, and ORC equipment, but it has also risen interests in the refrigeration and air-conditioning industry [69, 155]. More recently, it has been investigated for the two-phase loop thermosyphon (TPLT), a promising highly effective method for cooling in electronics [161].

Refrigerant R-1336mzz(Z) has been considered as a potential substitute to R-245fa, that because of its high NBP (306.6 K), is a regarded as suitable working fluid for next generation of high-temperature ORC systems and heat pumps [145]. Besides, it is classified A1 (lower toxicity and no flame propagation) [38].

R-1243zf has been regarded as a suitable alternative refrigerants for room air conditioners, in place of the widely used R-134a, an HFC, having similar critical temperature and NBP. Additionally, it is characterized by very low GWP and ODP, however its high flammability (not yet classified under ASHRAE Standard 34) is of major concern for the fluid to be used as a pure refrigerant, thus to date it is currently considered mainly as a component for blends [156].

In the following section, the available experimental data for vapor pressure, PvT properties, viscosity and thermal conductivity are presented and analyzed for the four low-GWP refrigerants. These properties are the ones for which a significant number of new studies have been found in the literature. Because refrigerant R-1233zd(E) was already reviewed in the 2018's article by Bobbo et al. [65], for this fluid only the sets of data identified subsequently are further analyzed and discussed. Specifically, REFPROP version 10.0 was used for the properties analysis of the four fluids, and the same software edition is intended hereafter when referring to the EOSs.

5.2 Thermodynamic properties

For each refrigerant considered in the analysis, Table 5.3 lists the EOSs implemented in REFPROP that were used to compute the reference properties from which to

Table 5.3: Equations of state used in the analysis.

Refrigerant	EOS	EOS uncertainties		
		Vapor pressure	*PvT* properties	Speed of sound
R-1233zd(E)	Mondéjar et al. (2015) [162]	0.22%	0.020%	0.131%
R-1224yd(Z)	Akasaka et al. (2017)	0.05%	0.5% (saturated liquid density) 0.1% (liquid density) in the critical region, may exceed 1%[a]	0.03% (vapor)
R-1336mzz(Z)	McLinden and Akasaka (2018)	0.05%	0.01% (liquid densities) 0.02% (vapor)	0.05% (vapor)
R-1243zf	Akasaka (2017)	0.10%	0.05% (liquid densities) 0.6% (vapor densities) > 1% in the critical region	n.d.

[a] because of a lack of reliable experimental data in the critical region, as originally reported by the authors.

calculate the deviations of the experimental data. The declared uncertainties for the ranges of validity of each EOS are also reported.

5.2.1 Vapor pressure

Table 5.4 lists the available data sets of experimentally measured vapor pressure for the selected refrigerants. A new set, by Beltramino et al. [155], was identified in this work for R-1224yd(Z), covering the temperature range 274–338 K, whereas the others were found in the two previous studies, mentioned at the beginning of this chapter. Figs. 5.1a–5.1d represent the calculated deviations.

R-1233zd(E)

For R-1233zd(E), four more data sets were added from the previous study by Bobbo et al. [65], namely, the ones by Yin et al. [163], Sakoda et al. [164], Li et al. [165], and Tanaka et al. [166], resulting in a total number of 256 vapor pressure data. Fig. 5.1a shows that, overall, the better agreement between the experimental measurements and the EOS is within the range between the NBP and T_{crit}. Instead, in the region at lower temperatures, in particular, the highest deviations occur. This is evident with the set by Li et al. [165], that reports 95 data over the reduced

Table 5.4: Data sets of experimental vapor pressure considered in the study.

Refrigerant	**Reference**	**No. data**	**T_{range} (K)**	**AAD%**
R-1233zd(E)	Yin et al. (2021)	18	288–373	0.12
	Sakoda et al. (2020)	12	300–410	0.21
	Li et al. (2019)	95	253–431	0.15
	Tanaka (2017)	11	300–400	0.29
	Di Nicola et al. (2017) (CNR-ITC)	32	293–353	0.33
	Di Nicola et al. (2017) (UnivPM)	49	234–375	0.59
	Mondéjar et al. (2015)	23	280–438	0.09
	Hulse et al. (2012)	16	263–353	1.93
R-1224yd(Z)	Beltramino et al. (2022)	66	274–338	0.45
	Bobbo et el. (2020)	31	293–353	0.42
	Sakoda and Higashi (2019)	15	310–410	0.35
R-1336mzz(Z)	Li et al. (2020)	91	278–443	0.23
	McLinden and Akasaka (2020)	18	330–440	0.03
	Sakoda et al. (2020)	17	290–410	0.18
	Tanaka et al. (2016)	13	324–443	0.10
R-1243zf	Yin et al. (2020)	26	253–376	0.11
	Yang et al. (2019)	17	273–353	0.16
	Higashi et al. (2018)	20	310–377	0.03
	Brown et al. (2013)	83	234–373	0.16

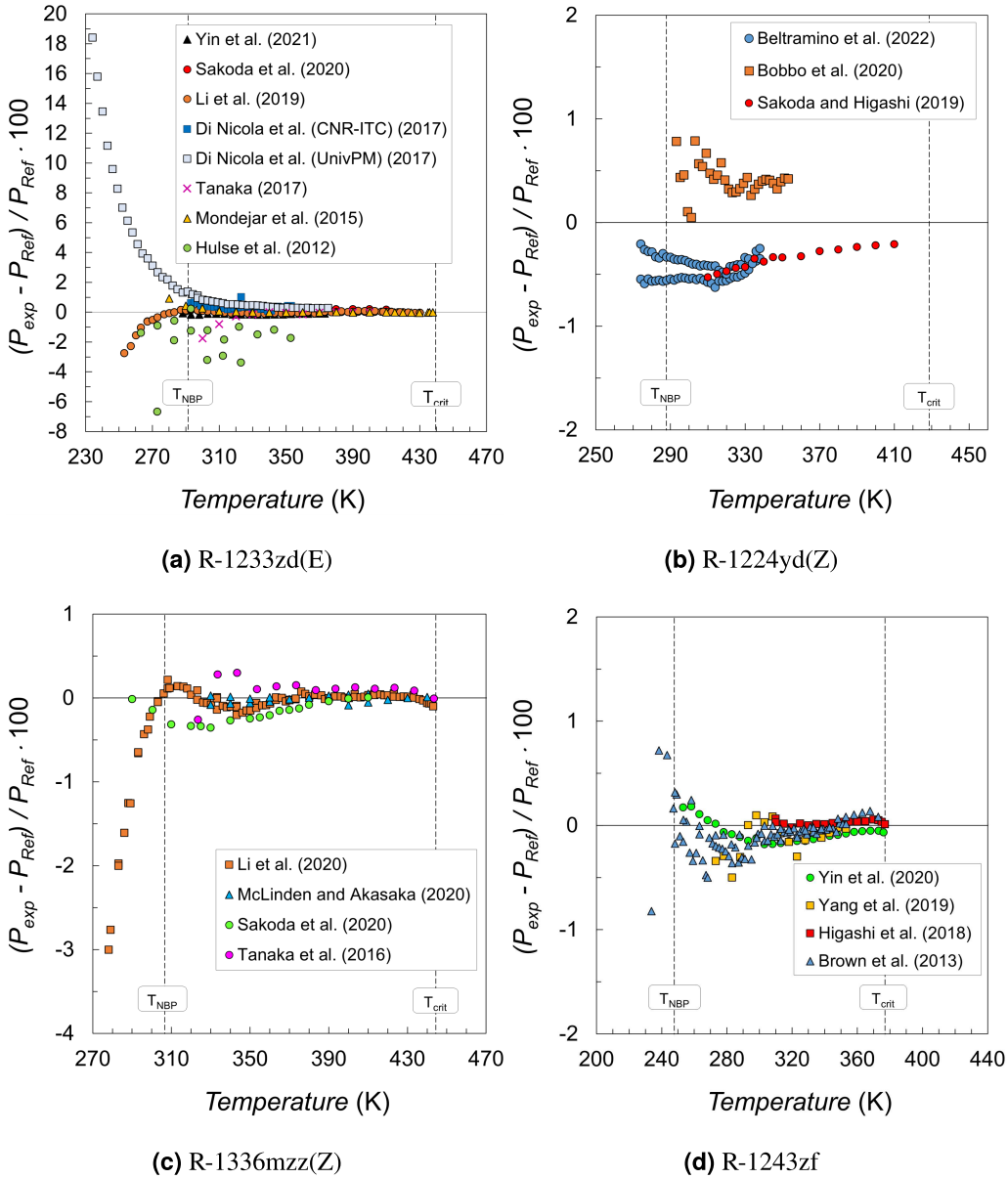

(a) R-1233zd(E) **(b)** R-1224yd(Z)

(c) R-1336mzz(Z) **(d)** R-1243zf

Figure 5.1: Deviation for available experimental vapor pressure data.

temperature range T_r = 0.58–0.98 with an average absolute deviation (AAD%) equal to 0.15 %, and a maximum absolute deviation (MAD%) of 2.71 %. Similarly, this was observed for the set by Di Nicola et al. (UnivPM) [167], consisting of 49 measurements (T_r = 0.53–0.86) with AAD% = 0.59 % and MAD% = 18.41 %.

Differently, the set by Sakoda et al. [164] provides 12 measurements at higher temperatures in the range T_r = 0.68–0.93, with AAD% = 0.21% and MAD% = 0.41%. The best agreement with the used EOS is with the set by Mondéjar et al. [162], reporting 23 experimental data (AAD% = 0.09% and MAD% = 0.92%) and by Yin et al. [165], with AAD% = 0.12%, MAD% = 0.15%. Actually, the very low AAD% and MAD% for the measurements by Mondéjar et al. [162] is attributable to the fact that the EOS was formulated on this data set only, due to a lack of accurate experimental measurements [162].

R-1224yd(Z)

As to R-1224yd(Z), only three studies reported vapor pressure measurements, consisting in a total of 112 experimental data. Fig. 5.1b shows that in this case many vapor pressure data present an absolute deviation within ±0.5 %. In terms of AAD%, the three studies are quite comparable: 0.45%, 0.42%, and 0.35%, for the study by Beltramino et al. [155] (66 measurements, with MAD% = 0.63 %), Bobbo et al. [127] (31 measurements, MAD% = 0.79 %), and Sakoda and Higashi [119], reporting 15 experimental data. The best correspondence for the EOS is found with this set, having MAD% = 0.53% and the lowest AAD% among the three studies.

R-1336mzz(Z)

For R-1336mzz(Z) (Fig. 5.1c), the analysis comprised four data sets, with 139 experimental data overall. Relative deviations are mostly well within ±0.25 %. Sakoda et al. [164] report 17 experimental data over the range T_r = 0.65–0.92, with AAD% = 0.18 % and MAD% = 0.36 %. McLinden and Akasaka [168] presented 18 vapor pressure measurements in the range of reduced temperature T_r = 0.74–0.99, with AAD% = 0.03 % and MAD% = 0.09 %, representing the best agreement between the experimental data and the reference EOS. In a similar range of reduced temperature T_r = 0.73–1.00, Tanaka et al. [169] provided 13 vapor pressure measurements, with AAD% = 0.10 %, and MAD% = 0.30 % that occurs at T_r = 0.77. Differently, Li et al. [170] reported 91 data covering also the lower-temperature region (T_r = 0.63–1.00), for which the AAD% is 0.23 %, and the MAD% is 3.00 % at the lowest investigated temperature (278.18 K) and pressure (0.030 MPa), representing the measurements with the highest discrepancy between the experimental data sets and the EOS. The bias is negative for all the studies: −0.176 %, −0.014 %, −0.188 %, for the sets by Sakoda et al. [164], McLinden

and Akasaka [168], and Li et al. [170], except for the one by Tanaka et al. [169] (0.104 %).

R-1243zf

Fig. 5.1d represents the vapor pressure deviations for R-1243zf. The four identified data sets provide a total of 146 experimental data. Very good agreement for the EOS is with the measurements by Higashi et al. [171] (AAD% = 0.03 %, MAD% = 0.07 %), which reports 20 experimental data in the range of reduced temperature T_r = 0.82–1. Deviations are scattered and higher for temperatures approximately below 300 K for the set by Brown et al. [172] (83 vapor pressure data for T_r = 0.62–0.99), with values increasing as the temperature diminishes, resulting in a maximum deviation MAD% = 0.82 % at the lowest vapor pressure data (0.053 MPa). Good correspondence between the EOS and the experimental values is for the data by Yin et al. [172] (26 experimental vapor pressure, for T_r = 0.67–1.00), with AAD% = 0.11 % and MAD% = 0.18 %. In the case of the data set by Yang et al. [173], reporting 17 measurements for T_r = 0.73–0.94, the AAD% and MAD% are 0.16 % and 0.50 %, respectively.

Notably, near the critical point, good agreement is observed among the different data sets as well as between the experimental data and the EOS.

5.2.2 PvT properties

In Table 5.5, the studies that have been considered for the *PvT* properties are itemized. For each refrigerant, experimental measurements of density are in the compressed liquid, superheated vapor, saturation, and supercritical states, except for R-1336mzz(Z), for which studies on saturated densities were not identified. A representation in *P-T* diagrams of the investigated fluid regions is provided in the figures from 5.2a to 5.2d.

PvT properties deviations for R-1233zd(E), R-1224yd(Z), R-1336mzz(Z), and R-1243zf with respect to the EOS implemented in REFPROP are represented in Figs. 5.3a–5.3d.

R-1233zd(E)

A new data set by Tanaka [166] was identified for R-1233zd(E), consisting in 11 experimental saturated liquid densities in the temperature range 300–400 K, taking the total number of *PvT* data to 532. The AAD% is 0.21 % and the bias is −0.13 %, whereas the MAD% is 0.24 %, indicating therefore good agreement with the reference EOS. Noteworthy, among the four analyzed refrigerants, R-1233zd(E) possesses the highest number of studies about *PvT* properties.

Table 5.5: Sets of experimental data for PvT properties of selected refrigerants.

Refrigerant	Reference	No. data[a]		T_{range} (K)	P_{range} (MPa)	AAD%
		PvT	ρ_{sat}			
R-1233zd(E)	*Compressed liquid*					
	Fedele et al. (2018) (CNR-ITC)	93		283–363	0.133–35.002	0.04
	Mondejar et al. (2015)	117		215–444	0.476–24.079	0.01
	Romeo et al. (2017)	30		274–333	1.000–25.010	0.02
	Tanaka (2016b)	39		329–440	0.777–9.765	0.65
	Superheated vapor					
	Yin et al. (2021)	63		303–373	0.091–0.99	0.10
	Fedele et al. (2018) (UnivPM)	60		308–373	0.167–0.693	0.41
	Mondejar et al. (2015)	43		350–440	0.255–1.923	0.05
	Tanaka (2016b)	33		328–443	0.777–9.770	7.74
	Supercritical region					
	Mondejar et al. (2015)	5		444	3.858–5.619	0.02
	Tanaka (2016b)	25		440–444	3.773–8.632	2.02
	Saturation					
	Tanaka (2016a)		11^{l}	300–400	0.136–1.793	
	Hulse et al. (2012)		13^{l}	243–293	0.011–0.108	0.15
R-1224yd(Z)	*Compressed liquid*					
	Fedele et al. (2020)	93		283–363	0.25–35	0.05
	Lago et al. (2022) (to be published)	80		273–353	1–35	0.03
	Sakoda and Higashi (2019)	16		354–413	1.98–6.41	0.09
	Superheated vapor					
	Sakoda and Higashi (2019)	30		330–420	0.361–1.823	0.19
	Saturation					
	Fedele et al. (2020)		9^{l}	283–363		0.04
	Sakoda and Higashi (2019)		$9^{l} + 8^{v}$	409–429		1.80
R-1336mzz(Z)	*Compressed liquid*					
	McLinden and Akasaka (2020)	97		230–440	0.79–35.7	0.02
	Sun et al. (2018)	137		283–373	0.1–100	0.03
	Superheated vapor					
	McLinden and Akasaka (2020)	1		460	2.74	0.01
	Supercritical region					
	McLinden and Akasaka (2020)	7		450–460	3.29–4.74	0.13
	All fluid regions[b]					
	Tanaka et al. (2016)	344		323–503	0.17–9.93	
R-1243zf	*Compressed liquid*					
	Higashi and Sakoda (2018)	28		328–376	2.18–6.9	0.25
	Di Nicola et al. (2013)	302		278–368	1.30–35	0.03
	Superheated vapor					
	Higashi and Sakoda (2018)	22		330-430	1.11–3.5	0.95
	Yin et al. (2020)	128		253–368	0.11–2.89	0.35
	Di Nicola et al. (2013)	99		278–368	0.26–0.91	0.62
	Supercritical region					
	Higashi and Sakoda (2018)	25		378–430	3.65–6.90	0.10
	Saturation					
	Higashi and Sakoda (2018)		$6^{l} + 7^{v}$	361–377		0.97

[a] (l) liquid, (v) vapor
[b] including the single-phase and the two-phase regions

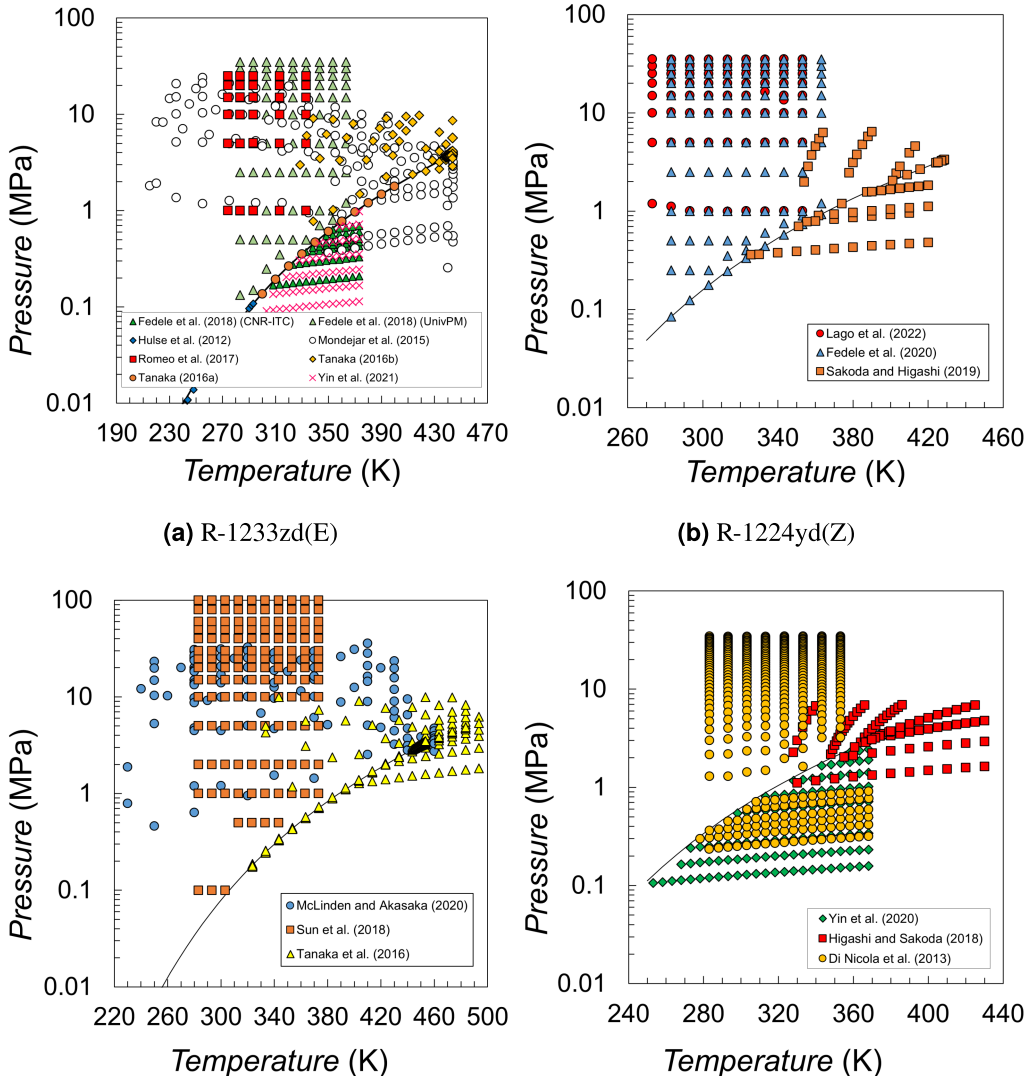

(a) R-1233zd(E) **(b)** R-1224yd(Z)

(c) R-1336mzz(Z) **(d)** R-1243zf

Figure 5.2: Experimental PvT data for the considered refrigerants.

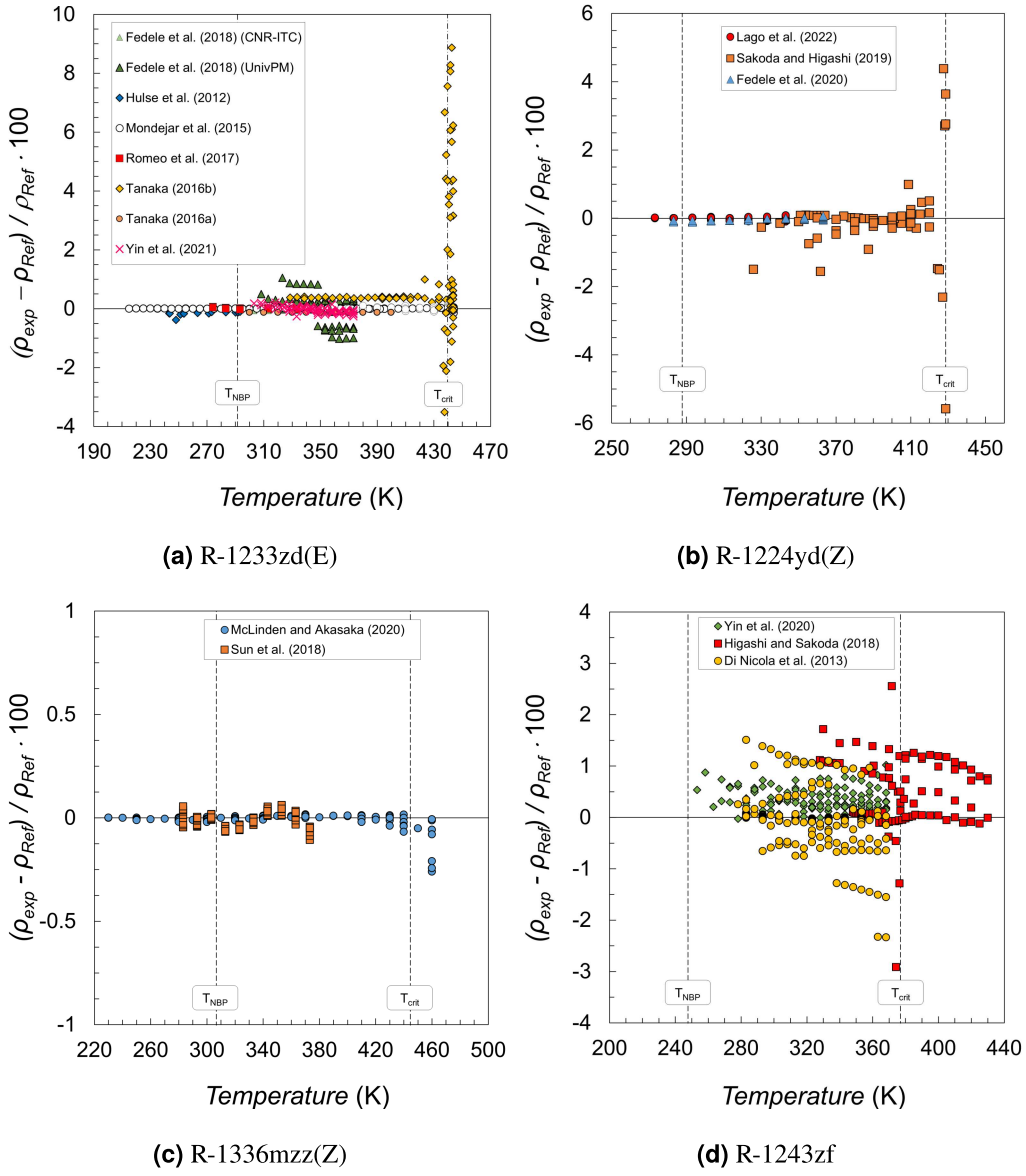

(a) R-1233zd(E) **(b)** R-1224yd(Z)

(c) R-1336mzz(Z) **(d)** R-1243zf

Figure 5.3: Calculated deviations for the refrigerant PvT properties with respect to REFPROP.

R-1224yd(Z)

There are 6 available data sets for R-1224yd(Z), with 245 experimental data overall. In the liquid phase, Fedele et al. [174] measured 93 densities in the range of reduced temperature T_r = 0.65–0.85 and the largest reduced pressure range P_r = 0.08–10.51 investigated for this fluid, with AAD% = 0.05 % and MAD% = 0.12 %, showing good correspondence with REFPROP. Sakoda and Higashi [119] reported 16 PvT measurements for T_r = 0.83–0.94 and P_r = 0.60–1.92, with AAD% = 0.09 % and MAD% = 0.29 %, whereas the set by Lago et al. (to be published) consists of 80 liquid densities for T_r = 0.64–0.82 and P_r = 0.30–10.57, with the lowest AAD% = 0.03 % and MAD% = 0.1 %, representing experimental data that well match the reference properties obtained with the EOS.

For the vapor phase, the one by Sakoda and Higashi [119] is the only available data set, reporting 30 data in the reduced temperature T_r = 0.77–0.98 and pressure P_r = 0.11–0.55, with AAD% = 0.19 % and MAD% = 0.57 %.

For the saturated densities, Sakoda and Higashi [119] presented 9 liquid densities and 8 vapor densities, in the range of reduced temperature T_r = 0.76–1. For the measurements approaching the critical temperature, the deviations are the highest, with MAD% = 5.58 %, whereas at lower temperatures some scattering is observed. Overall, the AAD% is 1.81 %, but with low bias (−0.03 %). Fedele et al. [174] also provided 9 saturated liquid densities, farther from the critical region and for T_r = 0.66–0.85. In this case, sound agreement is found with respect to REFPROP: the AAD% is 0.04 %, with bias −0.02 %. The MAD% is also very low (0.07 %).

R-1336mzz(Z)

For R-1336mzz(Z), 5 experimental data sets were found, with 586 measurements altogether. In the liquid phase, the study by McLinden and Akasaka [168] provides 97 measurements over a wide range of temperature (T_r = 0.52–0.99) and pressure (P_r = 0.16–12.33), with very low MAD% = 0.07 %, occurring near the critical point, and AAD% = 0.01 %, representing very good agreement with the used EOS. A single measurement from the same set was attributable to the density for the vapor phase, again with very low relative deviation (−0.01 %). The other set in the subcooled liquid region is by Sun et al. [175], with 137 experimental measurements over a restricted range of reduced temperature T_r = 0.64–0.84, but a very ample reduced pressure range (P_r = 0.04–34.55). The deviations are alternatively positive and negative, but reveal good consistency with REFPROP: the AAD% is 0.03% with bias −0.01 %, whereas the MAD% is 0.11 %.

In the supercritical region, 7 experimental data were reported by McLinden and Akasaka [168], for T_r = 1.01–1.04 and P_r = 1.14–1.64. The AAD% is 0.13 %, and the MAD% is 0.26 % at the highest investigated temperature (460 K).

Tanaka et al. [169] investigated the PvT properties over the range of temperature (T_r = 0.73–1.13) and pressure (P_r = 0.06–3.43)), reporting densities both for the single-phase and two-phase regions, with a total of 344 experimental data. Because a substantial amount of measurements were conducted in the two-phase regions, and thus represent "bulk" densities, deviations for these data were not calculated, since REFPROP can only provide either single-phase properties or saturated liquid and saturated vapor properties. Additionally, being the two-phase measurements not distinguished from the single-phase ones, the assessment of whether the experimental densities were in the single-phase rather than in the two-phase could have introduced major randomness in calculating deviations, especially for the data that lie very close to the vapor pressure curve. For these reasons, the deviations for the experimental PvT data for the set by Tanaka et al. [169] were not analyzed.

R-1243zf

Refrigerant R-1243zf presents 7 data sets of experimental PvT properties, with a total of 617 density measurements. The liquid densities measured by Di Nicola et al. [176] consist of 302 measurements in a constrained range of reduced temperature T_r = 0.75–0.94, but large reduced pressure P_r = 0.37–9.82, at eight different temperatures. The deviations distribute around the reference values with AAD% = 0.03 % and MAD% = 0.09 %, representing good agreement with the EOS. The set by Higashi and Sakoda [177] presents 28 experimental liquid densities along three isochores in the range T_r = 0.87–1.02 and P_r = 0.62–1.96, for which the AAD% is 0.25 % and the MAD% is 1.16 %.

For the vapor phase, Higashi and Sakoda [177] reported 22 experimental measurements for T_r = 0.88–1.14 and P_r = 0.32–1.00, with AAD% = 0.95 % and same bias, and MAD% = 1.72 %. Yin et al. [172] provided 128 experimental densities over the range of temperature T_r = 0.67–0.98 and pressure P_r = 0.11–2.89. In this case, the AAD% (0.35 %, and same bias) and MAD% (1.02 %) are lower, and deviations relative to the EOS are mostly positive. Di Nicola et al. [176] also provided measurements in the vapor phase with 99 data, for T_r = 0.74–0.98 and P_r = 0.07–0.26. Absolute deviations for this set are, in general, within ±1 %, except for few data all over the investigated temperature range. Specifically, between 330–370 K the maximum deviation (2.34 % at 368.15 K) occurs, whereas AAD% is 0.618 %, with bias −0.07 %.

Based on available studies, data for the supercritical region were reported by Higashi and Sakoda [177] only. The authors provided a set with 25 experimental densities over the range of temperature T_r = 1.00–1.14 and pressure P_r = 1.04–1.96, for which the AAD% is 0.42 % and the MAD% is 1.23 %.

The same study by Higashi and Sakoda [177] reports the only available data set of saturated densities for this fluid. It consists of 6 saturated liquid densities and 7

Table 5.6: Available experimental data sets of viscosity for the selected refrigerants.

Refrigerant	Reference	No. data*	T_{range} (K)	P_{range} (MPa)	AAD%
R-1233zd(E)	Zhao et al. (2021)	14^{satl}	303–432	0.150–3.220	5.98
	Cui et al. (2018)	12^{satl}	303–403	0.155–1.908	4.52
	Meng et al. (2018)	92^{cl}	243–373	0.200–40.000	0.59
	Miyara et al. (2018)	$61^{cl} + 28^{sv}$	314–474	1.005–4.074	2.59
	Hulse et al. (2012)	6^{cl}	270–380	0.100–1.350	55.71
R-1224yd(Z)	Alam et al. (2019)	$68^{cl} + 36^{sv}$	303–475	1.002–4.058	1.74
	Miyara et al. (2018)	$20^{cl} + 12^{sv}$	303–475	1.960–3.210	1.62
R-1336mzz(Z)	Zhang et al. (2022)	20^{satl}	303–399	0.089–2.787	4.90
	Alam et al. (2018)	$71^{cl} + 26^{sv}$	314–475	0.492–4.062	1.76
	Sun et al. (2018)	109^{cl}	253–353	0.100–40.000	1.08
R-1243zf	Zhao et al. (2021)	12^{satl}	293–373	0.510–3.250	8.67

* (satl), saturated liquid; (cl), compressed liquid; (sv), superheated vapor.

saturated vapor densities, covering the temperature range T_r = 0.96–1, including the density at the critical point. The AAD% is 0.97 %, whereas the MAD% is 2.91 %, for a measurement in proximity to the critical point (T_r = 0.99).

5.3 Transport properties

The experimental data sets that have been considered in the analysis for transport properties are illustrated in Table 5.6. Notably, only one new study for viscosity measurements has been identified in the literature in 2022 for these four fluids. Specifically, for R-1336mzz(Z) Zhang et al. [145] reported viscosity measurements for the saturated liquid. Overall, the available data sets for R-1233zd(E), R-1224yd(Z), R-1336mzz(Z), and R-1243zf are depicted in Figs. 5.4a–5.4d.

To calculate and analyze the deviation between the experimental and reference values for viscosity and thermal conductivity, REFPROP was used with the NIST recommended models and correlations. These are illustrated in Table 5.7. It is pointed out that, apart from the correlation for thermal conductivity of R-1233zd(E), REFPROP relies on ECS models to provide reference properties, due to a dearth of accurate experimental data [115].

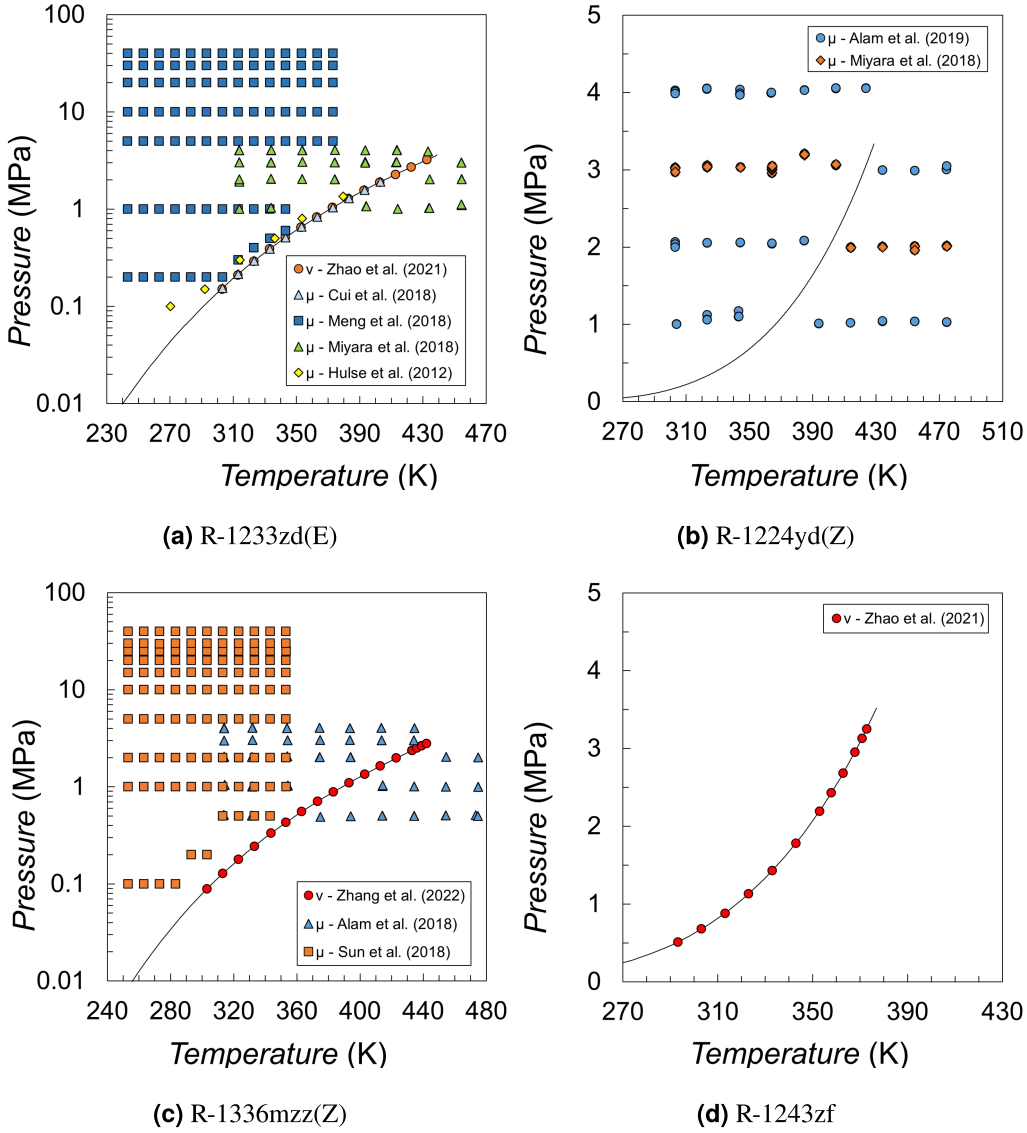

(a) R-1233zd(E)

(b) R-1224yd(Z)

(c) R-1336mzz(Z)

(d) R-1243zf

Figure 5.4: Available experimental viscosity data for the selected refrigerants.

Table 5.7: Recommended correlations and models by REFPROP, used in the transport properties analysis.

Refrigerant	Property	Correlation/Model (reference)	Uncertainties
R-1233zd(E)	Viscosity	ECS, based on R-134a (Huber [178])	Liquid: 4% over 243 to 433 K at pressures to 40 MPa, rising to 10% at 100 MPa. Gas: 4%.
	Therm. cond.	Correlation (Perkins et al. [179])	From 1% to 4% based on the temperature and pressure. Larger in the critical region.
R-1224yd(Z)	Viscosity and therm. cond.	ECS, based on R-134a (Huber [178])	Gas: 4% for viscosity, and 20% for therm. cond. Liquid: 4% for viscosity, and 20% for therm. cond. long saturation, and higher as pressure increases.
R-1336mzz(Z)	Viscosity and therm. cond.	ECS, based on R-134a (Huber [178])	Viscosity: 3% for saturated liquid from 300 to 435 K, 6% for vapor, higher elsewhere Therm. cond.: 3% along saturation and in gas phase, higher for higher pressures and near the CP.
R-1243zf	Viscosity and therm. cond.	ECS, based on R-134a (Huber [178])	Gas: 20% for viscosity and therm. cond. Liquid: 20% for viscosity and therm. cond. along saturation, higher as pressure increases.

5.3.1 Viscosity

The deviations for the experimental data sets of viscosity for R-1233zd(E), R-1224yd(Z), R-1336mzz(Z), and R-1243zf are depicted in Figs. 5.5a–5.5d, respectively.

R-1233zd(E)

Refrigerant R-1233zd(E) presents 5 data sets of viscosity measurements, providing a total of 213 experimental data. Zhao et al. [180] reported 14 measurements for kinematic viscosity of the saturated liquid, over the range of temperature 303–432 K, and pressure 0.150–3.220 MPa. Systematically positive, high deviations are observed for this data set, with AAD% = 5.98 %. In particular, the deviations exhibit a minimum (0.59 %) at T = 342.93 K, and increase as the experimental temperatures approach the NBP and the critical temperature. The MAD% is 20.97 % at 432.61 K, the closest data to the critical point. Cui et al. [181] provided 12 saturated liquid viscosity, for T = 303–403 K and P = 0.155–1.908 MPa, with AAD% = 4.52% and MAD% = 10.97 %, for which the deviations are systematically positive, and distribute similarly to that for the set by Zhao et al. [180]. For the set by Meng et al. [182], that reports 92 data in the compressed liquid region for T = 243–373 K, and over the very wide range of pressure P = 0.200–40.000 MPa, the deviations

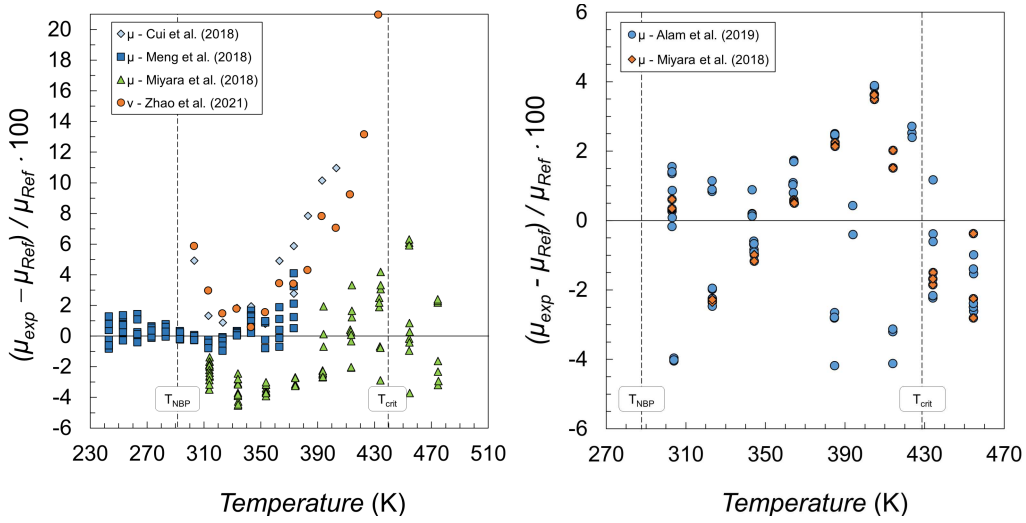

(a) R-1233zd(E) **(b)** R-1224yd(Z)

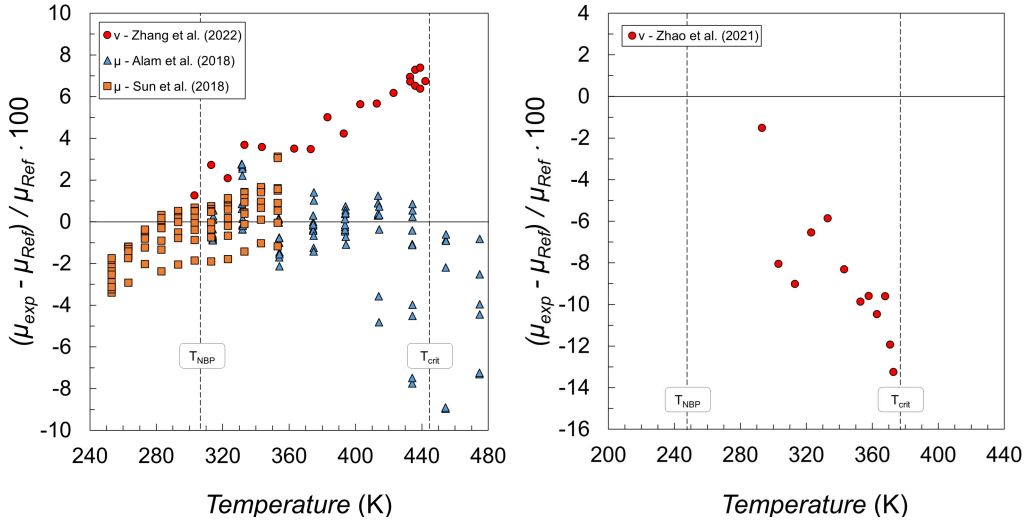

(c) R-1336mzz(Z) **(d)** R-1243zf

Figure 5.5: Calculated viscosity deviations for the four refrigerants.

are relatively much lower: the AAD% is 0.59 %, and the MAD% is 4.09 %. The subset of measurements at specific experimental temperatures shows both positive and negative deviations with respect to the REFPROP predictions. The study by Miyara et al. [183] comprises 61 compressed liquid and 28 superheated vapor viscosity measurements, in the range of temperature 314–474 K and pressure 1.005–4.074 MPa. For the measurements at temperatures above 390 K, the deviations at specific temperatures vary in a wider range, assuming both positive and negative values. The AAD% is 2.59 %, whereas the MAD% is 6.31 %. Hulse et al. [184] reported 6 viscosity measurements in the compressed liquid region, for T = 270–380 K and P = 0.100–1.350 MPa. In this case, the experimental data show very high deviations (AAD% = 55.71 %), that by far exceed the typical values that can be obtained with an ECS model for a pure fluid, that is within 5–10 % [115], and thus the same data set is left out from the representation with previously discussed studies.

R-1224yd(Z)

Two data sets of experimentally viscosity were found in the literature for R-1224yd(Z), that cover the compressed liquid and the superheated vapor phase, with 136 measurements in total. Alam et al. [185] reported 68 compressed liquid viscosity and 36 superheated viscosity, in the range of temperature 303–475 K and pressure 1.002–4.058 MPa. The deviations for the subsets of measurements at equivalent temperatures vary significantly, but for most the experimental viscosities are either higher or lower than the reference values. The AAD% is 1.74 %, whereas the MAD% is equal to 4.18 %. The measurements at the temperature of 474 K exceed the range of applicability of REFPROP model, thus the related deviations were excluded from the analysis. The set provided in study by Miyara et al. [186] (20 measurements in the compressed liquid region and 12 measurements in the superheated vapor region) covers the same temperature range of that by Alam et al. [185], but different pressures (1.960–3.210 MPa). These measurements exhibit AAD% = 1.62 % and MAD% = 3.63 %. Notably, the viscosity data by Miyara et al. [186] were obtained at almost identical pressures and temperatures to that of some measurements by Alam et al. [185], and for these the deviations are equivalent.

R-1336mzz(Z)

A total of 226 experimental viscosity measurements from three different data sets were found available for R-1336mzz(Z). For the year 2022, a new study by Zhang et al. [145] on experimental kinematic viscosity was identified for R-1336mzz(Z), that reports 20 saturated liquid data over the range of temperature 303–399 K

and pressure 0.089–2.787 MPa. The data set exhibit AAD% = 4.90 %. The deviations are systematically positive, increasing with increasing temperatures. The MAD% (7.39 %) is observed near the critical region. Alam et al. [133] reported 71 data for the compressed liquid and 26 for the superheated vapor, with AAD% = 1.76 %. The deviations with respect to REFPROP are within ±9.00 %, except for a single measurement that far exceeds this range, and yields the highest deviation (MAD% = 28.56 %). Additionally, the measurements that were performed at fixed temperatures and different pressures exhibit both positve and negative deviations, except for the experimental data above the critical temperature, whose deviations are negative. In the study by Sun et al. [175], which reports 109 data for the compressed liquid, a very wide range of pressure was investigated (0.100–40.000 MPa), for the temperatures between 253 K and 353 K, extending the measurements well below the NBP (306.6 K). The AAD% is 1.08 %, whereas the MAD% is 3.40 %. The data, that can be grouped into subsets with similar temperature but different pressures, for temperatures below 293.15 K show negative deviations with respect to the ECS REFPROP model, whilst for higher temperatures both positive and negative deviations are observed.

R-1243zf

Based on the experimental data for R-1243zf found in the literature, the set by Zhao et al. [145] is currently the only reported for kinematic viscosity. The 12 measurements were performed for the saturated liquid over the range of temperature 293–373 K and pressure 0.510–3.250 MPa. Systematically negative deviations are observed for this data set, with higher absolute values as temperature increases. At the highest reported temperature (372.84 K) and for the closest measurement to the critical temperature (376.93 K), the MAD% occurs (13.25 %), whereas the AAD% is 8.67 %.

5.3.2 Thermal conductivity

The collected data sets of thermal conductivity for R-1233zd(E), R-1224yd(Z), R-1336mzz(Z), and R-1243zf are outlined in Table 5.8. The distribution of the experimental measurements over the *P-T* plane is represented in Figs. 5.6a–5.6d, whereas the calculated deviations are provided in Figs. 5.7a–5.7d.

R-1233zd(E)

For refrigerant R-1233zd(E), currently two data sets of thermal conductivity are available, with 2519 measurements covering the regions for the compressed liquid, superheated vapor, and supercritical fluid.

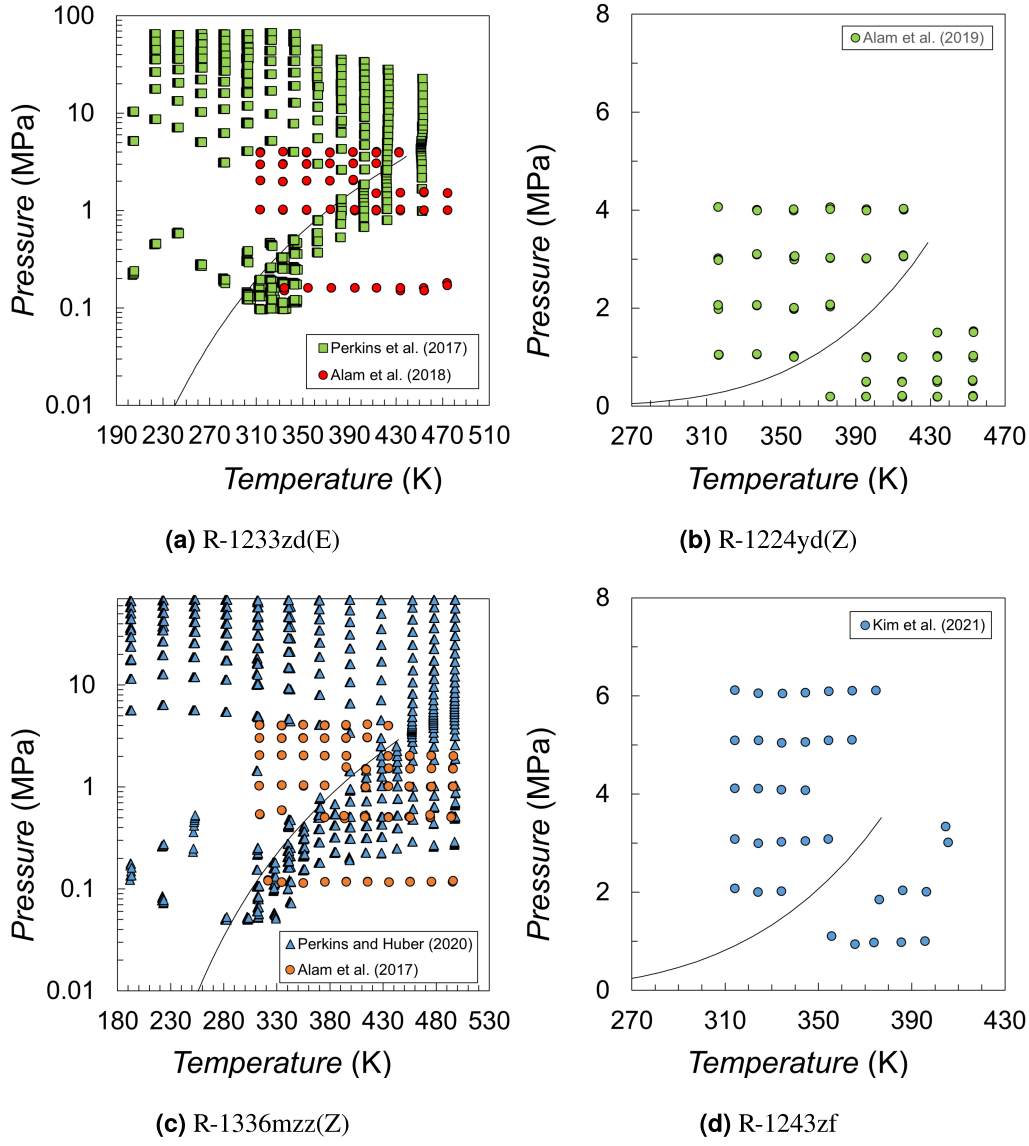

(a) R-1233zd(E)

(b) R-1224yd(Z)

(c) R-1336mzz(Z)

(d) R-1243zf

Figure 5.6: Experimental thermal conductivity measurements considered in the analysis.

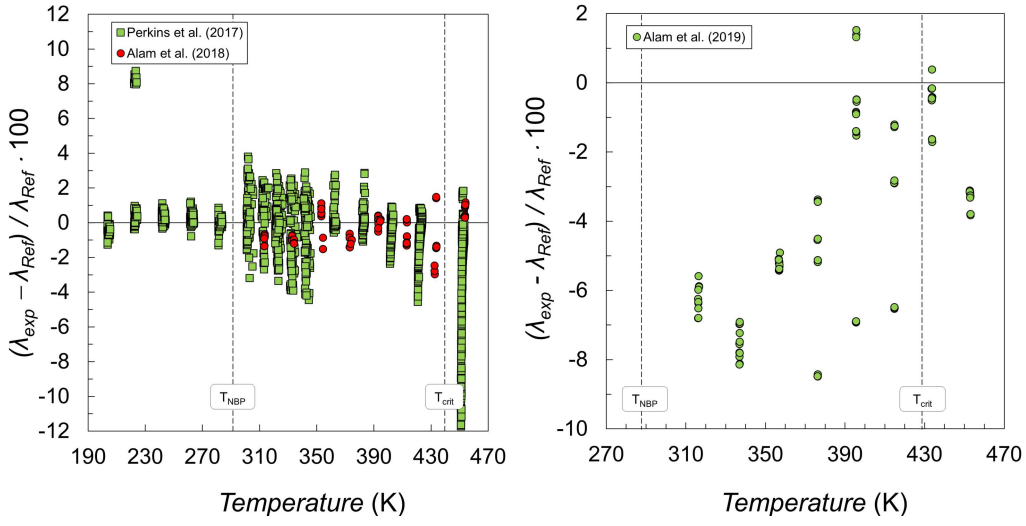

(a) R-1233zd(E)

(b) R-1224yd(Z)

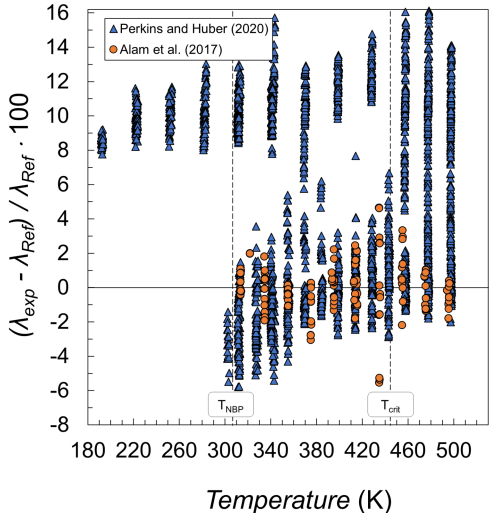

(c) R-1336mzz(Z)

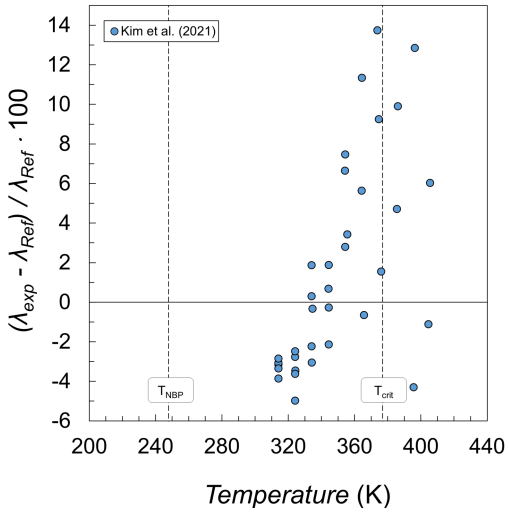

(d) R-1243zf

Figure 5.7: Calculated deviations for thermal conductivity with respect to reference REFPROP values.

Table 5.8: Available experimental data sets of thermal conductivity for the examined refrigerants.

Refrigerant	Reference	No. data*	T_{range} (K)	P_{range} (MPa)	AAD%
R-1233zd(E)	Alam et al. (2018)	$64^{cl} + 51^{sv}$	313–474	0.150–4.020	0.92
	Perkins et al. (2017)	$1453^{cl} + 635^{sv} + 316^{scr}$	204–453	0.096–66.618	4.11
R-1224yd(Z)	Alam et al. (2019)	$66^{cl} + 46^{sv}$	316–453	0.190–4.070	4.51
R-1336mzz(Z)	Perkins and Huber (2020)	$1323^{cl} + 1167^{sv} + 804^{scr}$	192–498	0.050–68.523	5.95
	Alam et al. (2017)	$74^{cl} + 92^{sv}$	313–496	0.114–4.106	1.08
R-1243zf	Kim et al. (2021)	$25^{cl} + 10^{sv}$	315–406	0.937–6.118	4.22

* (cl), compressed liquid; (sv), superheated vapor; (scr) supercritical region.

Alam et al. [187] measured 64 thermal conductivity data at liquid phase and 51 at vapor phase in the range of temperature 313–474 K and pressure 0.150–4.020 MPa. The deviations calculated in reference to REFPROP exhibit an AAD% equal to 0.92 %, and a MAD% of 2.98 %. The groups of data that were measured at equivalent temperatures but at different pressures show quite dissimilar deviations. Perkins et al. [179] provided a very large data set of thermal conductivity, based on which the currently recommended correlation in REFPROP was implemented. The measurements are 1453 in liquid phase, 635 in vapor phase, and 316 in the supercritical region. The data, covering an extensive range of temperature (204–453 K) and pressure (0.096–66.618 MPa) differ from the reference correlation implemented in REFPROP with AAD% = 4.51 %, but the MAD%, being very high, might indicate some issue with the reference model. In particular, the maximum deviation occurs for a measurement that in the *P-T* diagram lies very close to the vapor pressure curve (at $T = 341.875$ K and $P = 0.490$ MPa), in Fig. 5.7a plotted with data obtained with REFPROP. Similarly, many others measurements at different test conditions but in the vicinity of the vapor pressure curve exhibit very high deviations.

R-1224yd(Z)

The study by Alam et al. [185] is at present the only available publication reporting experimental thermal conductivity of R-1224yd(Z), consisting of 112 measurements in total (66 for the compressed liquid, 46 for the superheated vapor), conducted in the range of temperature 316–453 K and pressure 0.190–4.070 MPa, with AAD% = 4.51 %, and MAD% = 8.58 %. By considering the measurements as subsets of data performed at equivalent temperatures but different pressures, it can be observed that the calculated deviations for some subsets vary substantially. The extreme case is represented for the measurements at $T \approx 395$ K, whose deviations

in reference to REFPROP range from −6.93 % to 1.52 %.

R-1336mzz(Z)

For R-1336mzz(Z), two studies report experimental thermal conductivity measurements with 3460 data overall, including the regions of compressed liquid, superheated vapor, and supercritical fluid.

Perkins and Huber [188] provided the largest thermal conductivity data set for R-1336mzz(Z), reporting 3294 measurements (1323 in liquid phase, 1167 in vapor phase, and 804 in the supercritical region) over the wide range of temperature (192–498 K) and pressure (0.050–68.523 MPa). Due to the range of validity of the recommended ECS model in REFPROP 10.0 [115], for a lot of data (473) whose experimental pressures are higher than 46.0 MPa and with densities above 1637.3 kg/m^3, the deviations were not calculated. The remaining measurements exhibit an AAD% of 5.95 %, and a MAD% equal to 16.71 %. It can be observed that the subsets of data measured at similar temperatures but different pressure show very dissimilar deviations, and this, together with the restrictions in terms of queryable pressures and densities in REFPROP, might indicate issues with the recommended ECS model.

The set by Alam et al [189] includes 166 measurements (74 for the compressed liquid and 92 for the superheated vapor), for which the AAD% is 1.08 %, and the MAD% is 5.54 %. The discrepancy in terms of deviations for the subsets of data having the same temperature is lower if compared to the measurements by Perkins and Huber [188], however Alam et al. [189] provided measurements over a smaller range of temperature 313–496 K and pressure 0.114–4.106 MPa, thus also the related deviations at specific temperatures might vary in a more limited range.

R-1243zf

For refrigerant R-1243zf, only one experimental thermal conductivity data set by Kim et al. [159] has been found in the literature. The 35 measurements (25 in liquid phase, and 10 in vapor phase) were obtained in the ranges T = 315–406 K and P = 0.937–6.118 MPa. The data, exhibit an AAD% = 4.22 %, and the maximum deviation (MAD% = 13.74 %) for a measurement in the vapor phase, at a temperature that is close to the critical temperature, but well below the critical pressure.

5.4 Discussion

A first consideration is on the availability of experimental measurements for the examined thermophysical properties. While R-1233zd(E) is already provided with a consistent number of studies addressing the thermodynamic properties, the opposite is observed for the other three refrigerants. This gap further widens for the transport properties.

As to the calculated deviations, the vapor pressure data for R-1233zd(E) show that good agreement is achieved between the recommended EOS and the available data sets by Mondéjar et al. [162] in the temperature range between the NBP and the critical temperature. Differently, at temperatures below the NBP, significant discrepancy is observed for the set by Li et al. [165], as well as for the set by Di Nicola et al., considered in the 2018's refrigerant properties review [65]. Considering the recommended equation of state has been developed on a single data set of experimental data, in addition to the fact that the same data did not cover the whole declared range of validity of the software, the very high deviations are likely attributable to limited EOS capabilities in representing the fluid behavior at temperatures below the NBP. Such working conditions can be met, for instance, by low-pressure centrifugal chillers, for which this fluid has already been successfully employed. Consequently, a scarce ability to represent the fluid properties for temperatures below the NBP would also have shortcomings in the fine-tuning of a system design and performance.

Similarly to R-1233zd(E), for R-1336mzz(Z) high deviations are observed for the measurements by Li et al. [170] at temperatures below the NBP, far outreaching the declared estimated uncertainty for vapor pressure. Overall, for R-1336mzz(Z) much less experimental data are available, which might have been an inherent limit in the development of an accurate EOS. Nevertheless, it must be also considered that, since the pressure absolute uncertainty is normally constant, the relative experimental uncertainties for vapor pressure measurements increases as the pressure decreases, which can in part explain the high deviations at such measuring conditions. With regard to R-1243zf, the calculated AADs% show that better agreement with the reference EOS is obtained, with only slight dispersion of the deviations for the data at the lowest temperature. A different situation is observed for R-1224yd(Z), for which all the available data sets exhibit either positive or negative systematic deviations, that can be attributed to the adjustments of the measuring apparatuses. However, the AADs% for all the three vapor pressure data sets exceed the EOS declared estimated uncertainty, which very likely indicates the recommended equation will require future modifications.

As opposed to the vapor pressure data, better predictive capabilities of REFPROP EOSs is generally observed for the experimental PvT properties. Assessing the results based on the AADs%, however, very few data sets are represented within

the declared estimated uncertainties. This is particularly evident with the *PvT* data for R-1243zf: all the available data sets provide high deviations, generally greater than that for the other fluids. Again, the higher divergences for R-1243zf could be attributed to the lack of significant number of experimental data from which to develop an EOS. Singularities in terms of deviations are observed for *PvT* properties measured around the critical points for R-1233zd(E), R-1224yd(Z), and R-1243zf. However, being this fluid region normally more difficult to investigate experimentally, this worse agreement with the EOS can more easily attributed to the greater experimental uncertainties rather than to the EOS itself.

In fact, as outlined in Chapter 4, the Helmholtz energy-based equations, implemented in current REFPROP version for these fluids, incorporate dedicated terms (the Gaussian terms) to enhance the properties representation in the critical region.

Especially for those fluid which have been explored also for high-temperature heat pumps and ORC cycles, namely, R-1224yd(Z), R-1336mzz(Z), and R-1233zd(E), an inaccurate representation of the fluid behavior near the critical point could imply several inconsistencies with the real fluid behavior whenever, for instance, either the condensing or the evaporating side of the equipment operates in conditions that approach the critical region. Consequently, until significant number of accurate data become available to enhance the properties prediction capabilities, it could be wise considering an interval around the critical region in which the calculated properties must be handled more carefully. Based on the calculated deviations for the *PvT* data of the four refrigerants, this could be assumed as equal to $T_{crit} \pm 6\,\mathrm{K}$.

Differently from the analyzed thermodynamic properties, the comparison of the experimental viscosity and thermal conductivity measurements with the reference models and correlations clearly indicate that, for the considered novel refrigerants, there are still major issues concerned with the NIST software, mainly due to the inherent limits related to the implementation of theoretical ECS models, for which higher deviations are normally expected. Furthermore, the recommended models and correlations for the transport properties of these novel fluids generally lack in flexibility to represent the experimental data that are measured at similar temperatures but different pressures. This characteristic is particularly evident in the distribution of the thermal conductivity deviations for R-1336mzz(Z) (Fig. 5.7c), for which the reference model proves consistent only within a subset of measurements performed at temperatures between the NBP and the critical temperature. In general, however, as discussed in Section 4.8, the established transient hot-wire technique for measuring thermal conductivity allows to reproduce the experimental measurements within an uncertainty of 1 %, at least far from the critical region and low pressure conditions.

5.5 Conclusions

The literature search for newly available experimental data measurements for novel halogenated olefin, low-GWP refrigerants allowed to retrieve new studies reporting experimental measurements of technically interesting thermophysical properties. Based on the overall number of collected data sets, and in compliance with the state-of-the-art of property prediction tools, refrigerants R-1233zd(E), R-1224yd(Z), R-1336mzz(Z), and R-1243zf have been investigated to assess the capacity of accurately and conveniently extrapolate the fluid behavior over wide ranges of temperatures and pressures, encompassing all the suitable working conditions for the four refrigerants.

The deviation analysis provided valuable insights on the knowledge of these potential working fluids, shedding lights on the reliability of the current version (10.0) of NIST commercial database REFPROP, the reference standard for the air-conditioning, refrigeration, and heat pump industry. Because of a general low amount of available experimental measurements for both the thermodynamic and transport properties, the reference equations of state and correlations proved in turn affected by a still limited effectiveness, particularly for the conditions at temperatures below the normal boiling point, and around the critical region. Additionally, for the PvT properties of R-1336mzz(Z) and for thermal conductivity measurements of R-1233zd(E), a substantial lack of correspondence with some calculated values are observed in the vicinity of the saturation boundaries, so that the computed values were erroneously referred to the liquid phase rather than to the actual under-examination vapor phase, or vice versa.

In general, the major issues arose with crucial properties viscosity and thermal conductivity for which, although the values of these properties appeared to be mostly represented within the models/correlations estimated uncertainties, the excessively large ranges in which the measurements can be considered in agreement with REFPROP translate in an insufficient accuracy, precision, and reliability of the predicted properties. As a result, in spite of the availability of properties estimation tools is of great technical importance, especially to promote and widen the applications of these new generation of refrigerants, the simulation applications that integrates the same recommended formulations for the optimization of the design and performance of HVAC systems operating with these promising working fluids can be highly hindered in terms of trustworthiness that, as made evident by means of the properties analysis, cannot be taken for granted, regardless of the software recommendations.

Nomenclature

Acronyms

AAD%	percentage average absolute deviation
COP	coefficient of performance
CP	critical point
EOS	equation of state
GHG	greenhouse gas
GWP	Global Warming Potential
MAD%	percentage maximum absolute deviation
NBP	Normal Boiling Point temperature
Q_{vol}	volumetric heat capacity
TEWI	Total Equivalent Warming Impact

Symbols

λ	thermal conductivity
μ	dynamic viscosity
ν	kinematic viscosity
ρ	density
σ	surface tension
c_p	isobaric specific heat capacity
c_p^0	ideal-gas specific heat capacity
c_v	isochoric specific heat capacity
P	pressure
P_{sat}	vapor pressure
T	temperature
v	specific volume
w	speed of sound

Bibliography

[1] IPCC. "Summary for Policymakers". In: *Climate Change 2021: The Physical Science Basis. Contribution of Working Group I to the Sixth Assessment Report of the Intergovernmental Panel on Climate Change*. Ed. by V. Masson-Delmotte et al. Cambridge University Press, 2021, pp. 3–32. DOI: 10.1017/9781009157896.001.

[2] H. Ritchie and M. Roser. "Energy". In: *Our World in Data* (2020). URL: https://ourworldindata.org/energy.

[3] *Overview of Greenhouse Gases*. United States Environmental Protection Agency (EPA). 2019. URL: https://www.epa.gov/ghgemissions/.

[4] IPCC. "Summary for Policymakers". In: *Global Warming of 1.5°C. An IPCC Special Report on the impacts of global warming of 1.5°C above pre-industrial levels and related global greenhouse gas emission pathways, in the context of strengthening the global response to the threat of climate change, sustainable development, and efforts to eradicate poverty*. Ed. by V. Masson-Delmotte et al. Cambridge University Press, 2018. DOI: 10.1017/9781009157940.001.

[5] X. L. Yue and Q. X. Gao. "Contributions of natural systems and human activity to greenhouse gas emissions". In: *Advances in Climate Change Research* (2018).

[6] J. G. J. Olivier and J. A. H. W. Peters. *Trends in global CO2 and total greenhouse gas emissions: 2020 report*. Report. PBL Netherlands Environmental Assessment Agency, 2020.

[7] A. Ollila. "The Greenhouse Effect Definition". In: *Physical Science International Journal* (2019). DOI: 10.9734/PSIJ/2019/v23i230149.

[8] IPCC. *Climate Change 2013: The Physical Science Basis. Contribution of Working Group I to the Fifth Assessment Report of the Intergovernmental Panel on Climate Change*. Technical Summary. 2013.

[9] V. Morlet V., D. Coulomb, and J. L. Dupont. *The impact of the refrigeration sector on climate change, 35th Informatory Note on refrigeration technologies.* Informatory note. IIF-IIR, 2017.

[10] P. Forster et al. "The Earth's Energy Budget, Climate Feedbacks and Climate Sensitivity". In: *Climate Change 2021: The Physical Science Basis. Contribution of Working Group I to the Sixth Assessment Report of the Intergovernmental Panel on Climate Change*. Cambridge University Press, 2021. Chap. 7. DOI: 10.1017/9781009157896.001.

[11] *Fluorinated greenhouse gases*. European Commission. 2022. URL: https://ec.europa.eu/clima/eu-action/fluorinated-greenhouse-gases_en.

[12] IPCC. "Technical Summary". In: *Climate Change 2007: The Physical Science Basis. Contribution of Working Group I to the Fourth Assessment Report of the Intergovernmental Panel on Climate Change*. Ed. by P. Forster et al. Cambridge University Press, 2007.

[13] J. M. Calm. "The next generation of refrigerants – Historical review, considerations, and outlook". In: *International Journal of Refrigeration* (2008). DOI: https://doi.org/10.1016/j.ijrefrig.2008.01.013.

[14] Ø. Hodnebrog, S. B. Dalsøren, and G. Myhre. "Lifetimes, direct and indirect radiative forcing, and global warming potentials of ethane (C2H6), propane (C3H8), and butane (C4H10)". In: *Atmospheric Science Letters* (2018). DOI: https://doi.org/10.1002/asl.804.

[15] T. Oltersdorf et al. *Briefing: One step forward, two steps back. A deep dive into the climate impact of modern fluorinated refrigerants*. Briefing. ECOS, 2021.

[16] L. Maizland. *Global Climate Agreements: Successes and Failures*. Ed. by Council on Foreign Relations. 2021. URL: https://www.cfr.org/backgrounder/paris-global-climate-change-agreements.

[17] A. Azar and R. Nosbers. *Implications of natural refrigerants for cooling technologies: Converting from HFCs/HCFCs to natural refrigerants*. Deutsche Gesellschaft für Internationale Zusammenarbeit (GIZ) GmbH, 2018.

[18] EEA. *Fluorinated greenhouse gases 2021*. Report. European Environment Agency, 2021. URL: https://www.eea.europa.eu/publications/fluorinated-greenhouse-gases-2021.

[19] European Commission. *Phasing down F-gases and ozone depleting substances to deliver on our climate targets*. 2022. DOI: 10.2834/209635.

[20] *Green Deal: Phasing down fluorinated greenhouse gases and ozone depleting substances*. European Commission. 2022. URL: https://ec.europa.eu/commission/presscorner/detail/en/IP_22_2189.

[21] IPCC. "Summary for Policymakers". In: *Climate Change 2022: Mitigation of Climate Change. Contribution of Working Group III to the Sixth Assessment Report of the Intergovernmental Panel on Climate Change*. Ed. by P. R. Shukla. Cambridge University Press, 2022. DOI: 10.1017/9781009157926.001.

[22] G. J. M. Velders et al. "The importance of the Montreal Protocol in protecting climate". In: *Proceedings of the National Academy of Sciences* (2007). DOI: 10.1073/pnas.0610328104.

[23] Cool Coalition, Climate, and Clean Air Coalition. *Sustainable Cooling in support of a Resilient and Climate Proof Recovery*. UNEP, 2021.

[24] UNEP and IEA. *Cooling Emissions and Policy Synthesis Report*. UNEP, Nairobi and IEA, Paris, 2020.

[25] G. J. M. Velders et al. "The large contribution of projected HFC emissions to future climate forcing". In: *Proceedings of the National Academy of Sciences* (2009). DOI: 10.1073/pnas.0902817106.

[26] Y. Xu et al. "The role of HFCs in mitigating 21st century climate change". In: *Atmospheric Chemistry and Physics* (2013). DOI: 10.5194/acp-13-6083-2013.

[27] *Short-Lived Climate Pollutants (SLCPs)*. Climate & Clean Air Coalition (CCAC). URL: https://www.ccacoalition.org/en/content/short-lived-climate-pollutants-slcps.

[28] G. Fox. *Refrigerants in building services*. Building Services Research and Information Association (BSRIA), UK, 2022. ISBN: 978-0-86022-791-5.

[29] IPCC. In: *Climate Change 2021: The Physical Science Basis. Contribution of Working Group I to the Sixth Assessment Report of the Intergovernmental Panel on Climate Change*. Ed. by V. Masson-Delmotte et al. 2021. Chap. 7. DOI: 10.1017/9781009157896.001.

[30] AIRAH. *Methods of calculating Total Equivalent Warming Impact (TEWI) 2012*. 2012.

[31] R. Peixoto and F. Polonara. *2018 report of the refrigeration, air conditioning and heat pumps technical options committee*. Report. UNEP, 2018.

[32] H. Wan et al. “A comprehensive review of life cycle climate performance (LCCP) for air conditioning systems”. In: *International Journal of Refrigeration* (2021). DOI: https://doi.org/10.1016/j.ijrefrig.2021.06.026.

[33] M. O. McLinden, C. J. Seeton, and A. Pearson. “New refrigerants and system configurations for vapor-compression refrigeration”. In: *Science* (2020). DOI: 10.1126/science.abe3692.

[34] M. O. McLinden and M. L. Huber. “(R)Evolution of Refrigerants”. In: *Journal of Chemical & Engineering Data* (2020). DOI: 10.1021/acs.jced.0c00338.

[35] S. Ebnesajjad. “Refrigeration Cycle and Refrigerant Selection: How Refrigerant Gases Work?” In: *Concise Handbook of Fluorocarbon Gases*. John Wiley & Sons, Ltd, 2021. Chap. 5. DOI: https://doi.org/10.1002/9781119323228.ch5.

[36] J. Sheff and D. Groff. *Guide to Refrigerant Regulation and Policy*. 2019. URL: https://www.hvacrbusiness.com/refrigerant-regulation-policy-guide.html.

[37] G. Wright. *An introduction to A2L refrigerants and their use in Refrigeration, Air Conditioning and Heat Pump applications*. Guidance note. Federation of Environmental Trade Associations (FETA), 2017.

[38] ISO Central Secretary. *Refrigerating systems and heat pumps — Safety and environmental requirements. Part 1: Definitions, classification and selection criteria*. Standard ISO 5149-1:2014(E). International Organization for Standardization, 2014.

[39] D. K. Kim et al., eds. *Improving Refrigerant Flammability Limit Test Methods Based on ASTM E681*. Vol. 2215. Purdue University, 2018. URL: https://docs.lib.purdue.edu/iracc/1883.

[40] ISO Central Secretary. *Refrigerants — Designation and safety classification*. Standard ISO 817:2014(E). Geneva, CH: International Organization for Standardization, June 2014.

[41] *Addition Of Subclass 2L Refrigerants Proposed For ASHRAE Refrigerant Safety Standard*. ASHRAE. 2015. URL: https://www.ashrae.org/about/news/2015/addition-of-subclass-2l-refrigerants-proposed-for-ashrae-refrigerant-safety-standard.

[42] A. N. Le Gendre. “Chemical, Physical, and Environmental Properties of ASHRAE 34 and ISO 817”. In: *A Guide to the Safe Refrigerant Transition*. Ed. by AHRI. 2020.

[43] M. O. McLinden et al. "A thermodynamic analysis of refrigerants: Possibilities and tradeoffs for Low-GWP refrigerants". In: *International Journal of Refrigeration* (2014). DOI: https://doi.org/10.1016/j.ijrefrig.2013.09.032.

[44] *Transitioning to Low-GWP Refrigerants*. ACHR News. 2022. URL: https://www.achrnews.com/articles/145955-transitioning-to-low-gwp-refrigerants.

[45] I. Dincer. "Refrigerants". In: *Refrigeration Systems and Applications*. John Wiley & Sons, Ltd, 2017. Chap. 2. DOI: https://doi.org/10.1002/9781119230793.ch2.

[46] C. W. Booten et al. "Refrigerants: Market Trends and Supply Chain Assessment". In: (2020). DOI: 10.2172/1599577.

[47] IPCC. *IPCC/TEAP Special Report: Safeguarding the Ozone Layer and the Global Climate System*. Report. IPCC, 2005. Chap. Refrigeration.

[48] ASHRAE. *ASHRAE Position Document on Natural Refrigerants*. 2014.

[49] A. Cavallini and C. Zilio. "Carbon dioxide as a natural refrigerant". In: *International Journal of Low-carbon Technologies* (2007). DOI: 10.1093/ijlct/2.3.225.

[50] *Adoption of new air-conditioning safety standard a milestone for climate-friendly cooling*. Environmental Investigation Agency (EIA) UK. 2022. URL: https://eia-international.org/news/adoption-of-new-air-conditioning-safety-standard-a-milestone-for-climate-friendly-cooling/.

[51] L. Fedele, S. Bobbo, and D. Menegazzo. "An update on the thermophysical properties data available for pure low GWP refrigerants". In: 6th IIR Conference on Thermophysical Properties and Transfer Processes of Refrigerants. International Institute of Refrigeration (IIR). 2021. DOI: http://dx.doi.org/10.18462/iir.TPTPR.2021.1985.

[52] MolView. 2022. URL: https://molview.org/.

[53] I. H. Bell et al. "Survey of Data and Models for Refrigerant Mixtures Containing Halogenated Olefins". In: *Journal of Chemical & Engineering Data* (2021). DOI: 10.1021/acs.jced.1c00192.

[54] P. Giménez-Prades et al. "Novel molecules as working fluids for refrigeration, heat pump and organic Rankine cycle systems". In: *Renewable and Sustainable Energy Reviews* (2022). DOI: https://doi.org/10.1016/j.rser.2022.112549.

[55] J.F. Bornman et al. *Environmental Effects Assessment Panel: Summary update 2021 for policymakers*. UNEP, 2021.

[56] *PFAS ban proposal delayed*. Coolingpost. 2022. URL: https://www.coolingpost.com/world-news/pfas-ban-proposal-delayed/.

[57] ASME History and Heritage Committee. *Perkins Vapor-Compression Cycle for Refrigeration. A Historic Mechanical Engineering Landmark*. American Society of Mechanical Engineers (ASME), 2020.

[58] D. Didion. "The Influence of the Thermophysical Fluid Properties of the New Ozone-Safe Refrigerants on Performance". In: (1999).

[59] I. Dincer. "General Aspects of Thermodynamics". In: *Refrigeration Systems and Applications*. John Wiley & Sons, Ltd, 2017. Chap. 1. DOI: https://doi.org/10.1002/9781119230793.ch2.

[60] Y. Hwang and M. R. Reinhard. "Natural Refrigerants". In: *Mechanical Engineering* (1998). DOI: 10.1115/1.1998-OCT-7.

[61] D. Wu, B. Hu, and R.Z. Wang. "Vapor compression heat pumps with pure Low-GWP refrigerants". In: *Renewable and Sustainable Energy Reviews* (). DOI: https://doi.org/10.1016/j.rser.2020.110571.

[62] B. Pavkovic. "Refrigerants - Part 1: Properties and air-conditioning applications". In: *REHVA* (Oct. 2013).

[63] A. Domanski. *Low-gwp refrigerants: Status and Outlook*. Informatory note. IIF-IIR, 2022.

[64] G.F. Hundy, A.R. Trott, and T.C. Welch. "Chapter 3 - Refrigerants". In: *Refrigeration, Air Conditioning and Heat Pumps (Fifth Edition)*. Fifth Edition. Butterworth-Heinemann, 2016, pp. 41–58. DOI: https://doi.org/10.1016/B978-0-08-100647-4.00003-6.

[65] S. Bobbo et al. "Low GWP halocarbon refrigerants: A review of thermophysical properties". In: *International Journal of Refrigeration* (2018). DOI: https://doi.org/10.1016/j.ijrefrig.2018.03.027.

[66] W. A. Wakeham and C. A. Nieto De Castro. "Technological Importance". In: *Transport Properties of Fluids: Their Correlation, Prediction and Estimation*. Cambridge University Press, 1996, pp. 6–16.

[67] M. O. McLinden et al. "Possibilities, limits, and tradeoffs for refrigerants in the vapor compression cycle". In: *ASHRAE Transactions: Gaithersburg, MD, USA* (2012).

[68] M. O. McLinden and D. A. Didion. "The Search for Alternative Refrigerants – A Molecular Approach". In: (1988).

[69] A. Cavallini. "The state-of-the-art on Refrigerants". In: *Journal of Physics: Conference Series* (2020). DOI: 10.1088/1742-6596/1599/1/012001.

[70] P. Giménez-Prades et al. "Novel molecules as working fluids for refrigeration, heat pump and organic Rankine cycle systems". In: *Renewable and Sustainable Energy Reviews* (2022). DOI: https://doi.org/10.1016/j.rser.2022.112549.

[71] A. K. Vuppaladadiyam et al. "Progress in the development and use of refrigerants and unintended environmental consequences". In: *Science of The Total Environment* (2022). DOI: https://doi.org/10.1016/j.scitotenv.2022.153670.

[72] *Refrigerant criteria*. SWEP International AB. 2019. URL: https://www.swep.net/refrigerant-handbook/5.-refrigerants/sd7/.

[73] I. Dincer. "Refrigerants". In: *Refrigeration Systems and Applications*. John Wiley & Sons, Ltd, 2017. Chap. 2, pp. 71–126. ISBN: 9781119230793. DOI: https://doi.org/10.1002/9781119230793.ch2.

[74] L. Cecchinato et al. "L'effetto della presenza di gas incondensabili nelle apparecchiature frigorifere domestiche". In: 2004.

[75] R. Brignoli et al. "Refrigerant performance evaluation including effects of transport properties and optimized heat exchangers". In: *International Journal of Refrigeration* (2017). DOI: https://doi.org/10.1016/j.ijrefrig.2017.05.014.

[76] P. A. Domanski et al. "A thermodynamic analysis of refrigerants: Performance limits of the vapor compression cycle". In: *International Journal of Refrigeration* (2014). DOI: https://doi.org/10.1016/j.ijrefrig.2013.09.036.

[77] P. A. Domanski et al. "Low-GWP refrigerants for medium and high-pressure applications". In: *International Journal of Refrigeration* (2017). DOI: https://doi.org/10.1016/j.ijrefrig.2017.08.019.

[78] Bitzer. *Refrigerant report 21*. Report. BITZER Kühlmaschinenbau GmbH, 2021. URL: https://www.bitzer-refrigerantreport.com/.

[79] J. S. Brown et al. "Thermophysical properties and heat transfer and pressure drop performance potentials of hydrofluoro-olefins, hydrochlorofluoro-olefins, and their blends". In: *HVAC&R Research* (2014). DOI: 10.1080/10789669.2013.854146.

[80] J. S. Brown, C. Zilio, and A. Cavallini. "The fluorinated olefin R-1234ze(Z) as a high-temperature heat pumping refrigerant". In: *International Journal of Refrigeration* (2009). DOI: https://doi.org/10.1016/j.ijrefrig.2009.03.002.

[81] R. K. Shah and D. P. Sekulic. "Basic Thermal Design Theory for Recuperators". In: *Fundamentals of Heat Exchanger Design*. John Wiley & Sons, Ltd, 2003. Chap. 7.

[82] M. O. McLinden et al. "Limited options for low-global-warming-potential refrigerants". In: *Nature Communications* (2017). DOI: https://doi.org/10.1038/ncomms14476.

[83] L. P. M. Colombo et al. "Design and assessment of an experimental facility for the characterization of flow boiling of azeotropic refrigerants in horizontal tubes". In: *Journal of Physics: Conference Series* (). DOI: 10.1088/1742-6596/1224/1/012037.

[84] H. Lee. "Compact Heat Exchangers". In: *Thermal Design*. John Wiley & Sons, Ltd, 2022. Chap. 4.

[85] "Overview of Heat Exchanger Design Methodology". In: *Fundamentals of Heat Exchanger Design*. John Wiley & Sons, Ltd, 2003. Chap. 2, pp. 78–96. ISBN: 9780470172605.

[86] A. Cavallini and L. Mattarolo. "Trasmissione globale del calore. Scambiatori di calore". In: *Trasmissione del calore*. 1985. Chap. 10.

[87] S. Saleem, C. R. Bradshaw, and C. K. Bach. "Development of Design Guidelines for Fin-and-Tube Heat Exchangers with Low-GWP Refrigerants". In: *International Journal of Refrigeration* (2022). DOI: https://doi.org/10.1016/j.ijrefrig.2022.06.037.

[88] Ø. Wilhelmsen et al. "Thermodynamic Modeling with Equations of State: Present Challenges with Established Methods". In: *Industrial & Engineering Chemistry Research* (2017). DOI: 10.1021/acs.iecr.7b00317.

[89] M. R. Riazi. "Characterization and Properties of Petroleum Fractions". In: *PVT Relations and Equations of State*. ASTM International, 2005, pp. 329–364.

[90] R. T. Jacobsen et al. "Multiparameter Equations of State". In: *Equations of State for Fluids and Fluid Mixtures*. Elsevier, 2000. DOI: https://doi.org/10.1016/S1874-5644(00)80008-9.

[91] E. Hendriks et al. "Industrial Requirements for Thermodynamics and Transport Properties". In: *Industrial & Engineering Chemistry Research* (2010). DOI: 10.1021/ie101231b.

[92] R. Span et al. “Multiparameter equations of state — recent trends and future challenges”. In: *Fluid Phase Equilibria* (). DOI: https://doi.org/10.1016/S0378-3812(01)00416-2.

[93] M. J. Assael. “The Importance of Thermophysical Properties in Optimum Design and Energy Saving”. In: *Energy and Environment - Technological Challenges for the Future*. Springer, 2001, pp. 329–364. DOI: 10.1007/978-4-431-68325-4.

[94] A. Cavallini and L. Mattarolo. “Il gas ideale”. In: *Termodinamica Applicata*. 1985. Chap. 3, pp. 231–284.

[95] R. T. Jacobsen et al. “The Virial Equation of State”. In: *Equations of State for Fluids and Fluid Mixtures*. Elsevier, 2000. DOI: https://doi.org/10.1016/S1874-5644(00)80008-9.

[96] J. D. van der Waals. “De Continuiteit van den Gas-En Vloeisoftoestand”. Ph.D. Thesis. Hoogeschool te Leiden: Leiden, 1873.

[97] Y. S. Wei and R. J. Sadus. “Equations of state for the calculation of fluid-phase equilibria”. In: *AIChE Journal* (2000). DOI: https://doi.org/10.1002/aic.690460119.

[98] R. T. Jacobsen et al. “Cubic and Generalized Van Der Waals Equations”. In: *Equations of State for Fluids and Fluid Mixtures*. Elsevier, 2000. DOI: https://doi.org/10.1016/S1874-5644(00)80008-9.

[99] O. Redlich and J. N. S. Kwong. “On the Thermodynamics of Solutions. V. An Equation of State. Fugacities of Gaseous Solutions.” In: *Chemical Reviews* (1949). DOI: 10.1021/cr60137a013.

[100] G. Soave. “Equilibrium constants from a modified Redlich-Kwong equation of state”. In: *Chemical Engineering Science* (1972). DOI: https://doi.org/10.1016/0009-2509(72)80096-4.

[101] A. Rivera-Alvarez et al. “Predicting the Slope of the Temperature–Entropy Vapor Saturation Curve for Working Fluid Selection Based on Lee–Kesler Modeling”. In: *Industrial & Engineering Chemistry Research* (2020). DOI: 10.1021/acs.iecr.9b05736.

[102] D. Y. Peng and D. B. Robinson. “A New Two-Constant Equation of State”. In: *Industrial & Engineering Chemistry Fundamentals* (1976). DOI: 10.1021/i160057a011.

[103] R. Span et al. “Thermophysical Properties and Applications in Refrigeration System of the Low-GWP Refrigerant R1243zf and Its Blends”. In: *Fluid Phase Equilibria* (). DOI: https://doi.org/10.1007/s10765-021-02902-0.

[104] J. O. Valderrama. "The State of the Cubic Equations of State". In: *Industrial & Engineering Chemistry Research* (2003). DOI: 10.1021/ie020447b.

[105] I. H. Bell and A. Jäger. "Helmholtz Energy Transformations of Common Cubic Equations of State". In: *Journal of Research of the National Institute of Standards and Technology* (2016). DOI: 10.6028/jres.121.011.

[106] J. J. Martin and Y. C. Hou. "Development of an equation of state for gases". In: *AIChE Journal* (1955). DOI: https://doi.org/10.1002/aic.690010203.

[107] R. De Santis, F. Gironi, and L. Marrelli. "Vapor-Liquid Equilibrium from a Hard-Sphere Equation of State". In: *Industrial & Engineering Chemistry Fundamentals* (1976). DOI: 10.1021/i160059a006.

[108] B. A. Younglove and M. O. McLinden. "An International Standard Equation of State for the Thermodynamic Properties of Refrigerant 123 (2,2-Dichloro-1,1,1-Trifluoroethane)". In: *Journal of Physical and Chemical Reference Data* (1994). DOI: 10.1063/1.555950.

[109] E. W. Lemmon and R. Tillner-Roth. "A Helmholtz energy equation of state for calculating the thermodynamic properties of fluid mixtures". In: *Fluid Phase Equilibria* (1999). DOI: https://doi.org/10.1016/S0378-3812(99)00262-9.

[110] E. W. Lemmon and R. T. Jacobsen. "A New Functional Form and New Fitting Techniques for Equations of State with Application to Pentafluoroethane (HFC-125)". In: *Journal of Physical and Chemical Reference Data* (2005). DOI: 10.1063/1.1797813.

[111] I. H. Bell et al. "Pure and Pseudo-pure Fluid Thermophysical Property Evaluation and the Open-Source Thermophysical Property Library CoolProp". In: *Industrial & Engineering Chemistry Research* (2014). DOI: 10.1021/ie4033999.

[112] R. Akasaka and E. W. Lemmon. "Fundamental Equations of State for cis-1,3,3,3-Tetrafluoropropene [R-1234ze(Z)] and 3,3,3-Trifluoropropene (R-1243zf)". In: *Journal of Chemical & Engineering Data* (2019). DOI: 10.1021/acs.jced.9b00007.

[113] E. W. Lemmon et al. *NIST Standard Reference Database 23: Reference Fluid Thermodynamic and Transport Properties-REFPROP, Version 10.0, National Institute of Standards and Technology*. 2018. DOI: https://doi.org/10.18434/T4/1502528.

[114] J. Brown et al. *CYCLE_D-HX: NIST Vapor Compression Cycle Model Accounting for Refrigerant Thermodynamic and Transport Properties; Version 2, User's Guide*. 2021. DOI: https://doi.org/10.6028/NIST.TN.2134.

[115] M. L. Huber et al. "The NIST REFPROP Database for Highly Accurate Properties of Industrially Important Fluids". In: *Industrial & Engineering Chemistry Research* (2022). DOI: 10.1021/acs.iecr.2c01427.

[116] Simulink Documentation. *Simulation and Model-Based Design*. 2022. URL: https://www.mathworks.com/products/simulink.html.

[117] Modelica Association. *Modelica® - A Unified Object-Oriented Language for Physical Systems Modeling. Tutorial*. 2022. URL: http://www.modelica.org/documents/ModelicaTutorial14.pdf.

[118] E. Mickoleit, C. Breitkopf, and A. Jäger. "Influence of equations of state and mixture models on the design of a refrigeration process". In: *International Journal of Refrigeration* (2021). DOI: https://doi.org/10.1016/j.ijrefrig.2020.10.017.

[119] N. Sakoda and Y. Higashi. "Measurements of PvT Properties, Vapor Pressures, Saturated Densities, and Critical Parameters for cis-1-Chloro-2,3,3,3-tetrafluoropropene (R1224yd(Z))". In: *Journal of Chemical & Engineering Data* (2019). DOI: 10.1021/acs.jced.9b00374.

[120] L. Fedele et al. "Compressed Liquid Density Measurements for 1,1,1,2,3,3,3-Heptafluoropropane (R227ea)". In: *Journal of Chemical & Engineering Data* (2007). DOI: 10.1021/je700260f.

[121] *Working principles of vibrating-tube densitometers*. Instrumentation Tools. 2017. URL: https://instrumentationtools.com/densitometers-working-principle/.

[122] L. Fedele et al. "PρT Experimental Measurements and Data Correlation of Pentaerythritol Esters". In: *Journal of Chemical & Engineering Data* (2007). DOI: 10.1021/je060271a.

[123] Y. Higashi et al. "Measurements of PρT properties, vapor pressures, saturated densities, and critical parameters for R1234ze(Z) and R245fa". In: *International Journal of Refrigeration* (2015). DOI: https://doi.org/10.1016/j.ijrefrig.2014.12.007.

[124] N. Sakoda et al. "Measurements of PvT properties, saturated densities, and critical parameters of R1132(E)". In: *International Journal of Refrigeration* (2022). DOI: https://doi.org/10.1016/j.ijrefrig.2022.05.012.

[125] S. Okazaki et al. “Procedures for determining the critical parameters of fluids”. In: *Review of Scientific Instruments* (1983). DOI: 10.1063/1.1137208.

[126] X. Yao et al. “A new apparatus for measurement of the critical p-ρ-T properties based on the variable-volume method”. In: *International Journal of Refrigeration* (2022). DOI: https://doi.org/10.1016/j.ijrefrig.2022.01.011.

[127] S. Bobbo et al. “Saturated Pressure Measurements of cis-1-Chloro-2,3,3,3-tetrafluoropropene (R1224yd (Z)) Saturation Pressure”. In: *Journal of Chemical & Engineering Data* (2020). DOI: 10.1021/acs.jced.0c00231.

[128] Q. Zhong et al. “Adiabatic calorimeter for isochoric specific heat capacity measurements and experimental data of compressed liquid R1234yf”. In: *The Journal of Chemical Thermodynamics* (2018). DOI: https://doi.org/10.1016/j.jct.2018.05.022.

[129] B. Sheng et al. “The isobaric heat capacity of 2,3,3,3-tetrafluoroprop-1-ene (R1234yf) at temperatures from (230 to 285) K and pressures up to 8 MPa using a new flow calorimeter”. In: *The Journal of Chemical Thermodynamics* (2022). DOI: https://doi.org/10.1016/j.jct.2021.106626.

[130] X. Peng et al. “Experimental Speed of Sound for cis-1,3,3,3-Tetrafluoropropene (R1234ze(Z)) and Hexafluoropropene (R1216) in Gaseous Phase”. In: *International Journal of Refrigeration* (2022). DOI: https://doi.org/10.1016/j.ijrefrig.2022.08.024.

[131] Q. Liu et al. “Speed of Sound Measurements Using a Cylindrical Resonator for Gaseous Carbon Dioxide and Propene”. In: *Journal of Chemical & Engineering Data* (2014). DOI: 10.1021/je500424b.

[132] A. Miyara and M. J. Alam. “Development and Validation of Tandem Capillary Tubes Method to Measure Viscosity of Fluids”. In: *Transactions of the Japan Society of Refrigerating and Air Conditioning Engineers* (2019). DOI: 10.11322/tjsrae.18-47_EM_OA.

[133] M. J. Alam et al. “Measurement of Viscosity of cis-1,1,1,4,4,4-Hexafluoro-2-butene (R-1336mzz(Z)) by Tandem Capillary Tubes Method”. In: *Journal of Chemical & Engineering Data* (2018). DOI: 10.1021/acs.jced.8b00036.

[134] Y. Liu et al. “Surface tension and parachor for a new low-GWP refrigerant R1123/R32/R1234yf and its constituent binary pairs”. In: *International Journal of Refrigeration* (2021). DOI: https://doi.org/10.1016/j.ijrefrig.2021.09.021.

[135] B. Stâlhane and S. Pyk. "Ny Metod För Bestämning Av Värmeledningkoefficienter". In: *Teknisk Tidskrift* (1931).

[136] M. J. Assael, K. Antoniadis, and W. Wakeham. "Historical Evolution of the Transient Hot-Wire Technique". In: *International Journal of Thermophysics* (2010). DOI: 10.1007/s10765-010-0814-9.

[137] M. Scattolini et al. "Thermal Conductivity Measurements for trans-1,3,3,3-Tetrafluoropropene (R1234ze(E)) in Liquid Phase". In: 19th International Refrigeration and Air Conditioning Conference at Purdue. 2022. URL: https://docs.lib.purdue.edu/iracc/2412/.

[138] L. Fedele, S. Bobbo, and D. Menegazzo. "An update on the thermophysical properties data available for low GWP refrigerants". In: *6th IIR Conference on Thermophysical Properties and Transfer Processes of Refrigerants* (2021). DOI: http://dx.doi.org/10.18462/iir.TPTPR.2021.1985.

[139] IPCC. The Earth's Energy Budget, Climate Feedbacks and Climate Sensitivity. Supplementary Material. In: *Climate Change 2021: The Physical Science Basis. Contribution of Working Group I to the Sixth Assessment Report of the Intergovernmental Panel on Climate Change*. Ed. by V. Masson-Delmotte et al. 2021. Chap. 7. DOI: 10.1017/9781009157896.001.

[140] T. Sako et al. "Measurement of critical properties of fluorinated ethers and amines". In: *Fluid phase equilibria* (1998). DOI: https://doi.org/10.1016/S0378-3812(97)00249-5.

[141] K. Tanaka and R. Akasaka. "Experimental determination of the critical parameters for trans-1-chloro-3,3,3-trifluoroprop-1-ene [R1233zd(E)] and cis-1-chloro-2,3,3,3-tetrafluoroprop-1-ene [R1224yd(Z)]". In: *International Journal of Refrigeration* (2021). DOI: https://doi.org/10.1016/j.ijrefrig.2021.07.010.

[142] B. Sheng et al. "Measurements of isobaric specific heat capacity (c_p) for pure trans-1,3,3,3-tetrafluoropropene and (trans-1,3,3,3-Tetrafluoropropene + 1,1,1,2-tetrafluoroethane) binary mixtures at temperatures from (231.84 to 338.68) K and pressures up to 8.2 MPa". In: *The Journal of Chemical Thermodynamics* (2022). DOI: https://doi.org/10.1016/j.jct.2022.106821.

[143] M. J. Alam et al. "Viscosity Measurement of cis-1,3,3,3-tetrafluoropropene (R1234ze(Z)) by Tandem Capillary Tubes Method". In: *International Journal of Refrigeration* (2021). DOI: https://doi.org/10.1016/j.ijrefrig.2021.04.004.

[144] D. Mondal et al. “Viscosity measurement for trans-1,1,1,4,4,4-hexafluoro-2-butene (R1336mzz(E)) in liquid and vapor phases”. In: *International Journal of Refrigeration* (2022). DOI: https://doi.org/10.1016/j.ijrefrig.2021.10.006.

[145] X. Zhang et al. “Experimental investigation of saturated liquid kinematic viscosity and surface tension of two isomeric refrigerants trans-1,1,1,4,4,4-hexafluoro-butene (R1336mzz(E)) and cis-1,1,1,4,4,4-hexafluoro-butene (R1336mzz(Z)) by surface light scattering”. In: *Fluid Phase Equilibria* (2022). DOI: https://doi.org/10.1016/j.fluid.2022.113468.

[146] C. Xu et al. “Experimental and theoretical study on liquid viscosity of R1336mzz(E)”. In: *CIESC Journal* (2021). DOI: 10.11949/0438-1157.20201597.

[147] X. Peng et al. “Experimental speed of sound for trans-1-Chloro-3,3,3-trifluoroprop-1-ene (R1233zd(E)) and trans-1,1,1,4,4,4-Hexafluorobut-2-ene (R1336mzz(E)) in gaseous phase”. In: *The Journal of Chemical Thermodynamics* (2022). DOI: https://doi.org/10.1016/j.jct.2022.106808.

[148] D. Mondal et al. “Thermal conductivity measurement and correlation at saturation condition of HFO refrigerant trans-1,1,1,4,4,4-hexafluoro-2-butene (R1336mzz(E))”. In: *International Journal of Refrigeration* (2021). DOI: https://doi.org/10.1016/j.ijrefrig.2021.05.005.

[149] Guo Haowen et al. “Experimental and Theoretical Research on the Saturated Liquid Thermal Conductivity of HFO-1336mzz(E)”. In: *Industrial & Engineering Chemistry Research* (2021). DOI: 10.1021/acs.iecr.1c01228.

[150] N. Sakoda, Y. Higashi, and R. Akasaka. “Measurements of PvT Properties, Vapor Pressures, Saturated Densities, and Critical Parameters for trans-1,1,1,4,4,4-Hexafluoro-2-butene (R1336mzz(E))”. In: *Journal of Chemical & Engineering Data* (2021). DOI: 10.1021/acs.jced.0c00848.

[151] U. A. Perera et al. “Measurements of saturation pressures for the novel refrigerant R1132(E)”. In: *International Journal of Refrigeration* (2022). DOI: https://doi.org/10.1016/j.ijrefrig.2021.12.014.

[152] K. Tanaka et al. “Vapor Pressure, (P,ρ,T) Behavior, Saturated Densities, and Surface Tension of trans-1, 2-Dichloroethene [R1130 (E)]”. In: *International Journal of Thermophysics* (2022). DOI: https://doi.org/10.1007/s10765-022-02986-2.

[153] U. A. Perera et al. “PvT Properties, Saturation Pressures, Saturated Densities, and Critical Parameters of Trifluoroiodomethane (CF3I; R-13I1)”. In: *Journal of Chemical & Engineering Data* (2022). DOI: 10.1021/acs.jced.2c00182.

[154] Y. Kano. “Multi-property evaluation for a gas sample based on the acoustic and electromagnetic resonances measurement in a cylindrical cavity”. In: *The Journal of Chemical Thermodynamics* (2021). DOI: https://doi.org/10.1016/j.jct.2021.106448.

[155] G. Beltramino et al. “Saturation Vapour Pressure Measurements of Refrigerant R1224yd(z) From 274 K to 338 K”. In: *International Journal of Refrigeration* (2022). DOI: https://doi.org/10.1016/j.ijrefrig.2022.09.026.

[156] B. Sheng et al. “The isochoric special heat capacity for 3,3,3-trifluoroprop-1-ene (R1243zf) at temperatures from (299 to 351) K and pressures up to 11 MPa”. In: *The Journal of Chemical Thermodynamics* (2021).

[157] L. Ding et al. “Measurements of isochoric specific heat capacity for 3,3,3-trifluoroprop-1-ene (R1243zf) at temperatures from (250 to 300) K and pressures up to 10 MPa”. In: *The Journal of Chemical Thermodynamics* (2021). DOI: https://doi.org/10.1016/j.jct.2021.106494.

[158] H. Chen et al. “Experimental Speed of Sound for 3,3,3-Trifluoropropene (R-1243zf) in Gaseous Phase Measured with Cylindrical Resonator”. In: *Journal of Chemical & Engineering Data* (2021). DOI: 10.1021/acs.jced.1c00098.

[159] D. Kim et al. “Thermal conductivity measurements and correlations of pure R1243zf and binary mixtures of R32 + R1243zf and R32 + R1234yf”. In: *International Journal of Refrigeration* (2021). DOI: https://doi.org/10.1016/j.ijrefrig.2021.07.019.

[160] C. Arpagaus et al. “High temperature heat pumps: Market overview, state of the art, research status, refrigerants, and application potentials”. In: *Energy* (2018). DOI: https://doi.org/10.1016/j.energy.2018.03.166.

[161] B. Albertsen and G. Schmitz. “Experimental parameter studies on a two-phase loop thermosyphon cooling system with R1233zd(E) and R1224yd(Z)”. In: *International Journal of Refrigeration* (2021). DOI: https://doi.org/10.1016/j.ijrefrig.2021.07.036.

[162] M. E. Mondéjar et al. “Thermodynamic Properties of trans-1-Chloro-3,3,3-trifluoropropene (R1233zd(E)): Vapor Pressure, (p, ρ, T) Behavior, and Speed of Sound Measurements, and Equation of State”. In: *Journal of Chemical & Engineering Data* (2015). DOI: 10.1021/acs.jced.5b00348.

[163] J. Yin et al. “Experimental vapor pressures and gaseous pvT properties of trans-1-Chloro-3,3,3-trifluoropropene (R1233zd(E))”. In: *International Journal of Refrigeration* (2021). DOI: https://doi.org/10.1016/j.ijrefrig.2020.09.010.

[164] N. Sakoda, Y. Higashi, and R. Akasaka. “Measurements of Vapor Pressures for trans-1-Chloro-3,3,3-trifluoropropene (R1233zd(E)) and cis-1,1,1,4,4,4-Hexafluoro-2-butene (R1336mzz(Z))”. In: *Journal of Chemical & Engineering Data* (2020). DOI: 10.1021/acs.jced.0c00239.

[165] S. Li et al. “Vapor Pressure Measurements and Correlation for trans-1-Chloro-3,3,3-trifluoroprop-1-ene”. In: *Journal of Chemical & Engineering Data* (2019). DOI: 10.1021/acs.jced.9b00001.

[166] K. Tanaka. “Measurement of saturated vapor pressure and saturated liquid density of HCFO-1233zd(E) and HCFO-1233xf”. In: *Transactions of the Japan Society of Refrigerating and Air Conditioning Engineers* (2016). DOI: 10.11322/tjsrae.15-48_OA.

[167] G. Di Nicola et al. “Saturated Pressure Measurements of trans-1-Chloro-3, 3, 3-trifluoroprop-1-ene (R1233zd (E))”. In: *Journal of Chemical & Engineering Data* (). DOI: 10.1021/acs.jced.6b00916.

[168] M. O. McLinden and R. Akasaka. “Thermodynamic Properties of cis-1,1,1,4,4,4-Hexafluorobutene [R-1336mzz(Z)]: Vapor Pressure, (p, ρ, T) Behavior, and Speed of Sound Measurements and Equation of State”. In: *Journal of Chemical & Engineering Data* (2020). DOI: 10.1021/acs.jced.9b01198.

[169] K. Tanaka et al. “Thermodynamic Properties of cis-1,1,1,4,4,4-Hexafluoro-2-butene (HFO-1336mzz(Z)): Measurements of the pρT Property and Determinations of Vapor Pressures, Saturated Liquid and Vapor Densities, and Critical Parameters”. In: *Journal of Chemical & Engineering Data* (2016). DOI: 10.1021/acs.jced.6b00169.

[170] S. Li et al. “Vapor Pressure Measurements and Correlation for cis-1,1,1,4,4,4-Hexafluoro-2-butene (HFO-1336mzz(Z))”. In: *Journal of Chemical & Engineering Data* (2020). DOI: 10.1021/acs.jced.0c00024.

[171] Y. Higashi et al. "Measurements of Saturation Pressures for Trifluoroethene (R1123) and 3,3,3-Trifluoropropene (R1243zf)". In: *Journal of Chemical & Engineering Data* (2018). DOI: 10.1021/acs.jced.7b00818.

[172] J. Yin et al. "Saturated vapor pressure and gaseous pvT property measurements for 3,3,3-trifluoroprop-1-ene (R1243zf)". In: *International Journal of Refrigeration* (2020). DOI: https://doi.org/10.1016/j.ijrefrig.2020.04.021.

[173] Z. Yang et al. "Experimental measurements of saturated vapor pressure and isothermal vapor-liquid equilibria for 1,1,1,2-Tetrafluoroethane (HFC-134a) + 3,3,3-trifluoropropene (HFO-1243zf) binary system". In: *Fluid Phase Equilibria* (2019). DOI: https://doi.org/10.1016/j.fluid.2019.06.020.

[174] L. Fedele et al. "HCFO refrigerant cis-1-chloro-2,3,3,3 tetrafluoropropene [R1224yd(Z)]: Experimental assessment and correlation of the liquid density". In: *International Journal of Refrigeration* (2020). DOI: https://doi.org/10.1016/j.ijrefrig.2020.06.001.

[175] Y. Sun et al. "Measurement and Correlation of the Liquid Density and Viscosity of HFO-1336mzz(Z) (cis-1,1,1,4,4,4-Hexafluoro-2-butene) at High Pressure". In: *Journal of Chemical & Engineering Data* (2019). DOI: 10.1021/acs.jced.8b00713.

[176] G. Di Nicola et al. "Subcooled liquid density measurements and PvT measurements in the vapor phase for 3,3,3-trifluoroprop-1-ene (R1243zf)". In: *International Journal of Refrigeration* (2013). DOI: https://doi.org/10.1016/j.ijrefrig.2013.08.004.

[177] Y. Higashi and N. Sakoda. "Measurements of PvT Properties, Saturated Densities, and Critical Parameters for 3,3,3-Trifluoropropene (HFO1243zf)". In: *Journal of Chemical & Engineering Data* (2018). DOI: 10.1021/acs.jced.8b00452.

[178] M. L. Huber. "Models for Viscosity, Thermal Conductivity, and Surface Tension of Selected Pure Fluids as Implemented in REFPROP v10.0". In: (2018). DOI: https://doi.org/10.6028/NIST.IR.8209.

[179] R. A. Perkins, M. L. Huber, and M. J. Assael. "Measurement and Correlation of the Thermal Conductivity of trans-1-Chloro-3,3,3-trifluoropropene (R1233zd(E))". In: *Journal of Chemical & Engineering Data* (2017). DOI: 10.1021/acs.jced.7b00106.

[180] G. Zhao et al. “Saturated liquid kinematic viscosity, surface tension and thermal diffusivity of two low-GWP refrigerants 3,3,3-trifluoropropene (R1243zf) and trans-1-chloro-3,3,3-trifluoro-1-propene (R1233zd(E)) by light scattering method”. In: *International Journal of Refrigeration* (2021). DOI: https://doi.org/10.1016/j.ijrefrig.2021.03.012.

[181] J. Cui et al. “Saturated Liquid Dynamic Viscosity and Surface Tension of trans-1-Chloro-3,3,3-trifluoropropene and Dodecafluoro-2-methylpentan-3-one”. In: *Journal of Chemical & Engineering Data* (2018). DOI: 10.1021/acs.jced.7b00902.

[182] X. Meng, C. Wen, and J. Wu. “Measurement and correlation of the liquid viscosity of trans-1-chloro-3,3,3-trifluoropropene (R1233zd(E))”. In: *The Journal of Chemical Thermodynamics* (2018). DOI: https://doi.org/10.1016/j.jct.2018.04.001.

[183] A. Miyara, M. J. Alam, and K. Kariya. “Measurement of viscosity of trans-1-chloro-3,3,3-trifluoropropene (R-1233zd(E)) by tandem capillary tubes method”. In: *International Journal of Refrigeration* (2018). DOI: https://doi.org/10.1016/j.ijrefrig.2018.05.021.

[184] R. J. Hulse et al. “Physical Properties of HCFO-1233zd(E)”. In: *Journal of Chemical & Engineering Data* (2012). DOI: 10.1021/je300776s.

[185] M. J. Alam et al. “Measurement of thermal conductivity and viscosity of cis-1-chloro-2,3,3,3-tetrafluoropropene (R-1224yd(Z))”. In: *International Journal of Refrigeration* (2019). DOI: https://doi.org/10.1016/j.ijrefrig.2019.05.033.

[186] A. Miyara, M. J. Alam, and K. Kariya. “Measurements of Transport Properties of Low Gwp Refrigerant HCFO-1224yd(Z) (cis-1-chloro-2,3,3,3-tetrafluoropropene; CF3CF=CHCl)”. In: *Int. J. Refrig.* (2018). DOI: http://dx.doi.org/10.18462/iir.hfo.2018.1139.

[187] M. J. Alam et al. “Measurement of thermal conductivity and correlations at saturated state of refrigerant trans-1-chloro-3,3,3-trifluoropropene (R-1233zd(E))”. In: *International Journal of Refrigeration* (2018). DOI: https://doi.org/10.1016/j.ijrefrig.2018.02.004.

[188] R. A. Perkins and M. L. Huber. “Measurement and Correlation of the Thermal Conductivity of cis-1, 1, 1, 4, 4, 4-hexafluoro-2-butene”. In: *International journal of thermophysics* (2020).

[189] M. J. Alam et al. “Measurement of thermal conductivity of cis-1,1,1,4,4,4-hexafluoro-2-butene (R-1336mzz(Z)) by the transient hot-wire method”. In: *International Journal of Refrigeration* (2017). DOI: https://doi.org/10.1016/j.ijrefrig.2017.08.014.